Effects of Winglets on the Drag of a Low-Aspect-Ratio Configuration

Leigh Ann Smith and Richard L. Campbell

Effects of Winglets on the Drag of a Low-Aspect-Ratio Configuration

Leigh Ann Smith and Richard L. Campbell
Langley Research Center • Hampton, Virginia

Contents

Figures:

Abstract

A wind-tunnel investigation has been performed to determine the effect of winglets on the induced drag of a low-aspect-ratio wing configuration at Mach numbers between 0.30 and 0.85 and a nominal angle-of-attack range from −2° to 20°. Results of the tests at the cruise lift coefficient showed significant increases in lift-drag ratio for the winglet configuration relative to a wing-alone configuration designed for the same lift coefficient and Mach number. Further, even larger increases in lift-drag ratio were observed at lift coefficients above the design value at all Mach numbers tested. The addition of these winglets had a negligible effect on the static lateral-directional stability characteristics of the configuration. No tests were made to determine the effect of these winglets at supersonic Mach numbers, where increases in drag caused by winglets might be more significant. Computational analyses were also performed for the two configurations studied. Linear and small-disturbance formulations were used. The codes were found to give reasonable performance estimates sufficient for predicting changes of this magnitude.

Introduction

Reducing drag is a major concern for aircraft designers. Reduced drag yields such benefits as smaller, quieter engines that require less fuel and aircraft with increased range and/or payload capacities. Winglets have been found to yield significant reductions in the induced drag of a configuration when properly sized and placed (Whitcomb 1976). However, winglets have been investigated largely for high-aspect-ratio configurations with little emphasis on low-aspect-ratio effects. Recently, Kuhlman et al. (1988) investigated winglet effects for low-aspect-ratio configurations, determining that the percentage drag reduction afforded by winglets depends only on the ratio of winglet length to wing span, not on aspect ratio or wing sweep. In their study, Kuhlman et al. explored the effect of winglets on the performance of generic low-aspect-ratio configurations, including various planforms and leading-edge sweeps, at transonic conditions (Kuhlman et al. 1988).

The Kuhlman study produced two configurations with identical fuselages and identical wing planforms, one with winglets and one without, that are each designed for minimum drag. Both models use the same airfoil thickness distributions but have camber and twist distributions that have been optimized independently for minimum induced drag. This report investigates experimentally and numerically the performance of these designs. Results are presented for the two models over a range of subsonic Mach numbers and angles of attack to document any performance benefits or penalties that result from the addition of winglets. Some lateral-directional data are also presented to allow an assessment of the possible penalties that result from the addition of winglets on the configuration tested.

Symbols

The results presented in this report are referred to the stability-axis system for the longitudinal aerodynamic characteristics and to the body-axis system for the lateral-directional aerodynamic characteristics. Force and moment data have been reduced to conventional coefficient form based on the geometry of the baseline wing planform. Moments are referenced to the quarter-chord point of the mean aerodynamic chord of the baseline wing.

AR aspect ratio, $\dfrac{b^2}{S}$

b wing span, 24.000 in.

$\bar{c}$ mean aerodynamic chord, 12.365 in.

C_A axial force coefficient, $\dfrac{\text{Axial force}}{qS}$

C_D drag coefficient, $\dfrac{\text{Drag}}{qS}$

$C_{D,0}$ drag coefficient at zero lift

C_L lift coefficient, $\dfrac{\text{Lift}}{qS}$

C_{L_α} lift curve slope, $\dfrac{\partial C_L}{\partial \alpha}$, per degree

C_l configuration rolling-moment coefficient, $\dfrac{\text{Rolling moment}}{qSb}$

C_{l_β}	rate of change of rolling-moment coefficient with sideslip angle, $\dfrac{\partial C_l}{\partial \beta}$, per degree
C_m	pitching-moment coefficient, $\dfrac{\text{Pitching moment}}{qS\bar{c}}$
$C_{m_{C_L}}$	longitudinal stability derivative, $\dfrac{\partial C_m}{\partial C_L}$
$C_{m,0}$	pitching-moment coefficient at zero lift
C_N	normal force coefficient, $\dfrac{\text{Normal force}}{qS}$
C_n	yawing-moment coefficient, $\dfrac{\text{Yawing moment}}{qSb}$
C_{n_β}	rate of change of yawing-moment coefficient with sideslip angle, $\dfrac{\partial C_n}{\partial \beta}$, per degree
C_p	pressure coefficient
C_Y	configuration side-force coefficient, $\dfrac{\text{Side force}}{qS}$
C_{Y_β}	rate of change of side-force coefficient with sideslip angle, $\dfrac{\partial C_Y}{\partial \beta}$, per degree
e	Oswald's efficiency factor
L/D	lift-drag ratio
M	free-stream Mach number
q	free-stream dynamic pressure, psi
S	wing reference area, 258.900 in^2
x	streamwise coordinate value measured from nose, in.
y	spanwise coordinate value measured from center of fuselage, in.
z	vertical coordinate value measured from center of fuselage, in.
α	angle of attack, deg
β	angle of sideslip, deg
η	wing semispan station

Abbreviations:

VLM	vortex lattice method
WBPPW	wing-body-pod-pylon-winglet

Method

Models

The aerodynamic design of the models used in the present study has been described by Kuhlman et al. (1988, 1989). Kuhlman et al. sought to reduce induced drag on two identical planforms by optimizing wing twist and camber for one planform and by adding a winglet and optimizing wing and winglet twist and camber distributions for the other. The planforms are mounted midway on a cylindrical fuselage with an ogive nose. These two wing shapes are each designed to achieve minimum induced drag at the design condition of $M = 0.80$ and $C_L = 0.30$. A NACA 64A006 airfoil thickness distribution is used for both wings.

The configurations as designed by Kuhlman et al. are duplicated in the hardware for this test. Both wings have the same cropped delta planform with a leading-edge sweep of 50°, a span of 24.000 in., a taper ratio of 0.203, and an aspect ratio of 2.2. Sketches of both models are shown in figure 1, and coordinates are listed in tables 1 and 2.

The winglet planform was selected based on design criteria developed for transport-type aircraft by Whitcomb (1976). Similarly proven criteria for low-aspect ratios were not readily available. Winglet leading-edge sweep is 50° to match wing sweep, and winglet taper ratio is 0.5. Winglet length is fixed at 15 percent of wing semispan with a cant angle of 15° outboard from vertical. The winglet twist distribution was optimized using the same airfoil at all winglet stations. Winglets are mounted at the aft portion of the wingtip with a root chord equal to 60 percent of the wingtip chord. The resulting winglets have a total area equal to 2.27 percent of the wing area, and their span projected to the plane of the wing increases the configuration span by 3.88 percent relative to the wing alone.

Test Facility

Wind-tunnel testing for this project was performed in the Langley 7- by 10-Foot High-Speed Tunnel (HST). This tunnel is a closed-circuit atmospheric tunnel with a rectangular unventilated test section. It has a maximum Mach number capability of 0.94. The tunnel is equipped with a centerline vertical-strut model support system (Schaefer 1965), which

was used for all models in this test. Tunnel calibration information is provided by Fox and Huffman (1977). Photographs of the models installed in the tunnel are shown in figure 2.

Test Procedures

Testing was performed over a Mach number range of 0.30 to 0.85 and a Reynolds number range of 1.9 to 4.0×10^6. Nominal angle-of-attack sweeps ranged from $-2.0°$ to $20.0°$ depending on Mach number. The upper angle-of-attack limit was determined by a safety load limit on the sting. This limit allowed for a nominal angle of attack of $20.0°$ at the lower end of the Mach range, and $10.0°$ at the upper end. Angle-of-attack sweeps were run at all Mach numbers with the baseline model inverted as a check for tunnel flow angularity.

Additionally, angle-of-attack sweeps were run for two yaw angles, $2.5°$ and $-2.5°$, for both configurations. These sweeps were completed over the same Mach number range previously described. They were included in order to observe the sideslip characteristics of the models and to check for any degradation in lateral-directional stability characteristics caused by the presence of the winglets.

Transition grit strips, sized using the method of Braslow and Knox (1958), were applied to the model to induce boundary-layer transition at a fixed location. The strips were applied 0.6 in. from the leading edge of the wing on the upper and lower surfaces and 0.6 in. from the nose of the model. Strips were applied to the winglet 0.5 in. from the leading edge on the upper and lower surfaces. Grit size no. 150 was used on the nose and winglets, and no. 120 on the wings. All strips were 0.0625 in. wide.

Instrumentation

A six-component electrical strain-gauge balance was used to obtain force and moment data for this test. Angle of attack was measured by an accelerometer placed at the base of the sting with measurements corrected for sting bending. Electronic scanning pressure transducers were used to measure base and cavity pressures, which were used to correct drag measurements.

The strain-gauge balance measurements are known to be accurate to within 0.5 percent of full scale. This degree of accuracy represents ±0.0051 in C_N at $M = 0.85$ and ±0.0266 at $M = 0.50$. The C_A accuracy is ±0.0003 at $M = 0.85$ and ±0.0013 at $M = 0.50$. The accelerometer has an accuracy of $\pm0.01°$. No uncertainty studies were conducted to assess the uncertainty of this experimental setup.

Theoretical Analysis

Theoretical analyses were performed for the two configurations. Two different computational methods were used for each configuration to assess the ability of these codes to predict wind-tunnel performance results for these configurations.

The wing-body-pod-pylon-winglet (WBPPW) transonic small disturbance code by Boppe (1987) was chosen as the primary computational analysis tool for this study. This code was also one of the codes used by Kuhlman et al. (1988, 1989) in the original design of the models. It is capable of modeling two-dimensional airfoils and complex three-dimensional aircraft geometries with associated pods, pylons, and winglets at transonic speeds below Mach 1.0. This code has been used successfully for a wide range of configurations. It solves a version of the small-disturbance equation that has been extended to improve the results for configurations with swept shocks. Thus it is most appropriately used at transonic Mach numbers and for angles of attack near zero. Flow solutions for a wing-body case are obtained through calculations on two rectangular Cartesian grid systems: a global crude grid and embedded fine grids on the wing. These fine grids are embedded at 18 different stations on the wing. Further details of the code and its gridding system are documented by Boppe (1987). Two-dimensional laminar and turbulent boundary-layer calculations (Bradshaw and Ferriss 1971) simulate viscous effects on the wing.

The vortex lattice method (VLM) code described by Margason and Lamar (1971) and Lamar and Herbert (1982), was also used to compute the longitudinal forces and moments for the wing-body and the wing-body-winglet configuration. This code represents the lifting surfaces with a network of vortices and can model multiple planforms having twist, camber, and dihedral. Its ability to vary the dihedral along the span was used to model the winglet. The fuselage was also modeled as part of the wing with no camber and a planform corresponding to the maximum half-width line. An estimate of compressibility effects was included using the Prandtl-Glauert correction factor.

Results and Discussion

Presentation of Results

The data obtained from this test are presented in figures 3 to 9. Figures 3 to 8 present longitudinal aerodynamic characteristics, and figure 9 presents lateral-directional stability characteristics. All theoretical data are presented in figures 10 to 13.

3

Experimental Results

Figure 3 illustrates the behavior of C_L with increasing α for both configurations. Above $M = 0.30$, the winglet model has the steeper lift-curve slope because of the effective aspect ratio increase. However, the baseline model consistently has higher lift values than those the winglet model has at $\alpha < 6°$ for all Mach numbers. This phenomenon is caused by the different twist distributions required to optimize the span loading for the two wings at the design point of $M = 0.80$ and $C_L = 0.30$. At $M = 0.30$, the lift curve of the baseline model is consistently higher than that of the winglet model.

Figure 4 details the change in drag with lift for the two configurations. For values of C_L ranging from approximately 0.25 to 0.70, the drag for the winglet model is equal to or less than that of the baseline. The minimum C_D values for both configurations are almost equal, but the data are insufficient to determine the exact difference. One would expect the winglet model to have slightly greater minimum drag because of its 2-percent greater wetted area and corresponding increase in skin-friction drag. This effect is shown clearly at $M = 0.30$ and 0.60, for which the difference in minimum drag is about 5 percent.

Figure 5 shows the longitudinal stability characteristics. These models are tailless, and thus the stability is based on wing performance and fuselage effects. Over the entire C_L range the differences in twist distribution for the two models cause differences in their spanwise wing loading and thus differences in their pitching-moment characteristics away from the design C_L. At the design C_L of 0.30, both wings are designed to have an elliptic span loading and thus, have a similar value of C_m at that condition. Above the design C_L, the winglets increase the lift at the wingtips and thus give the winglet model a slightly more negative pitching moment than that of the baseline model. For $M = 0.60$ and below, where higher values of C_L are obtained, the break in the $C_{m_{C_L}}$ curve indicating separation and pitch instability occurs around $C_L = 0.60$. The winglet model curve has the sharper break, an indication of a more significant lift loss behind the moment center at the wingtip.

The plots in figure 6 clearly show that the winglets increase L/D at values of C_L between 0.20 and 0.70 for all Mach numbers. At the design condition ($M = 0.80$, $C_L = 0.30$) L/D is increased by about 11 percent, while L/D increases of approximately 20 percent are observed at C_L values of approximately 0.60 for $M = 0.80$. As C_L increases, the induced drag becomes a larger fraction of the

total drag, and the winglets cause a constant percent reduction in induced-drag coefficient (Kuhlman et al. 1988). This phenomenon causes the increase in percent change in L/D as C_L increases. Loss of attached flow causes trends seen most clearly at the lower Mach numbers ($M \leq 0.70$), for which the percentage L/D improvement caused by winglets is eliminated at or above $C_L \approx 0.70$. This loss of L/D improvement corresponds to loss of lift in the tip region, which could be attributed to flow separation on the winglets or wingtip.

The C_D versus C_L^2 plots (fig. 7) show that there is a reduction in induced drag for the winglet model. For each curve, the slope of the straight line plotted through the data is inversely proportional to the value of Oswald's efficiency factor e as illustrated by the equation

$$C_D = C_{D,0} + \frac{C_L^2}{\pi \text{AR} e} \qquad (1)$$

This line is fitted to the points in the linear part of the curve (where C_L^2 is between 0.05 and 0.16). The line through the winglet data has the smaller slope and thus a higher value of e and lower induced drag.

Figure 8 summarizes the longitudinal data for the design C_L over the range of Mach numbers tested. For the design $C_L = 0.30$, the lift-curve slope is more positive for the winglet configuration than for the baseline configuration at all Mach numbers, an improvement which is also reflected in the lift-drag ratios shown in figure 6. The winglet configuration values of $C_{m_{C_L}}$ at $C_L = 0.30$ are also more negative than those of the baseline model, an indication of increased longitudinal stability, and the winglet model has a less negative pitching moment at zero lift.

Drag data are also illustrated for the Mach number range at the design lift coefficient. The data gathered are insufficient to determine the drag-rise Mach number because it appears to be in excess of the 0.85 maximum Mach number obtained. The drag data for the design C_L do show that the winglet configuration can achieve the desired lift with less drag than the baseline configuration for all Mach numbers.

Review of the longitudinal data for the design C_L indicates that the winglet configuration can achieve the desired lift with less drag, lower pitching moment, and greater longitudinal stability than the baseline configuration. However, a possible concern for application of winglets to low-aspect-ratio wings is the effect on lateral-directional stability. Lateral-directional stability was briefly reviewed in this investigation. Figure 9 presents lateral-directional stability derivatives for three of the Mach numbers tested.

The trends for the winglet configuration show slightly increased stability relative to the wing-alone configuration; however, most of the differences are within the error band for balance accuracy. Both configurations are unstable because they lack vertical tails.

Theory Comparisons

Results of the theoretical analyses are presented in figures 10 to 12. In the WBPPW code these values are calculated for a single flow condition, and thus the theory curves result from several calculations taken point by point. The VLM code computes an α sweep for a given Mach number in a single calculation.

Figure 10 shows a comparison of lift-curve slopes for the experimental data and the two codes for both the baseline model and the winglet model at $M = 0.30$ and $M = 0.80$. As the formulation of the WBPPW code leads us to expect, the best agreement occurs for small values of α and transonic Mach numbers. The WBPPW code predicts the lift-curve slope for the baseline configuration at the cruise Mach number of 0.80 for the values of α shown. The slope is slightly underpredicted for the winglet model at that Mach number. At $M = 0.30$ the experimental curve is underpredicted for both configurations, with agreement only at the lowest values of α. For the VLM code, the lift curves shown match very well along the linear portion of the curve, especially at the lower Mach numbers. The VLM code accurately predicts the shift in lift-curve slope caused by the addition of the winglets.

Figure 11 shows comparisons between experimental drag data and the code predictions. The WBPPW curve agrees with the experiment in trends but is not close in actual values.

The adjusted WBPPW and VLM curves were created by supplementing the theoretical induced-drag calculations with information gained by experiment. The value of $C_{D,0}$ was extrapolated from the experimental C_D-versus-C_L^2 curve (fig. 7) and combined with the induced-drag value calculated by each code to get the total drag as predicted by equation (1). This procedure was necessary because the VLM code has no $C_{D,0}$ calculation, and the WBPPW code calculates $C_{D,0}$ only indirectly.

In the WBPPW code, the induced drag is computed directly from the formula $C_L^2/\pi ARe$, and $C_{D,0}$ is calculated by subtracting induced drag from the pressure drag calculation and adding an estimated skin-friction drag. The calculated $C_{D,0}$, therefore, is different for each point on a given curve. Therefore, replacing $C_{D,0}$ with a constant value from the experiment changes the shape of the curve.

The resulting agreement between the experimental values and the adjusted WBPPW drag calculations in figure 11 indicates that most of the error in the original value of C_D computed by the WBPPW code is in the $C_{D,0}$ calculation, not in the induced-drag calculation. No attempt is made in this adjusted calculation to account for wave drag due to lift; the agreement seen here indicates that it is not present at these conditions, and the theoretical pressure distributions (fig. 13) support this conclusion. This technique also yields similar drag predictions for the VLM results for values of C_L between 0.10 and 0.50, with the predicted drag values matching the experimental drag values more closely for the winglet configuration than for the baseline configuration.

The last comparison between the codes and experiment is shown in figure 12. The VLM estimates show better agreement than those from the WBPPW code, with the winglet data showing better agreement than the baseline data. The WBPPW code is good for rough estimates of pitching-moment coefficient but not for detailed calculations. Again, the WBPPW curve agrees with the $M = 0.80$ data better than with the $M = 0.30$ data. One possible source of the discrepancies seen here for the WBPPW curves are the loads calculated on the fuselage. Inaccurate lift distributions over the length of the fuselage can greatly affect pitching-moment calculations. The grid around the fuselage is a coarse one, and pressure plots (fig. 14) indicate that the lift is only sparsely predicted across the fuselage, especially in the nose region.

Table 3 compares the values of Oswald's efficiency factor e determined theoretically (for two Mach numbers) and experimentally (for all Mach numbers). Experimentally, this value was obtained from the inverse of the slope of the C_D-versus-C_L^2 plots (fig. 7). This technique was also used with VLM data to estimate a VLM e value. It gave a result that the resulting VLM e values are much too high for the baseline shape, but the predictions for the winglet model are reasonably accurate. For the WBPPW results, the value of e is computed by means of a fast Fourier analysis applied to the configuration span-load distribution. The WBPPW code only applies this analysis when winglets are not present, however, and thus no winglet-on predicted values are presented. Although a good estimate was made for $M = 0.30$, the WBPPW code overestimated the value of e by about 9 percent for $M = 0.80$. This lower experimental value for e indicates that the baseline wing may not be achieving the elliptical loading predicted by the codes. Because no pressure data were obtained, no experimental span-load data exist to determine the

cause of this discrepancy. Also, because no theoretical e value is available for the winglet case, it is not known if the winglet configuration experienced a similar discrepancy from the estimated efficiency.

Comparing the results of the two codes shows they agree similarly with the experimental data. The two codes give reasonable performance estimates for the two low-aspect-ratio configurations studied here. Hence the two wings should come sufficiently close to meeting the design objective of minimum drag at $M = 0.80$ and $C_L = 0.30$ and so the effects of winglets on these configurations can be assessed accurately.

Concluding Remarks

This study indicates that at the design Mach number of 0.80 winglets improve the lift-draft ratio of the cropped delta wings by 11 percent at a lift coefficient of 0.30 and by 20 percent at a lift coefficient of 0.60. The addition of winglets greatly reduces the induced drag of the configuration and increases the lift-curve slope. Results indicate that the addition of winglets does not adversely affect the static stability characteristics of the configuration as long as separation does not occur on the wing or winglet. Comparisons of wind-tunnel data to theory show that the wing-body-pod-pylon-winglet (WBPPW) and vortex lattice method (VLM) codes give reasonable performance estimates for the low-aspect-ratio configurations studied herein.

NASA Langley Research Center
Hampton, VA 23681-0001
October 17, 1995

References

Boppe, Charles W. 1987: *Aerodynamic Analysis for Aircraft With Nacelles, Pylons, and Winglets at Transonic Speeds.* NASA CR-4066.

Bradshaw, P.; and Ferriss, D. H. 1971: Calculation of Boundary-Layer Development Using the Turbulent Energy Equation: Compressible Flow on Adiabatic Walls. *J. Fluid Mech.*, vol. 46, pt. 1, pp. 83–110.

Braslow, A. L.; and Knox, E. C. 1958: *Simplified Method for Determination of Critical Height of Distributed Roughness Particles for Boundary-Layer Transition at Mach Numbers From 0 to 5.* NACA TN 4363.

Fox, Charles H., Jr.; and Huffman, Jarrett K. 1977: *Calibration and Test Capabilities of the Langley 7- by 10-Foot High Speed Tunnel.* NASA TM X-74027.

Kuhlman, John M.; Liaw, Paul; and Cerney, Michael J. 1988: *Theoretical/Numerical Study of Feasibility of Use of Winglets on Low Aspect Ratio Wings at Subsonic and Transonic Mach Numbers To Reduce Drag.* NASA CR-4174.

Kuhlman, John M.; and Brown, Christopher K. 1989: *Computational Design of Low Aspect Ratio Wing-Winglet Configurations for Transonic Wind-Tunnel Tests.* NASA CR-181939.

Lamar, John E.; and Herbert, Henry E. 1982: *Production Version of the Extended NASA/Langley Vortex Lattice FORTRAN Computer Program, Volume I—User's Guide.* NASA TM-83303.

Margason, Richard J.; and Lamar, John E. 1971: *Vortex-Lattice FORTRAN Program for Estimating Subsonic Aerodynamic Characteristics of Complex Planforms.* NASA TN D-6142.

Schaefer, William T., Jr. 1965: *Characteristics of Major Active Wind Tunnels at the Langley Research Center.* NASA TM X-1130.

Whitcomb, Richard T. 1976: *Design Approach and Selected Wind-Tunnel Results at High Subsonic Speeds for Wing-Tip Mounted Winglets.* NASA TN D-8260.

Table 1. Wing Coordinates for Baseline Model

Station 1						Station 2					
Upper surface			Lower surface			Upper surface			Lower surface		
x	y	z	x	y	z	x	y	z	x	y	z
17.4438	2.0614	−0.0430	17.4438	2.0616	−0.0422	18.3850	2.8731	−0.1216	18.3850	2.8747	−0.1314
17.4671	2.0712	−0.0168	17.4671	2.0766	−0.0677	18.4069	2.8661	−0.0759	18.4069	2.8783	−0.1551
17.5216	2.0896	0.0107	17.5216	2.1093	−0.0892	18.4580	2.8602	−0.0380	18.4580	2.8821	−0.1796
17.5605	2.0995	0.0266	17.5605	2.1307	−0.1007	18.4945	2.8573	−0.0187	18.4945	2.8836	−0.1893
17.6382	2.1107	0.0563	17.6382	2.1656	−0.1206	18.5676	2.8523	0.0133	18.5676	2.8855	−0.2022
17.8327	2.1182	0.1214	17.8327	2.2076	−0.1535	18.7501	2.8423	0.0781	18.7501	2.8880	−0.2182
18.2216	2.1123	0.2291	18.2216	2.2275	−0.1779	19.1152	2.8263	0.1818	19.1152	2.8892	−0.2258
18.6105	2.1016	0.3178	18.6105	2.2306	−0.1828	19.4803	2.8134	0.2657	19.4803	2.8889	−0.2240
18.9994	2.0892	0.3899	18.9994	2.2286	−0.1843	19.8454	2.8026	0.3352	19.8454	2.8886	−0.2217
19.3883	2.0760	0.4526	19.3883	2.2271	−0.1856	20.2105	2.7935	0.3943	20.2105	2.8881	−0.2187
19.7772	2.0628	0.5067	19.7772	2.2261	−0.1857	20.5756	2.7854	0.4462	20.5756	2.8875	−0.2146
20.1661	2.0504	0.5523	20.1661	2.2244	−0.1852	20.9407	2.7784	0.4918	20.9407	2.8869	−0.2106
20.5550	2.0390	0.5927	20.5550	2.2229	−0.1848	21.3058	2.7722	0.5318	21.3058	2.8863	−0.2066
20.9439	2.0287	0.6280	20.9439	2.2215	−0.1843	21.6709	2.7668	0.5665	21.6709	2.8856	−0.2024
21.3328	2.0191	0.6572	21.3328	2.2201	−0.1833	22.0360	2.7622	0.5966	22.0360	2.8849	−0.1980
22.1106	2.0054	0.7019	22.1106	2.2176	−0.1810	22.7662	2.7548	0.6445	22.7662	2.8835	−0.1887
22.8884	1.9985	0.7298	22.8884	2.2158	−0.1770	23.4964	2.7498	0.6768	23.4964	2.8819	−0.1783
23.6662	1.9990	0.7421	23.6662	2.2150	−0.1706	24.2266	2.7471	0.6943	24.2266	2.8799	−0.1656
24.4440	2.0077	0.7364	24.4440	2.2159	−0.1584	24.9568	2.7470	0.6952	24.9568	2.8771	−0.1477
25.2218	2.0223	0.7166	25.2218	2.2172	−0.1405	25.6871	2.7490	0.6821	25.6871	2.8737	−0.1252
25.9996	2.0412	0.6853	25.9996	2.2188	−0.1203	26.4173	2.7528	0.6578	26.4173	2.8700	−0.1013
26.7774	2.0635	0.6440	26.7774	2.2206	−0.0976	27.1475	2.7581	0.6230	27.1475	2.8661	−0.0758
27.5552	2.0876	0.5934	27.5552	2.2224	−0.0740	27.8777	2.7650	0.5787	27.8777	2.8621	−0.0500
28.3330	2.1135	0.5343	28.3330	2.2243	−0.0499	28.6079	2.7733	0.5252	28.6079	2.8582	−0.0247
29.1108	2.1395	0.4662	29.1108	2.2257	−0.0274	29.3381	2.7829	0.4630	29.3381	2.8546	−0.0015
29.8886	2.1654	0.3894	29.8886	2.2262	−0.0101	30.0683	2.7939	0.3916	30.0683	2.8519	0.0158
30.6664	2.1907	0.3018	30.6664	2.2259	−0.0031	30.7985	2.8064	0.3100	30.7985	2.8508	0.0227
31.4442	2.2119	0.2097	31.4442	2.2258	−0.0018	31.5287	2.8199	0.2233	31.5287	2.8507	0.0240
32.2220	2.2294	0.1184	32.2220	2.2260	−0.0006	32.2589	2.8333	0.1363	32.2589	2.8505	0.0250
32.9998	2.2422	0.0275	32.9998	2.2270	0.0071	32.9891	2.8464	0.0513	32.9891	2.8495	0.0316

Table 1. Continued

Station 3						Station 4					
Upper surface			Lower surface			Upper surface			Lower surface		
x	y	z	x	y	z	x	y	z	x	y	z
19.1372	3.5171	−0.1532	19.1372	3.5171	−0.1533	19.8894	4.1584	−0.1683	19.8894	4.1597	−0.1769
19.1580	3.5103	−0.1096	19.1580	3.5220	−0.1849	19.9090	4.1520	−0.1267	19.9090	4.1630	−0.1979
19.2064	3.5047	−0.0732	19.2064	3.5255	−0.2076	19.9548	4.1466	−0.0919	19.9548	4.1663	−0.2191
19.2410	3.5019	−0.0545	19.2410	3.5269	−0.2166	19.9875	4.1438	−0.0739	19.9875	4.1675	−0.2273
19.3102	3.4970	−0.0233	19.3102	3.5287	−0.2280	20.0529	4.1392	−0.0439	20.0529	4.1691	−0.2376
19.4833	3.4873	0.0398	19.4833	3.5308	−0.2415	20.2165	4.1297	0.0175	20.2165	4.1709	−0.2488
19.8294	3.4715	0.1417	19.8294	3.5313	−0.2453	20.5436	4.1143	0.1170	20.5436	4.1709	−0.2494
20.1754	3.4588	0.2246	20.1754	3.5305	−0.2403	20.8707	4.1018	0.1983	20.8707	4.1697	−0.2417
20.5215	3.4481	0.2937	20.5215	3.5297	−0.2349	21.1978	4.0913	0.2664	21.1978	4.1685	−0.2339
20.8676	3.4390	0.3529	20.8676	3.5288	−0.2291	21.5248	4.0823	0.3250	21.5248	4.1672	−0.2258
21.2137	3.4309	0.4049	21.2137	3.5277	−0.2223	21.8519	4.0742	0.3767	21.8519	4.1659	−0.2169
21.5597	3.4237	0.4512	21.5597	3.5267	−0.2156	22.1790	4.0671	0.4229	22.1790	4.1645	−0.2081
21.9058	3.4175	0.4919	21.9058	3.5257	−0.2090	22.5061	4.0608	0.4636	22.5061	4.1632	−0.1996
22.2519	3.4120	0.5275	22.2519	3.5247	−0.2023	22.8332	4.0553	0.4996	22.8332	4.1619	−0.1910
22.5980	3.4072	0.5587	22.5980	3.5236	−0.1955	23.1603	4.0503	0.5313	23.1603	4.1605	−0.1823
23.2901	3.3993	0.6092	23.2901	3.5215	−0.1817	23.8145	4.0423	0.5831	23.8145	4.1579	−0.1651
23.9823	3.3939	0.6445	23.9823	3.5192	−0.1670	24.4686	4.0366	0.6204	24.4686	4.1551	−0.1473
24.6744	3.3907	0.6655	24.6744	3.5166	−0.1504	25.1228	4.0329	0.6438	25.1228	4.1521	−0.1281
25.3665	3.3899	0.6703	25.3665	3.5134	−0.1292	25.7770	4.0318	0.6516	25.7770	4.1485	−0.1047
26.0587	3.3912	0.6616	26.0587	3.5095	−0.1043	26.4312	4.0326	0.6462	26.4312	4.1444	−0.0780
26.7509	3.3943	0.6419	26.7509	3.5055	−0.0782	27.0853	4.0351	0.6304	27.0853	4.1402	−0.0507
27.4430	3.3989	0.6119	27.4430	3.5013	−0.0511	27.7395	4.0391	0.6042	27.7395	4.1359	−0.0229
28.1351	3.4051	0.5724	28.1351	3.4971	−0.0241	28.3937	4.0445	0.5689	28.3937	4.1317	0.0046
28.8273	3.4126	0.5237	28.8273	3.4931	0.0020	29.0479	4.0514	0.5244	29.0479	4.1276	0.0307
29.5195	3.4215	0.4664	29.5195	3.4895	0.0256	29.7020	4.0596	0.4713	29.7020	4.1240	0.0541
30.2116	3.4317	0.3997	30.2116	3.4868	0.0428	30.3562	4.0692	0.4089	30.3562	4.1215	0.0709
30.9037	3.4437	0.3226	30.9037	3.4858	0.0496	31.0104	4.0805	0.3360	31.0104	4.1204	0.0773
31.5959	3.4563	0.2404	31.5959	3.4856	0.0506	31.6646	4.0926	0.2578	31.6646	4.1204	0.0777
32.2880	3.4691	0.1576	32.2880	3.4855	0.0513	32.3187	4.1047	0.1790	32.3187	4.1204	0.0776
32.9802	3.4819	0.0762	32.9802	3.4816	0.0766	32.9729	4.1168	0.1014	32.9729	4.1167	0.1018

Table 1. Continued

Station 5							Station 6					
Upper surface			Lower surface				Upper surface			Lower surface		
x	y	z	x	y	z		x	y	z	x	y	z
20.6416	4.7979	−0.1712	20.6416	4.7993	−0.1792		21.3938	5.4376	−0.1753	21.3938	5.4387	−0.1830
20.6601	4.7918	−0.1319	20.6601	4.8022	−0.1991		21.4111	5.4319	−0.1382	21.4111	5.4417	−0.2012
20.7032	4.7867	−0.0985	20.7032	4.8052	−0.2186		21.4516	5.4270	−0.1064	21.4516	5.4444	−0.2192
20.7340	4.7841	−0.0813	20.7340	4.8063	−0.2261		21.4805	5.4245	−0.0901	21.4805	5.4454	−0.2260
20.7957	4.7796	−0.0524	20.7957	4.8078	−0.2352		21.5384	5.4202	−0.0624	21.5384	5.4467	−0.2341
20.9497	4.7705	0.0068	20.9497	4.8092	−0.2444		21.6830	5.4114	−0.0053	21.6830	5.4479	−0.2415
21.2579	4.7555	0.1034	21.2579	4.8088	−0.2422		21.9721	5.3970	0.0880	21.9721	5.4471	−0.2368
21.5660	4.7433	0.1828	21.5660	4.8073	−0.2322		22.2613	5.3851	0.1649	22.2613	5.4453	−0.2251
21.8741	4.7330	0.2493	21.8741	4.8058	−0.2225		22.5505	5.3751	0.2299	22.5505	5.4435	−0.2137
22.1823	4.7241	0.3069	22.1823	4.8043	−0.2126		22.8396	5.3664	0.2860	22.8396	5.4417	−0.2022
22.4904	4.7162	0.3578	22.4904	4.8026	−0.2020		23.1288	5.3587	0.3360	23.1288	5.4399	−0.1900
22.7985	4.7092	0.4035	22.7985	4.8010	−0.1916		23.4180	5.3517	0.3809	23.4180	5.4381	−0.1782
23.1066	4.7029	0.4439	23.1066	4.7995	−0.1815		23.7071	5.3456	0.4209	23.7071	5.4363	−0.1668
23.4148	4.6973	0.4799	23.4148	4.7979	−0.1714		23.9963	5.3400	0.4564	23.9963	5.4345	−0.1555
23.7229	4.6925	0.5116	23.7229	4.7964	−0.1614		24.2855	5.3352	0.4880	24.2855	5.4328	−0.1442
24.3392	4.6844	0.5640	24.3392	4.7933	−0.1415		24.8638	5.3270	0.5408	24.8638	5.4294	−0.1219
24.9554	4.6785	0.6025	24.9554	4.7902	−0.1213		25.4421	5.3209	0.5802	25.4421	5.4260	−0.0998
25.5717	4.6746	0.6275	25.5717	4.7869	−0.1001		26.0205	5.3169	0.6067	26.0205	5.4224	−0.0768
26.1879	4.6731	0.6376	26.1879	4.7831	−0.0754		26.5988	5.3150	0.6189	26.5988	5.4184	−0.0507
26.8042	4.6734	0.6349	26.8042	4.7788	−0.0478		27.1772	5.3150	0.6190	27.1772	5.4140	−0.0221
27.4205	4.6753	0.6221	27.4205	4.7746	−0.0199		27.7555	5.3164	0.6093	27.7555	5.4096	0.0063
28.0367	4.6789	0.5993	28.0367	4.7702	0.0082		28.3338	5.3195	0.5901	28.3338	5.4052	0.0347
28.6530	4.6838	0.5674	28.6530	4.7660	0.0355		28.9122	5.3237	0.5620	28.9122	5.4010	0.0622
29.2692	4.6901	0.5268	29.2692	4.7621	0.0612		29.4905	5.3295	0.5253	29.4905	5.3970	0.0878
29.8855	4.6977	0.4775	29.8855	4.7585	0.0838		30.0688	5.3364	0.4803	30.0688	5.3935	0.1103
30.5018	4.7068	0.4189	30.5018	4.7560	0.1000		30.6472	5.3447	0.4262	30.6472	5.3911	0.1261
31.1180	4.7174	0.3501	31.1180	4.7552	0.1055		31.2255	5.3547	0.3619	31.2255	5.3902	0.1315
31.7343	4.7288	0.2758	31.7343	4.7552	0.1052		31.8038	5.3654	0.2922	31.8038	5.3903	0.1312
32.3505	4.7405	0.2007	32.3505	4.7554	0.1042		32.3822	5.3764	0.2216	32.3822	5.3905	0.1300
32.9668	4.7519	0.1269	32.9668	4.7518	0.1272		32.9605	5.3871	0.1522	32.9605	5.3870	0.1525

Table 1. Continued

Station 7							Station 8					
Upper surface			Lower surface				Upper surface			Lower surface		
x	y	z	x	y	z		x	y	z	x	y	z
22.1460	6.0757	−0.1691	22.1460	6.0758	−0.1691		22.8982	6.7126	−0.1547	22.8982	6.7136	−0.1614
22.1622	6.0704	−0.1343	22.1622	6.0795	−0.1932		22.9133	6.7075	−0.1222	22.9133	6.7161	−0.1770
22.2000	6.0657	−0.1042	22.2000	6.0820	−0.2097		22.9485	6.7032	−0.0938	22.9485	6.7183	−0.1921
22.2271	6.0633	−0.0885	22.2271	6.0830	−0.2159		22.9736	6.7009	−0.0790	22.9736	6.7192	−0.1976
22.2811	6.0592	−0.0621	22.2811	6.0840	−0.2229		23.0238	6.6971	−0.0539	23.0238	6.7201	−0.2036
22.4162	6.0508	−0.0076	22.4162	6.0849	−0.2287		23.1495	6.6890	−0.0020	23.1495	6.7208	−0.2078
22.6865	6.0370	0.0821	22.6865	6.0838	−0.2218		23.4008	6.6757	0.0839	23.4008	6.7195	−0.1992
22.9567	6.0255	0.1564	22.9567	6.0818	−0.2085		23.6521	6.6647	0.1552	23.6521	6.7172	−0.1847
23.2269	6.0158	0.2192	23.2269	6.0798	−0.1958		23.9035	6.6554	0.2157	23.9035	6.7150	−0.1708
23.4972	6.0074	0.2737	23.4972	6.0779	−0.1830		24.1548	6.6473	0.2683	24.1548	6.7129	−0.1569
23.7674	5.9999	0.3224	23.7674	6.0758	−0.1697		24.4061	6.6400	0.3155	24.4061	6.7107	−0.1428
24.0376	5.9931	0.3663	24.0376	6.0738	−0.1568		24.6574	6.6334	0.3581	24.6574	6.7086	−0.1290
24.3079	5.9870	0.4055	24.3079	6.0719	−0.1443		24.9087	6.6275	0.3962	24.9087	6.7066	−0.1156
24.5781	5.9816	0.4405	24.5781	6.0700	−0.1320		25.1600	6.6222	0.4305	25.1600	6.7045	−0.1025
24.8483	5.9768	0.4717	24.8483	6.0681	−0.1197		25.4113	6.6175	0.4611	25.4113	6.7025	−0.0895
25.3888	5.9686	0.5242	25.3888	6.0644	−0.0958		25.9140	6.6095	0.5128	25.9140	6.6986	−0.0644
25.9293	5.9625	0.5639	25.9293	6.0608	−0.0721		26.4166	6.6034	0.5524	26.4166	6.6948	−0.0395
26.4697	5.9583	0.5913	26.4697	6.0570	−0.0479		26.9192	6.5991	0.5805	26.9192	6.6910	−0.0145
27.0102	5.9562	0.6052	27.0102	6.0529	−0.0210		27.4219	6.5967	0.5955	27.4219	6.6867	0.0129
27.5507	5.9558	0.6076	27.5507	6.0484	0.0080		27.9245	6.5961	0.5996	27.9245	6.6823	0.0418
28.0911	5.9569	0.6005	28.0911	6.0440	0.0366		28.4271	6.5969	0.5949	28.4271	6.6779	0.0700
28.6316	5.9594	0.5842	28.6316	6.0396	0.0648		28.9298	6.5989	0.5811	28.9298	6.6737	0.0977
29.1720	5.9632	0.5594	29.1720	6.0354	0.0919		29.4324	6.6023	0.5593	29.4324	6.6696	0.1239
29.7125	5.9683	0.5264	29.7125	6.0316	0.1170		29.9350	6.6069	0.5294	29.9350	6.6658	0.1480
30.2530	5.9747	0.4851	30.2530	6.0282	0.1386		30.4377	6.6128	0.4915	30.4377	6.6627	0.1686
30.7934	5.9824	0.4350	30.7934	6.0259	0.1538		30.9403	6.6200	0.4450	30.9403	6.6605	0.1828
31.3339	5.9918	0.3748	31.3339	6.0251	0.1586		31.4429	6.6287	0.3888	31.4429	6.6599	0.1868
31.8744	6.0018	0.3094	31.8744	6.0253	0.1579		31.9455	6.6381	0.3272	31.9455	6.6601	0.1853
32.4148	6.0121	0.2430	32.4148	6.0255	0.1562		32.4482	6.6478	0.2647	32.4482	6.6605	0.1827
32.9553	6.0224	0.1774	32.9553	6.0222	0.1779		32.9508	6.6573	0.2030	32.9508	6.6573	0.2033

Table 1. Continued

Station 9						Station 10					
Upper surface			Lower surface			Upper surface			Lower surface		
x	y	z	x	y	z	x	y	z	x	y	z
23.6505	7.3506	−0.1478	23.6505	7.3517	−0.1540	24.4027	7.9863	−0.1261	24.4027	7.9872	−0.1319
23.6644	7.3460	−0.1174	23.6644	7.3538	−0.1685	24.4155	7.9820	−0.0980	24.4155	7.9893	−0.1449
23.6970	7.3419	−0.0909	23.6970	7.3559	−0.1820	24.4454	7.9782	−0.0734	24.4454	7.9912	−0.1571
23.7202	7.3396	−0.0770	23.7202	7.3566	−0.1869	24.4667	7.9762	−0.0603	24.4667	7.9918	−0.1614
23.7667	7.3360	−0.0534	23.7667	7.3575	−0.1920	24.5094	7.9727	−0.0381	24.5094	7.9925	−0.1657
23.8829	7.3285	−0.0042	23.8829	7.3579	−0.1949	24.6162	7.9656	0.0082	24.6162	7.9927	−0.1672
24.1152	7.3158	0.0776	24.1152	7.3563	−0.1845	24.8297	7.9537	0.0856	24.8297	7.9910	−0.1557
24.3476	7.3053	0.1457	24.3476	7.3538	−0.1690	25.0431	7.9437	0.1502	25.0431	7.9884	−0.1394
24.5800	7.2963	0.2037	24.5800	7.3516	−0.1542	25.2566	7.9352	0.2055	25.2566	7.9859	−0.1237
24.8124	7.2885	0.2544	24.8124	7.3493	−0.1394	25.4701	7.9276	0.2539	25.4701	7.9836	−0.1084
25.0448	7.2815	0.2999	25.0448	7.3470	−0.1245	25.6836	7.9210	0.2975	25.6836	7.9812	−0.0929
25.2771	7.2751	0.3411	25.2771	7.3447	−0.1098	25.8970	7.9149	0.3371	25.8970	7.9789	−0.0778
25.5095	7.2694	0.3782	25.5095	7.3426	−0.0957	26.1105	7.9093	0.3728	26.1105	7.9766	−0.0632
25.7419	7.2642	0.4116	25.7419	7.3404	−0.0819	26.3240	7.9043	0.4051	26.3240	7.9744	−0.0488
25.9743	7.2596	0.4416	25.9743	7.3383	−0.0681	26.5375	7.8998	0.4341	26.5375	7.9722	−0.0347
26.4390	7.2517	0.4927	26.4390	7.3342	−0.0416	26.9644	7.8921	0.4841	26.9644	7.9680	−0.0073
26.9038	7.2456	0.5323	26.9038	7.3302	−0.0157	27.3914	7.8861	0.5233	27.3914	7.9639	0.0193
27.3685	7.2412	0.5612	27.3685	7.3262	0.0104	27.8183	7.8816	0.5521	27.8183	7.9598	0.0458
27.8333	7.2386	0.5777	27.8333	7.3219	0.0385	28.2453	7.8789	0.5696	28.2453	7.9555	0.0738
28.2980	7.2376	0.5840	28.2980	7.3174	0.0677	28.6723	7.8777	0.5771	28.6723	7.9511	0.1027
28.7628	7.2379	0.5819	28.7628	7.3129	0.0961	29.0992	7.8779	0.5761	29.0992	7.9465	0.1314
29.2276	7.2396	0.5713	29.2276	7.3086	0.1237	29.5262	7.8791	0.5679	29.5262	7.9425	0.1581
29.6923	7.2424	0.5529	29.6923	7.3047	0.1497	29.9531	7.8815	0.5524	29.9531	7.9386	0.1829
30.1571	7.2464	0.5269	30.1571	7.3010	0.1734	30.3801	7.8852	0.5293	30.3801	7.9351	0.2053
30.6218	7.2517	0.4932	30.6218	7.2979	0.1938	30.8070	7.8898	0.4991	30.8070	7.9322	0.2242
31.0866	7.2582	0.4511	31.0866	7.2957	0.2076	31.2340	7.8958	0.4606	31.2340	7.9302	0.2369
31.5513	7.2661	0.3996	31.5513	7.2951	0.2118	31.6609	7.9031	0.4130	31.6609	7.9298	0.2401
32.0161	7.2748	0.3429	32.0161	7.2953	0.2105	32.0879	7.9111	0.3605	32.0879	7.9301	0.2380
32.4809	7.2837	0.2853	32.4809	7.2956	0.2082	32.5148	7.9195	0.3068	32.5148	7.9306	0.2347
32.9456	7.2926	0.2285	32.9456	7.2925	0.2287	32.9418	7.9278	0.2541	32.9418	7.9276	0.2542

Table 1. Continued

Station 11						Station 12					
Upper surface			Lower surface			Upper surface			Lower surface		
x	y	z	x	y	z	x	y	z	x	y	z
25.1549	8.6235	−0.1150	25.1549	8.6243	−0.1201	25.9071	9.2600	−0.0967	25.9071	9.2607	−0.1013
25.1666	8.6195	−0.0893	25.1666	8.6261	−0.1322	25.9176	9.2564	−0.0732	25.9176	9.2623	−0.1120
25.1938	8.6160	−0.0665	25.1938	8.6278	−0.1430	25.9422	9.2531	−0.0523	25.9422	9.2638	−0.1215
25.2133	8.6141	−0.0544	25.2133	8.6283	−0.1467	25.9598	9.2514	−0.0412	25.9598	9.2643	−0.1246
25.2522	8.6110	−0.0337	25.2522	8.6289	−0.1502	25.9949	9.2484	−0.0222	25.9949	9.2647	−0.1275
25.3495	8.6042	0.0096	25.3495	8.6289	−0.1505	26.0827	9.2423	0.0180	26.0827	9.2646	−0.1268
25.5440	8.5930	0.0822	25.5440	8.6271	−0.1380	26.2584	9.2318	0.0857	26.2584	9.2626	−0.1135
25.7386	8.5835	0.1433	25.7386	8.6244	−0.1211	26.4340	9.2230	0.1428	26.4340	9.2599	−0.0964
25.9331	8.5755	0.1956	25.9331	8.6219	−0.1049	26.6097	9.2153	0.1920	26.6097	9.2573	−0.0798
26.1277	8.5684	0.2417	26.1277	8.6194	−0.0891	26.7853	9.2086	0.2355	26.7853	9.2548	−0.0636
26.3222	8.5620	0.2834	26.3222	8.6170	−0.0730	26.9610	9.2026	0.2750	26.9610	9.2523	−0.0473
26.5168	8.5561	0.3213	26.5168	8.6146	−0.0574	27.1366	9.1970	0.3111	27.1366	9.2499	−0.0313
26.7113	8.5508	0.3557	26.7113	8.6122	−0.0422	27.3123	9.1919	0.3440	27.3123	9.2475	−0.0159
26.9059	8.5459	0.3870	26.9059	8.6099	−0.0274	27.4879	9.1873	0.3740	27.4879	9.2451	−0.0006
27.1004	8.5416	0.4152	27.1004	8.6077	−0.0127	27.6636	9.1830	0.4013	27.6636	9.2428	0.0143
27.4895	8.5340	0.4641	27.4895	8.6033	0.0156	28.0148	9.1757	0.4489	28.0148	9.2384	0.0434
27.8786	8.5281	0.5030	27.8786	8.5991	0.0431	28.3661	9.1697	0.4873	28.3661	9.2340	0.0716
28.2677	8.5235	0.5324	28.2677	8.5949	0.0704	28.7174	9.1652	0.5169	28.7174	9.2297	0.0991
28.6568	8.5205	0.5512	28.6568	8.5904	0.0988	29.0687	9.1621	0.5368	29.0687	9.2253	0.1278
29.0460	8.5191	0.5609	29.0460	8.5859	0.1279	29.4200	9.1604	0.5479	29.4200	9.2208	0.1567
29.4351	8.5187	0.5632	29.4351	8.5816	0.1556	29.7713	9.1599	0.5516	29.7713	9.2164	0.1851
29.8242	8.5195	0.5580	29.8242	8.5776	0.1821	30.1226	9.1602	0.5492	30.1226	9.2124	0.2109
30.2133	8.5214	0.5457	30.2133	8.5737	0.2069	30.4739	9.1616	0.5401	30.4739	9.2088	0.2349
30.6024	8.5244	0.5264	30.6024	8.5704	0.2291	30.8252	9.1641	0.5243	30.8252	9.2055	0.2562
30.9915	8.5285	0.5001	30.9915	8.5675	0.2477	31.1765	9.1675	0.5019	31.1765	9.2027	0.2741
31.3806	8.5337	0.4661	31.3806	8.5655	0.2604	31.5277	9.1721	0.4722	31.5277	9.2009	0.2861
31.7697	8.5403	0.4235	31.7697	8.5649	0.2640	31.8790	9.1779	0.4343	31.8790	9.2003	0.2896
32.1588	8.5476	0.3760	32.1588	8.5652	0.2626	32.2303	9.1845	0.3919	32.2303	9.2005	0.2883
32.5479	8.5552	0.3274	32.5479	8.5655	0.2600	32.5816	9.1913	0.3481	32.5816	9.2009	0.2857
32.9370	8.5623	0.2791	32.9370	8.5625	0.2796	32.9329	9.1978	0.3050	32.9329	9.1979	0.3051

Table 1. Continued

Station 13						Station 14					
Upper surface			Lower surface			Upper surface			Lower surface		
x	y	z	x	y	z	x	y	z	x	y	z
26.6593	9.8960	−0.0788	26.6593	9.8966	−0.0831	27.4115	10.5333	−0.0657	27.4115	10.5338	−0.0692
26.6687	9.8928	−0.0578	26.6687	9.8981	−0.0923	27.4198	10.5304	−0.0471	27.4198	10.5352	−0.0776
26.6906	9.8898	−0.0389	26.6906	9.8994	−0.1007	27.4391	10.5279	−0.0302	27.4391	10.5362	−0.0847
26.7063	9.8883	−0.0286	26.7063	9.8998	−0.1033	27.4529	10.5264	−0.0211	27.4529	10.5366	−0.0868
26.7377	9.8856	−0.0112	26.7377	9.9002	−0.1055	27.4804	10.5240	−0.0054	27.4804	10.5368	−0.0884
26.8160	9.8799	0.0256	26.8160	9.8999	−0.1039	27.5493	10.5189	0.0278	27.5493	10.5365	−0.0862
26.9728	9.8703	0.0878	26.9728	9.8978	−0.0903	27.6871	10.5102	0.0844	27.6871	10.5344	−0.0726
27.1295	9.8621	0.1408	27.1295	9.8951	−0.0731	27.8250	10.5027	0.1327	27.8250	10.5318	−0.0557
27.2863	9.8550	0.1867	27.2863	9.8926	−0.0565	27.9628	10.4962	0.1751	27.9628	10.5292	−0.0392
27.4430	9.8488	0.2274	27.4430	9.8900	−0.0401	28.1006	10.4903	0.2131	28.1006	10.5267	−0.0227
27.5997	9.8429	0.2647	27.5997	9.8875	−0.0235	28.2384	10.4849	0.2481	28.2384	10.5241	−0.0060
27.7565	9.8377	0.2990	27.7565	9.8850	−0.0074	28.3762	10.4799	0.2804	28.3762	10.5216	0.0104
27.9132	9.8329	0.3303	27.9132	9.8826	0.0084	28.5140	10.4753	0.3101	28.5140	10.5191	0.0264
28.0699	9.8284	0.3590	28.0699	9.8802	0.0241	28.6518	10.4710	0.3376	28.6518	10.5167	0.0423
28.2267	9.8243	0.3854	28.2267	9.8778	0.0393	28.7897	10.4672	0.3629	28.7897	10.5143	0.0580
28.5401	9.8172	0.4315	28.5401	9.8733	0.0690	29.0653	10.4602	0.4080	29.0653	10.5095	0.0885
28.8536	9.8113	0.4695	28.8536	9.8687	0.0978	29.3409	10.4543	0.4456	29.3409	10.5049	0.1179
29.1671	9.8068	0.4993	29.1671	9.8644	0.1258	29.6165	10.4496	0.4760	29.6165	10.5005	0.1468
29.4806	9.8035	0.5201	29.4806	9.8600	0.1546	29.8922	10.4462	0.4982	29.8922	10.4960	0.1761
29.7941	9.8015	0.5331	29.7941	9.8555	0.1835	30.1678	10.4439	0.5133	30.1678	10.4915	0.2051
30.1075	9.8006	0.5390	30.1075	9.8512	0.2115	30.4434	10.4424	0.5226	30.4434	10.4873	0.2320
30.4210	9.8006	0.5393	30.4210	9.8473	0.2369	30.7191	10.4420	0.5259	30.7191	10.4834	0.2574
30.7345	9.8015	0.5334	30.7345	9.8437	0.2603	30.9947	10.4424	0.5233	30.9947	10.4798	0.2807
31.0480	9.8033	0.5211	31.0480	9.8404	0.2811	31.2703	10.4437	0.5148	31.2703	10.4766	0.3013
31.3614	9.8062	0.5027	31.3614	9.8378	0.2983	31.5460	10.4458	0.5006	31.5460	10.4739	0.3186
31.6749	9.8101	0.4774	31.6749	9.8359	0.3101	31.8216	10.4491	0.4802	31.8216	10.4721	0.3308
31.9884	9.8152	0.4444	31.9884	9.8354	0.3139	32.0972	10.4532	0.4528	32.0972	10.4713	0.3358
32.3018	9.8210	0.4072	32.3018	9.8355	0.3131	32.3728	10.4581	0.4214	32.3728	10.4712	0.3364
32.6153	9.8270	0.3686	32.6153	9.8359	0.3110	32.6485	10.4632	0.3886	32.6485	10.4714	0.3356
32.9288	9.8327	0.3302	32.9288	9.8328	0.3304	32.9241	10.4684	0.3556	32.9241	10.4682	0.3559

Table 1. Concluded

Station 15						Station 16					
Upper surface			Lower surface			Upper surface			Lower surface		
x	y	z	x	y	z	x	y	z	x	y	z
28.1637	11.1708	−0.0567	28.1637	11.1713	−0.0598	29.1556	12.0000	−0.0089	29.1556	12.0000	−0.0178
28.1708	11.1683	−0.0405	28.1708	11.1723	−0.0669	29.1612	12.0000	0.0003	29.1612	12.0000	−0.0192
28.1875	11.1660	−0.0257	28.1875	11.1732	−0.0729	29.1744	12.0000	0.0132	29.1744	12.0000	−0.0217
28.1994	11.1648	−0.0177	28.1994	11.1736	−0.0745	29.1838	12.0000	0.0195	29.1838	12.0000	−0.0229
28.2231	11.1626	−0.0038	28.2231	11.1737	−0.0756	29.2026	12.0000	0.0301	29.2026	12.0000	−0.0234
28.2826	11.1580	0.0255	28.2826	11.1733	−0.0731	29.2496	12.0000	0.0529	29.2496	12.0000	−0.0205
28.4015	11.1503	0.0758	28.4015	11.1712	−0.0600	29.3436	12.0000	0.0925	29.3436	12.0000	−0.0086
28.5204	11.1436	0.1193	28.5204	11.1687	−0.0437	29.4376	12.0000	0.1275	29.4376	12.0000	0.0055
28.6392	11.1376	0.1580	28.6392	11.1662	−0.0275	29.5316	12.0000	0.1589	29.5316	12.0000	0.0206
28.7581	11.1322	0.1931	28.7581	11.1637	−0.0110	29.6256	12.0000	0.1886	29.6256	12.0000	0.0357
28.8770	11.1271	0.2256	28.8770	11.1611	0.0057	29.7196	12.0000	0.2165	29.7196	12.0000	0.0508
28.9959	11.1224	0.2560	28.9959	11.1586	0.0223	29.8136	12.0000	0.2425	29.8136	12.0000	0.0661
29.1148	11.1181	0.2843	29.1148	11.1561	0.0386	29.9076	12.0000	0.2673	29.9076	12.0000	0.0814
29.2337	11.1140	0.3106	29.2337	11.1536	0.0549	30.0016	12.0000	0.2908	30.0016	12.0000	0.0967
29.3526	11.1103	0.3352	29.3526	11.1511	0.0710	30.0956	12.0000	0.3129	30.0956	12.0000	0.1119
29.5903	11.1035	0.3791	29.5903	11.1462	0.1024	30.2837	12.0000	0.3533	30.2837	12.0000	0.1420
29.8281	11.0977	0.4166	29.8281	11.1415	0.1329	30.4717	12.0000	0.3891	30.4717	12.0000	0.1712
30.0659	11.0929	0.4475	30.0659	11.1369	0.1626	30.6597	12.0000	0.4197	30.6597	12.0000	0.1996
30.3036	11.0893	0.4712	30.3036	11.1323	0.1924	30.8477	12.0000	0.4444	30.8477	12.0000	0.2279
30.5414	11.0866	0.4883	30.5414	11.1278	0.2218	31.0357	12.0000	0.4637	31.0357	12.0000	0.2557
30.7792	11.0847	0.5005	30.7792	11.1236	0.2488	31.2237	12.0000	0.4786	31.2237	12.0000	0.2816
31.0169	11.0837	0.5070	31.0169	11.1196	0.2743	31.4117	12.0000	0.4890	31.4117	12.0000	0.3054
31.2547	11.0836	0.5081	31.2547	11.1161	0.2976	31.5997	12.0000	0.4946	31.5997	12.0000	0.3273
31.4925	11.0842	0.5040	31.4925	11.1129	0.3183	31.7877	12.0000	0.4957	31.7877	12.0000	0.3474
31.7303	11.0856	0.4945	31.7303	11.1101	0.3359	31.9758	12.0000	0.4921	31.9758	12.0000	0.3643
31.9680	11.0880	0.4795	31.9680	11.1082	0.3487	32.1638	12.0000	0.4836	32.1638	12.0000	0.3777
32.2058	11.0912	0.4586	32.2058	11.1071	0.3555	32.3518	12.0000	0.4708	32.3518	12.0000	0.3854
32.4436	11.0951	0.4338	32.4436	11.1067	0.3582	32.5398	12.0000	0.4542	32.5398	12.0000	0.3899
32.6813	11.0991	0.4077	32.6813	11.1065	0.3595	32.7278	12.0000	0.4338	32.7278	12.0000	0.3937
32.9191	11.1031	0.3811	32.9191	11.1031	0.3813	32.9158	12.0000	0.4093	32.9158	12.0000	0.4167

Table 2. Wing and Winglet Coordinates for Winglet Model

Station 1						Station 2					
Upper surface			Lower surface			Upper surface			Lower surface		
x	y	z	x	y	z	x	y	z	x	y	z
17.4531	2.0707	−0.0885	17.4531	2.0778	−0.0743	19.3468	3.6847	−0.2054	19.3468	3.6858	−0.2143
17.4764	2.0862	−0.0776	17.4764	2.0911	−0.0893	19.3672	3.6795	−0.1616	19.3672	3.6884	−0.2362
17.5308	2.1185	−0.0527	17.5308	2.1195	−0.1210	19.4149	3.6751	−0.1253	19.4149	3.6910	−0.2585
17.5696	2.1342	−0.0350	17.5696	2.1378	−0.1398	19.4489	3.6729	−0.1066	19.4489	3.6920	−0.2671
17.6472	2.1425	0.0000	17.6472	2.1702	−0.1626	19.5170	3.6692	−0.0752	19.5170	3.6934	−0.2780
17.8414	2.1529	0.0693	17.8414	2.2191	−0.1932	19.6872	3.6617	−0.0115	19.6872	3.6948	−0.2903
18.2297	2.1624	0.1715	18.2297	2.2442	−0.2227	20.0276	3.6493	0.0918	20.0276	3.6949	−0.2915
18.6180	2.1520	0.2581	18.6180	2.2476	−0.2313	20.3680	3.6392	0.1767	20.3680	3.6940	−0.2838
19.0064	2.1401	0.3310	19.0064	2.2475	−0.2367	20.7084	3.6306	0.2484	20.7084	3.6930	−0.2753
19.3947	2.1305	0.3910	19.3947	2.2442	−0.2396	21.0488	3.6232	0.3104	21.0488	3.6919	−0.2660
19.7830	2.1210	0.4433	19.7830	2.2398	−0.2422	21.3893	3.6167	0.3657	21.3893	3.6906	−0.2556
20.1713	2.1118	0.4882	20.1713	2.2354	−0.2444	21.7297	3.6108	0.4154	21.7297	3.6894	−0.2450
20.5596	2.1032	0.5261	20.5596	2.2323	−0.2462	22.0701	3.6054	0.4599	22.0701	3.6881	−0.2343
20.9479	2.0956	0.5588	20.9479	2.2308	−0.2472	22.4105	3.6008	0.4996	22.4105	3.6868	−0.2233
21.3362	2.0893	0.5878	21.3362	2.2296	−0.2477	22.7509	3.5965	0.5349	22.7509	3.6855	−0.2121
22.1129	2.0792	0.6320	22.1129	2.2279	−0.2476	23.4317	3.5895	0.5944	23.4317	3.6828	−0.1888
22.8895	2.0736	0.6597	22.8895	2.2269	−0.2454	24.1125	3.5840	0.6396	24.1125	3.6798	−0.1641
23.6661	2.0750	0.6719	23.6661	2.2262	−0.2393	24.7933	3.5803	0.6712	24.7933	3.6766	−0.1370
24.4428	2.0834	0.6684	24.4428	2.2263	−0.2274	25.4741	3.5784	0.6874	25.4741	3.6727	−0.1047
25.2194	2.0982	0.6518	25.2194	2.2275	−0.2088	26.1550	3.5779	0.6908	26.1550	3.6684	−0.0678
25.9960	2.1169	0.6239	25.9960	2.2301	−0.1859	26.8358	3.5788	0.6841	26.8358	3.6637	−0.0294
26.7727	2.1384	0.5867	26.7727	2.2327	−0.1607	27.5166	3.5807	0.6677	27.5166	3.6589	0.0108
27.5493	2.1629	0.5401	27.5493	2.2352	−0.1331	28.1974	3.5837	0.6426	28.1974	3.6541	0.0515
28.3259	2.1879	0.4860	28.3259	2.2376	−0.1053	28.8782	3.5876	0.6092	28.8782	3.6493	0.0920
29.1026	2.2140	0.4258	29.1026	2.2392	−0.0785	29.5590	3.5926	0.5679	29.5590	3.6446	0.1308
29.8792	2.2400	0.3555	29.8792	2.2400	−0.0534	30.2398	3.5985	0.5183	30.2398	3.6407	0.1644
30.6558	2.2633	0.2748	30.6558	2.2405	−0.0363	30.9207	3.6055	0.4594	30.9207	3.6377	0.1885
31.4324	2.2841	0.1934	31.4324	2.2408	−0.0286	31.6015	3.6130	0.3961	31.6015	3.6355	0.2078
32.2091	2.3033	0.1116	32.2091	2.2408	−0.0188	32.2823	3.6206	0.3326	32.2823	3.6332	0.2270
32.9857	2.3207	0.0296	32.9857	2.2408	−0.0019	32.9631	3.6280	0.2710	32.9631	3.6280	0.2710

Table 2. Continued

Station 3					
Upper surface			Lower surface		
x	y	z	x	y	z
21.0779	5.1514	−0.2383	21.0779	5.1523	−0.2461
21.0957	5.1468	−0.1998	21.0957	5.1546	−0.2649
21.1373	5.1429	−0.1671	21.1373	5.1567	−0.2836
21.1669	5.1409	−0.1502	21.1669	5.1576	−0.2906
21.2263	5.1375	−0.1217	21.2263	5.1586	−0.2991
21.3747	5.1305	−0.0631	21.3747	5.1595	−0.3069
21.6716	5.1190	0.0330	21.6716	5.1590	−0.3024
21.9684	5.1096	0.1126	21.9684	5.1575	−0.2902
22.2652	5.1016	0.1800	22.2652	5.1560	−0.2779
22.5620	5.0945	0.2388	22.5620	5.1545	−0.2652
22.8589	5.0882	0.2915	22.8589	5.1529	−0.2517
23.1557	5.0826	0.3391	23.1557	5.1513	−0.2383
23.4525	5.0775	0.3818	23.4525	5.1497	−0.2249
23.7494	5.0730	0.4204	23.7494	5.1481	−0.2115
24.0462	5.0688	0.4549	24.0462	5.1465	−0.1980
24.6399	5.0618	0.5137	24.6399	5.1433	−0.1708
25.2335	5.0564	0.5595	25.2335	5.1399	−0.1428
25.8272	5.0523	0.5926	25.8272	5.1364	−0.1133
26.4208	5.0500	0.6122	26.4208	5.1324	−0.0797
27.0145	5.0490	0.6204	27.0145	5.1282	−0.0438
27.6082	5.0492	0.6185	27.6082	5.1237	−0.0061
28.2018	5.0506	0.6077	28.2018	5.1191	0.0325
28.7955	5.0529	0.5886	28.7955	5.1145	0.0709
29.3891	5.0561	0.5616	29.3891	5.1101	0.1085
29.9828	5.0602	0.5269	29.9828	5.1059	0.1437
30.5765	5.0653	0.4842	30.5765	5.1023	0.1734
31.1701	5.0715	0.4321	31.1701	5.0999	0.1937
31.7638	5.0783	0.3756	31.7638	5.0981	0.2091
32.3574	5.0850	0.3188	32.3574	5.0962	0.2243
32.9511	5.0916	0.2630	32.9511	5.0916	0.2635

Station 4					
Upper surface			Lower surface		
x	y	z	x	y	z
21.9435	5.8832	−0.2414	21.9435	5.8841	−0.2488
21.9600	5.8789	−0.2054	21.9600	5.8861	−0.2659
21.9985	5.8752	−0.1747	21.9985	5.8881	−0.2829
22.0260	5.8733	−0.1587	22.0260	5.8889	−0.2892
22.0810	5.8701	−0.1317	22.0810	5.8897	−0.2964
22.2186	5.8634	−0.0760	22.2186	5.8904	−0.3024
22.4937	5.8526	0.0158	22.4937	5.8896	−0.2955
22.7687	5.8435	0.0920	22.7687	5.8879	−0.2818
23.0438	5.8358	0.1568	23.0438	5.8863	−0.2682
23.3189	5.8290	0.2134	23.3189	5.8847	−0.2544
23.5939	5.8230	0.2642	23.5939	5.8829	−0.2399
23.8690	5.8175	0.3101	23.8690	5.8812	−0.2256
24.1441	5.8125	0.3516	24.1441	5.8796	−0.2115
24.4192	5.8081	0.3889	24.4192	5.8779	−0.1973
24.6942	5.8041	0.4225	24.6942	5.8762	−0.1831
25.2444	5.7972	0.4799	25.2444	5.8728	−0.1550
25.7946	5.7919	0.5249	25.7946	5.8694	−0.1264
26.3447	5.7879	0.5581	26.3447	5.8659	−0.0965
26.8949	5.7855	0.5782	26.8949	5.8619	−0.0633
27.4450	5.7843	0.5879	27.4450	5.8578	−0.0281
27.9951	5.7844	0.5879	27.9951	5.8534	0.0085
28.5453	5.7854	0.5791	28.5453	5.8490	0.0455
29.0954	5.7874	0.5626	29.0954	5.8446	0.0821
29.6456	5.7903	0.5384	29.6456	5.8404	0.1178
30.1958	5.7940	0.5068	30.1958	5.8365	0.1508
30.7459	5.7988	0.4671	30.7459	5.8332	0.1784
31.2961	5.8045	0.4184	31.2961	5.8310	0.1965
31.8462	5.8109	0.3653	31.8462	5.8294	0.2099
32.3963	5.8173	0.3118	32.3963	5.8279	0.2230
32.9465	5.8235	0.2593	32.9465	5.8235	0.2599

Table 2. Continued

Station 5							Station 6					
Upper surface			Lower surface				Upper surface			Lower surface		
x	y	z	x	y	z		x	y	z	x	y	z
22.8091	6.6140	−0.2360	22.8091	6.6147	−0.2426		23.6747	7.3446	−0.2290	23.6747	7.3454	−0.2349
22.8243	6.6100	−0.2027	22.8243	6.6167	−0.2584		23.6886	7.3409	−0.1983	23.6886	7.3470	−0.2495
22.8598	6.6066	−0.1740	22.8598	6.6185	−0.2738		23.7210	7.3378	−0.1717	23.7210	7.3486	−0.2631
22.8851	6.6048	−0.1590	22.8851	6.6191	−0.2793		23.7442	7.3360	−0.1577	23.7442	7.3492	−0.2679
22.9358	6.6018	−0.1335	22.9358	6.6199	−0.2855		23.7905	7.3332	−0.1340	23.7905	7.3498	−0.2731
23.0624	6.5955	−0.0809	23.0624	6.6203	−0.2897		23.9063	7.3274	−0.0845	23.9063	7.3501	−0.2757
23.3158	6.5851	0.0063	23.3158	6.6193	−0.2809		24.1379	7.3175	−0.0023	24.1379	7.3488	−0.2652
23.5691	6.5764	0.0789	23.5691	6.6175	−0.2659		24.3695	7.3093	0.0664	24.3695	7.3469	−0.2493
23.8225	6.5691	0.1407	23.8225	6.6157	−0.2513		24.6012	7.3024	0.1250	24.6012	7.3451	−0.2339
24.0758	6.5627	0.1948	24.0758	6.6140	−0.2366		24.8328	7.2963	0.1764	24.8328	7.3433	−0.2185
24.3291	6.5569	0.2434	24.3291	6.6122	−0.2213		25.0644	7.2908	0.2226	25.0644	7.3414	−0.2029
24.5825	6.5516	0.2875	24.5825	6.6104	−0.2065		25.2960	7.2857	0.2646	25.2960	7.3396	−0.1876
24.8358	6.5468	0.3273	24.8358	6.6087	−0.1919		25.5276	7.2813	0.3025	25.5276	7.3378	−0.1726
25.0892	6.5426	0.3632	25.0892	6.6069	−0.1774		25.7592	7.2772	0.3368	25.7592	7.3361	−0.1579
25.3425	6.5387	0.3955	25.3425	6.6052	−0.1629		25.9908	7.2734	0.3678	25.9908	7.3343	−0.1432
25.8492	6.5321	0.4511	25.8492	6.6018	−0.1342		26.4540	7.2671	0.4212	26.4540	7.3309	−0.1145
26.3559	6.5269	0.4949	26.3559	6.5984	−0.1054		26.9173	7.2621	0.4635	26.9173	7.3275	−0.0857
26.8626	6.5230	0.5275	26.8626	6.5949	−0.0759		27.3805	7.2582	0.4955	27.3805	7.3240	−0.0566
27.3693	6.5206	0.5477	27.3693	6.5910	−0.0433		27.8437	7.2559	0.5158	27.8437	7.3202	−0.0249
27.8759	6.5194	0.5574	27.8759	6.5869	−0.0085		28.3069	7.2546	0.5262	28.3069	7.3163	0.0086
28.3826	6.5192	0.5588	28.3826	6.5827	0.0264		28.7702	7.2543	0.5290	28.7702	7.3123	0.0418
28.8893	6.5201	0.5520	28.8893	6.5785	0.0615		29.2334	7.2548	0.5240	29.2334	7.3083	0.0750
29.3960	6.5217	0.5376	29.3960	6.5744	0.0959		29.6966	7.2563	0.5118	29.6966	7.3045	0.1073
29.9027	6.5244	0.5160	29.9027	6.5705	0.1289		30.1599	7.2586	0.4927	30.1599	7.3008	0.1381
30.4094	6.5278	0.4872	30.4094	6.5669	0.1595		30.6231	7.2617	0.4667	30.6231	7.2975	0.1663
30.9161	6.5321	0.4506	30.9161	6.5639	0.1845		31.0863	7.2657	0.4332	31.0863	7.2948	0.1889
31.4227	6.5376	0.4053	31.4227	6.5620	0.2003		31.5495	7.2707	0.3912	31.5495	7.2932	0.2027
31.9294	6.5435	0.3553	31.9294	6.5606	0.2114		32.0127	7.2762	0.3448	32.0127	7.2921	0.2119
32.4361	6.5495	0.3050	32.4361	6.5594	0.2220		32.4760	7.2818	0.2980	32.4760	7.2910	0.2205
32.9428	6.5554	0.2561	32.9428	6.5553	0.2563		32.9392	7.2873	0.2523	32.9392	7.2872	0.2526

Table 2. Continued

Station 7						Station 8					
Upper surface			Lower surface			Upper surface			Lower surface		
x	y	z	x	y	z	x	y	z	x	y	z
24.5403	8.0743	−0.2150	24.5403	8.0750	−0.2206	25.4059	8.8036	−0.1966	25.4059	8.8042	−0.2016
24.5529	8.0710	−0.1870	24.5529	8.0765	−0.2334	25.4172	8.8006	−0.1713	25.4172	8.8055	−0.2131
24.5823	8.0681	−0.1626	24.5823	8.0780	−0.2455	25.4435	8.7979	−0.1490	25.4435	8.8068	−0.2235
24.6033	8.0666	−0.1496	24.6033	8.0784	−0.2496	25.4624	8.7965	−0.1371	25.4624	8.8072	−0.2270
24.6452	8.0639	−0.1275	24.6452	8.0790	−0.2539	25.5000	8.7941	−0.1168	25.5000	8.8076	−0.2304
24.7502	8.0584	−0.0814	24.7502	8.0791	−0.2550	25.5941	8.7889	−0.0742	25.5941	8.8076	−0.2302
24.9601	8.0492	−0.0043	24.9601	8.0776	−0.2432	25.7823	8.7805	−0.0027	25.7823	8.8060	−0.2173
25.1700	8.0416	0.0601	25.1700	8.0757	−0.2266	25.9705	8.7733	0.0573	25.9705	8.8039	−0.2001
25.3799	8.0350	0.1152	25.3799	8.0738	−0.2106	26.1587	8.7672	0.1086	26.1587	8.8020	−0.1839
25.5898	8.0292	0.1635	25.5898	8.0719	−0.1949	26.3469	8.7618	0.1538	26.3469	8.8001	−0.1681
25.7997	8.0240	0.2072	25.7997	8.0700	−0.1790	26.5351	8.7570	0.1946	26.5351	8.7983	−0.1522
26.0096	8.0194	0.2468	26.0096	8.0682	−0.1635	26.7233	8.7526	0.2317	26.7233	8.7964	−0.1367
26.2195	8.0151	0.2827	26.2195	8.0664	−0.1485	26.9115	8.7485	0.2654	26.9115	8.7946	−0.1217
26.4294	8.0112	0.3152	26.4294	8.0646	−0.1337	27.0997	8.7449	0.2959	27.0997	8.7929	−0.1070
26.6393	8.0077	0.3446	26.6393	8.0629	−0.1190	27.2879	8.7416	0.3236	27.2879	8.7912	−0.0926
27.0591	8.0016	0.3955	27.0591	8.0595	−0.0905	27.6643	8.7359	0.3716	27.6643	8.7878	−0.0646
27.4789	7.9968	0.4360	27.4789	8.0561	−0.0623	28.0407	8.7313	0.4101	28.0407	8.7846	−0.0371
27.8987	7.9931	0.4667	27.8987	8.0528	−0.0339	28.4171	8.7278	0.4395	28.4171	8.7813	−0.0097
28.3185	7.9907	0.4869	28.3185	8.0491	−0.0034	28.7935	8.7255	0.4591	28.7935	8.7779	0.0192
28.7384	7.9894	0.4987	28.7384	8.0454	0.0275	29.1700	8.7242	0.4700	29.1700	8.7743	0.0492
29.1582	7.9889	0.5023	29.1582	8.0417	0.0588	29.5464	8.7237	0.4736	29.5464	8.7708	0.0793
29.5780	7.9893	0.4985	29.5780	8.0380	0.0898	29.9228	8.7240	0.4715	29.9228	8.7673	0.1075
29.9978	7.9905	0.4882	29.9978	8.0344	0.1198	30.2992	8.7250	0.4630	30.2992	8.7641	0.1347
30.4176	7.9926	0.4711	30.4176	8.0310	0.1481	30.6756	8.7268	0.4482	30.6756	8.7611	0.1600
30.8374	7.9954	0.4476	30.8374	8.0280	0.1736	31.0520	8.7293	0.4273	31.0520	8.7584	0.1826
31.2572	7.9990	0.4169	31.2572	8.0256	0.1937	31.4284	8.7325	0.3995	31.4284	8.7564	0.1998
31.6770	8.0037	0.3779	31.6770	8.0243	0.2054	31.8048	8.7368	0.3638	31.8048	8.7552	0.2089
32.0968	8.0088	0.3348	32.0968	8.0234	0.2125	32.1812	8.7416	0.3242	32.1812	8.7547	0.2137
32.5166	8.0140	0.2913	32.5166	8.0226	0.2193	32.5576	8.7463	0.2841	32.5576	8.7542	0.2181
32.9364	8.0192	0.2484	32.9364	8.0190	0.2491	32.9340	8.7508	0.2457	32.9340	8.7509	0.2455

Table 2. Continued

Station 9						Station 10					
Upper surface			Lower surface			Upper surface			Lower surface		
x	y	z	x	y	z	x	y	z	x	y	z
26.2715	9.5319	−0.1729	26.2715	9.5324	−0.1772	27.1371	10.2594	−0.1378	27.1371	10.2599	−0.1416
26.2815	9.5293	−0.1503	26.2815	9.5337	−0.1874	27.1458	10.2570	−0.1179	27.1458	10.2609	−0.1502
26.3048	9.5269	−0.1302	26.3048	9.5347	−0.1963	27.1661	10.2549	−0.1001	27.1661	10.2618	−0.1577
26.3215	9.5255	−0.1195	26.3215	9.5351	−0.1992	27.1806	10.2538	−0.0905	27.1806	10.2621	−0.1599
26.3548	9.5234	−0.1011	26.3548	9.5354	−0.2017	27.2095	10.2518	−0.0739	27.2095	10.2623	−0.1617
26.4380	9.5187	−0.0621	26.4380	9.5352	−0.2005	27.2820	10.2476	−0.0388	27.2820	10.2620	−0.1596
26.6045	9.5109	0.0036	26.6045	9.5335	−0.1868	27.4268	10.2406	0.0207	27.4268	10.2603	−0.1453
26.7711	9.5043	0.0589	26.7711	9.5315	−0.1694	27.5717	10.2346	0.0709	27.5717	10.2583	−0.1281
26.9376	9.4986	0.1063	26.9376	9.5296	−0.1531	27.7166	10.2295	0.1140	27.7166	10.2564	−0.1121
27.1041	9.4937	0.1480	27.1041	9.5277	−0.1373	27.8614	10.2248	0.1521	27.8614	10.2545	−0.0967
27.2706	9.4892	0.1858	27.2706	9.5258	−0.1216	28.0063	10.2208	0.1865	28.0063	10.2527	−0.0814
27.4371	9.4851	0.2202	27.4371	9.5240	−0.1063	28.1512	10.2171	0.2180	28.1512	10.2510	−0.0666
27.6036	9.4813	0.2514	27.6036	9.5223	−0.0917	28.2960	10.2137	0.2466	28.2960	10.2493	−0.0524
27.7702	9.4780	0.2798	27.7702	9.5205	−0.0772	28.4409	10.2105	0.2726	28.4409	10.2476	−0.0385
27.9367	9.4749	0.3056	27.9367	9.5189	−0.0631	28.5858	10.2077	0.2963	28.5858	10.2460	−0.0250
28.2697	9.4696	0.3504	28.2697	9.5156	−0.0359	28.8755	10.2028	0.3376	28.8755	10.2429	0.0010
28.6028	9.4653	0.3866	28.6028	9.5125	−0.0095	29.1652	10.1988	0.3709	29.1652	10.2400	0.0260
28.9358	9.4619	0.4144	28.9358	9.5094	0.0166	29.4549	10.1957	0.3966	29.4549	10.2371	0.0504
29.2688	9.4598	0.4332	29.2688	9.5062	0.0438	29.7447	10.1937	0.4141	29.7447	10.2340	0.0753
29.6019	9.4584	0.4443	29.6019	9.5028	0.0716	30.0344	10.1925	0.4245	30.0344	10.2310	0.1003
29.9349	9.4579	0.4493	29.9349	9.4997	0.0982	30.3241	10.1918	0.4293	30.3241	10.2283	0.1237
30.2679	9.4580	0.4479	30.2679	9.4966	0.1239	30.6139	10.1920	0.4282	30.6139	10.2256	0.1459
30.6010	9.4589	0.4407	30.6010	9.4937	0.1483	30.9036	10.1928	0.4215	30.9036	10.2232	0.1666
30.9340	9.4604	0.4276	30.9340	9.4910	0.1706	31.1933	10.1942	0.4094	31.1933	10.2209	0.1850
31.2670	9.4626	0.4087	31.2670	9.4887	0.1902	31.4830	10.1963	0.3919	31.4830	10.2191	0.2007
31.6001	9.4657	0.3834	31.6001	9.4869	0.2046	31.7728	10.1991	0.3683	31.7728	10.2178	0.2115
31.9331	9.4695	0.3507	31.9331	9.4862	0.2115	32.0625	10.2028	0.3381	32.0625	10.2173	0.2155
32.2661	9.4739	0.3142	32.2661	9.4858	0.2144	32.3522	10.2068	0.3046	32.3522	10.2173	0.2157
32.5992	9.4783	0.2773	32.5992	9.4855	0.2168	32.6420	10.2107	0.2708	32.6420	10.2174	0.2158
32.9322	9.4825	0.2417	32.9322	9.4825	0.2420	32.9317	10.2145	0.2382	32.9317	10.2146	0.2386

Table 2. Continued

Station 11						Winglet station 1					
Upper surface			Lower surface			Outboard surface			Inboard surface		
x	y	z	x	y	z	x	y	z	x	y	z
28.0027	10.9830	−0.0736	28.0027	10.9834	−0.0768	31.7077	12.3346	1.1161	31.7077	12.3324	1.1163
28.0101	10.9809	−0.0560	28.0101	10.9842	−0.0838	31.7103	12.3382	1.1155	31.7103	12.3288	1.1169
28.0273	10.9790	−0.0401	28.0273	10.9849	−0.0897	31.7163	12.3397	1.1154	31.7163	12.3230	1.1177
28.0396	10.9779	−0.0315	28.0396	10.9851	−0.0912	31.7206	12.3398	1.1153	31.7206	12.3196	1.1182
28.0643	10.9762	−0.0165	28.0643	10.9851	−0.0919	31.7291	12.3393	1.1154	31.7291	12.3138	1.1190
28.1258	10.9724	0.0157	28.1258	10.9846	−0.0879	31.7505	12.3361	1.1159	31.7505	12.3011	1.1210
28.2490	10.9658	0.0710	28.2490	10.9827	−0.0715	31.7934	12.3269	1.1172	31.7934	12.2788	1.1242
28.3721	10.9602	0.1180	28.3721	10.9805	−0.0527	31.8362	12.3169	1.1186	31.8362	12.2589	1.1270
28.4952	10.9553	0.1586	28.4952	10.9784	−0.0352	31.8790	12.3070	1.1201	31.8790	12.2410	1.1296
28.6184	10.9510	0.1948	28.6184	10.9764	−0.0183	31.9219	12.2973	1.1215	31.9219	12.2246	1.1319
28.7415	10.9471	0.2279	28.7415	10.9744	−0.0015	31.9647	12.2875	1.1229	31.9647	12.2090	1.1342
28.8646	10.9435	0.2581	28.8646	10.9725	0.0146	32.0075	12.2778	1.1243	32.0075	12.1943	1.1363
28.9878	10.9401	0.2858	28.9878	10.9706	0.0301	32.0503	12.2680	1.1257	32.0503	12.1803	1.1383
29.1109	10.9372	0.3112	29.1109	10.9688	0.0452	32.0932	12.2583	1.1271	32.0932	12.1668	1.1402
29.2340	10.9344	0.3345	29.2340	10.9670	0.0600	32.1360	12.2487	1.1285	32.1360	12.1541	1.1421
29.4803	10.9294	0.3753	29.4803	10.9637	0.0881	32.2217	12.2294	1.1312	32.2217	12.1301	1.1455
29.7265	10.9255	0.4087	29.7265	10.9605	0.1146	32.3073	12.2101	1.1340	32.3073	12.1081	1.1487
29.9728	10.9224	0.4350	29.9728	10.9575	0.1400	32.3930	12.1906	1.1368	32.3930	12.0879	1.1516
30.2191	10.9202	0.4533	30.2191	10.9545	0.1652	32.4786	12.1707	1.1397	32.4786	12.0700	1.1542
30.4653	10.9188	0.4652	30.4653	10.9516	0.1896	32.5643	12.1505	1.1426	32.5643	12.0540	1.1566
30.7116	10.9180	0.4716	30.7116	10.9490	0.2118	32.6500	12.1315	1.1454	32.6500	12.0388	1.1587
30.9579	10.9179	0.4725	30.9579	10.9466	0.2325	32.7356	12.1128	1.1481	32.7356	12.0256	1.1607
31.2041	10.9184	0.4682	31.2041	10.9443	0.2511	32.8213	12.0947	1.1506	32.8213	12.0140	1.1623
31.4504	10.9195	0.4588	31.4504	10.9424	0.2676	32.9069	12.0774	1.1532	32.9069	12.0044	1.1637
31.6967	10.9212	0.4447	31.6967	10.9407	0.2813	32.9926	12.0613	1.1555	32.9926	11.9968	1.1647
31.9429	10.9235	0.4254	31.9429	10.9395	0.2910	33.0783	12.0474	1.1575	33.0783	11.9918	1.1655
32.1892	10.9265	0.4005	32.1892	10.9391	0.2945	33.1639	12.0365	1.1590	33.1639	11.9898	1.1658
32.4355	10.9298	0.3730	32.4355	10.9390	0.2954	33.2496	12.0274	1.1604	33.2496	11.9895	1.1658
32.6817	10.9330	0.3457	32.6817	10.9389	0.2965	33.3352	12.0186	1.1617	33.3352	11.9895	1.1658
32.9280	10.9361	0.3205	32.9280	10.9360	0.3206	33.4209	12.0090	1.1629	33.4209	12.0088	1.1631

Table 2. Concluded

Winglet station 2						Winglet station 3					
Outboard surface			Inboard surface			Outboard surface			Inboard surface		
x	y	z	x	y	z	x	y	z	x	y	z
32.5121	12.3617	1.7942	32.5121	12.3601	1.7944	32.9449	12.3776	2.1590	32.9449	12.3763	2.1591
32.5141	12.3645	1.7938	32.5141	12.3574	1.7948	32.9465	12.3787	2.1587	32.9465	12.3728	2.1596
32.5186	12.3657	1.7936	32.5186	12.3530	1.7954	32.9504	12.3797	2.1586	32.9504	12.3692	2.1601
32.5219	12.3658	1.7936	32.5219	12.3505	1.7958	32.9531	12.3798	2.1585	32.9531	12.3672	2.1604
32.5285	12.3654	1.7937	32.5285	12.3462	1.7964	32.9586	12.3797	2.1586	32.9586	12.3637	2.1609
32.5448	12.3632	1.7940	32.5448	12.3366	1.7978	32.9722	12.3780	2.1588	32.9722	12.3561	2.1620
32.5775	12.3565	1.7950	32.5775	12.3199	1.8002	32.9995	12.3730	2.1595	32.9995	12.3428	2.1639
32.6102	12.3492	1.7960	32.6102	12.3052	1.8023	33.0268	12.3675	2.1603	33.0268	12.3311	2.1656
32.6430	12.3421	1.7970	32.6430	12.2920	1.8042	33.0542	12.3620	2.1611	33.0542	12.3206	2.1671
32.6757	12.3350	1.7981	32.6757	12.2797	1.8060	33.0815	12.3566	2.1619	33.0815	12.3110	2.1685
32.7084	12.3278	1.7991	32.7084	12.2682	1.8077	33.1088	12.3512	2.1627	33.1088	12.3019	2.1698
32.7411	12.3208	1.8001	32.7411	12.2573	1.8093	33.1361	12.3459	2.1635	33.1361	12.2934	2.1710
32.7738	12.3137	1.8011	32.7738	12.2470	1.8108	33.1634	12.3405	2.1642	33.1634	12.2853	2.1722
32.8065	12.3067	1.8021	32.8065	12.2371	1.8122	33.1907	12.3352	2.1650	33.1907	12.2776	2.1733
32.8392	12.2996	1.8031	32.8392	12.2278	1.8136	33.2180	12.3299	2.1658	33.2180	12.2703	2.1743
32.9047	12.2856	1.8052	32.9047	12.2101	1.8161	33.2727	12.3192	2.1673	33.2727	12.2567	2.1763
32.9701	12.2716	1.8072	32.9701	12.1940	1.8184	33.3273	12.3085	2.1688	33.3273	12.2443	2.1781
33.0355	12.2574	1.8092	33.0355	12.1793	1.8205	33.3819	12.2978	2.1704	33.3819	12.2331	2.1797
33.1010	12.2429	1.8113	33.1010	12.1663	1.8223	33.4366	12.2868	2.1720	33.4366	12.2233	2.1811
33.1664	12.2282	1.8134	33.1664	12.1548	1.8241	33.4912	12.2756	2.1736	33.4912	12.2147	2.1824
33.2318	12.2146	1.8154	33.2318	12.1436	1.8257	33.5458	12.2656	2.1750	33.5458	12.2063	2.1835
33.2973	12.2013	1.8174	33.2973	12.1339	1.8271	33.6005	12.2557	2.1764	33.6005	12.1990	2.1846
33.3627	12.1884	1.8192	33.3627	12.1255	1.8282	33.6551	12.2461	2.1778	33.6551	12.1929	2.1855
33.4281	12.1761	1.8210	33.4281	12.1186	1.8293	33.7097	12.2371	2.1792	33.7097	12.1880	2.1862
33.4935	12.1648	1.8226	33.4935	12.1133	1.8300	33.7644	12.2289	2.1803	33.7644	12.1843	2.1867
33.5590	12.1550	1.8240	33.5590	12.1098	1.8305	33.8190	12.2219	2.1813	33.8190	12.1823	2.1871
33.6244	12.1476	1.8251	33.6244	12.1088	1.8307	33.8736	12.2170	2.1820	33.8736	12.1823	2.1870
33.6898	12.1416	1.8259	33.6898	12.1090	1.8307	33.9282	12.2131	2.1826	33.9282	12.1833	2.1869
33.7553	12.1358	1.8268	33.7553	12.1095	1.8306	33.9829	12.2095	2.1831	33.9829	12.1846	2.1867
33.8207	12.1294	1.8276	33.8207	12.1293	1.8277	34.0375	12.2053	2.1837	34.0375	12.2053	2.1837

Table 3. Experimental and Predicted Values of Oswald's Efficiency Factor

Mach number	Experimental e value for—		WBPPW e value for baseline model	VLM e value for—	
	Baseline model	Winglet model		Baseline model	Winglet model
0.30	0.956	1.144	0.947	1.013	1.082
.60	.872	1.145			
.70	.861	1.171			
.75	.871	1.100			
.775	.847	1.145			
.80	.853	1.128	.940	1.089	1.074
.825	.844	1.083			
.85	.840	1.122			
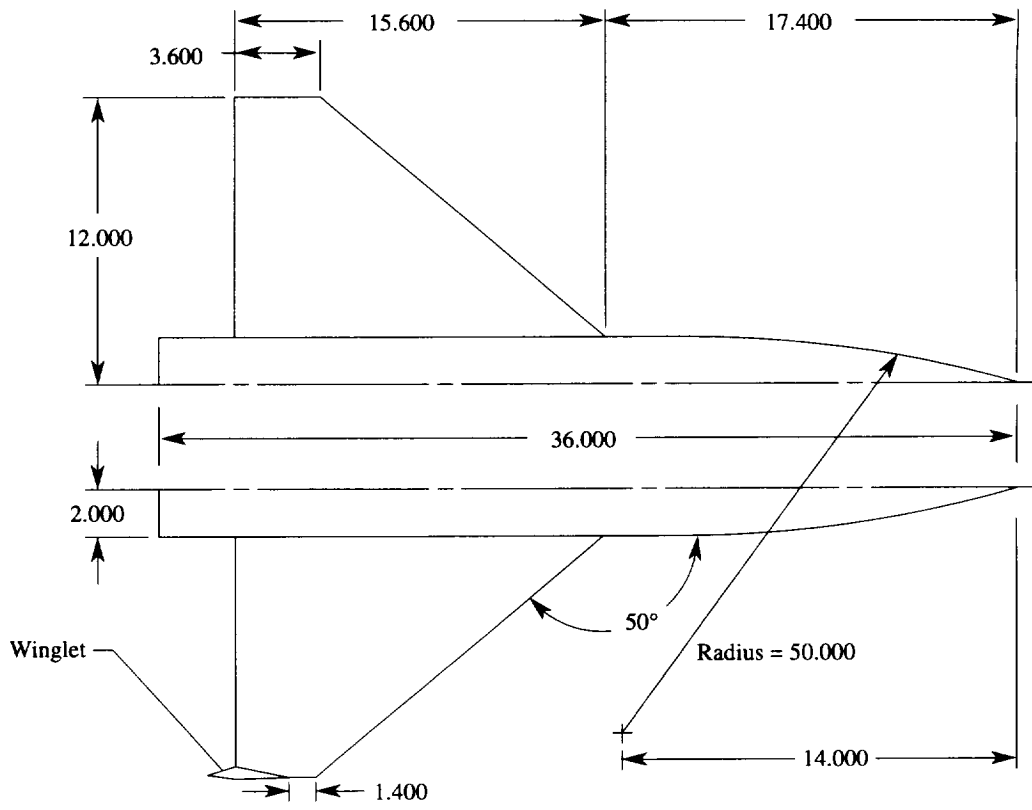
(a) Planform view of model.
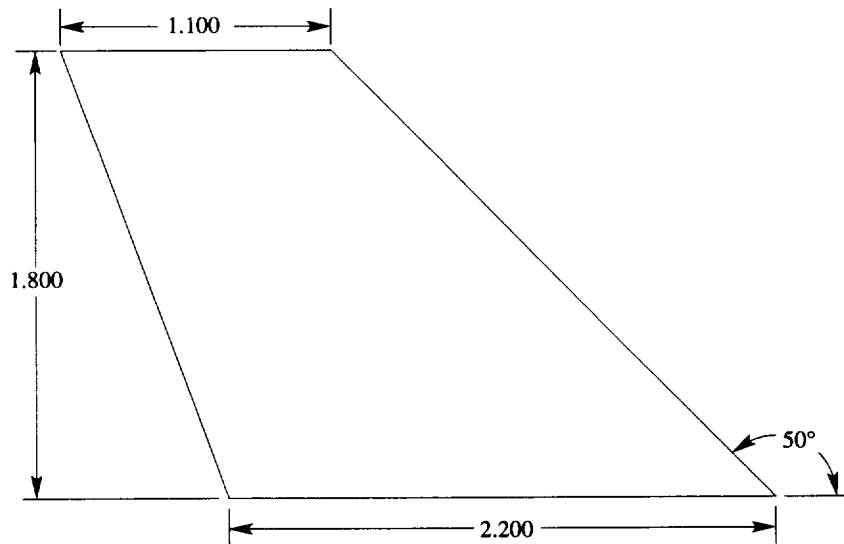
(b) Planform view of winglet.

Figure 1. Model dimensions; all linear dimensions in inches.
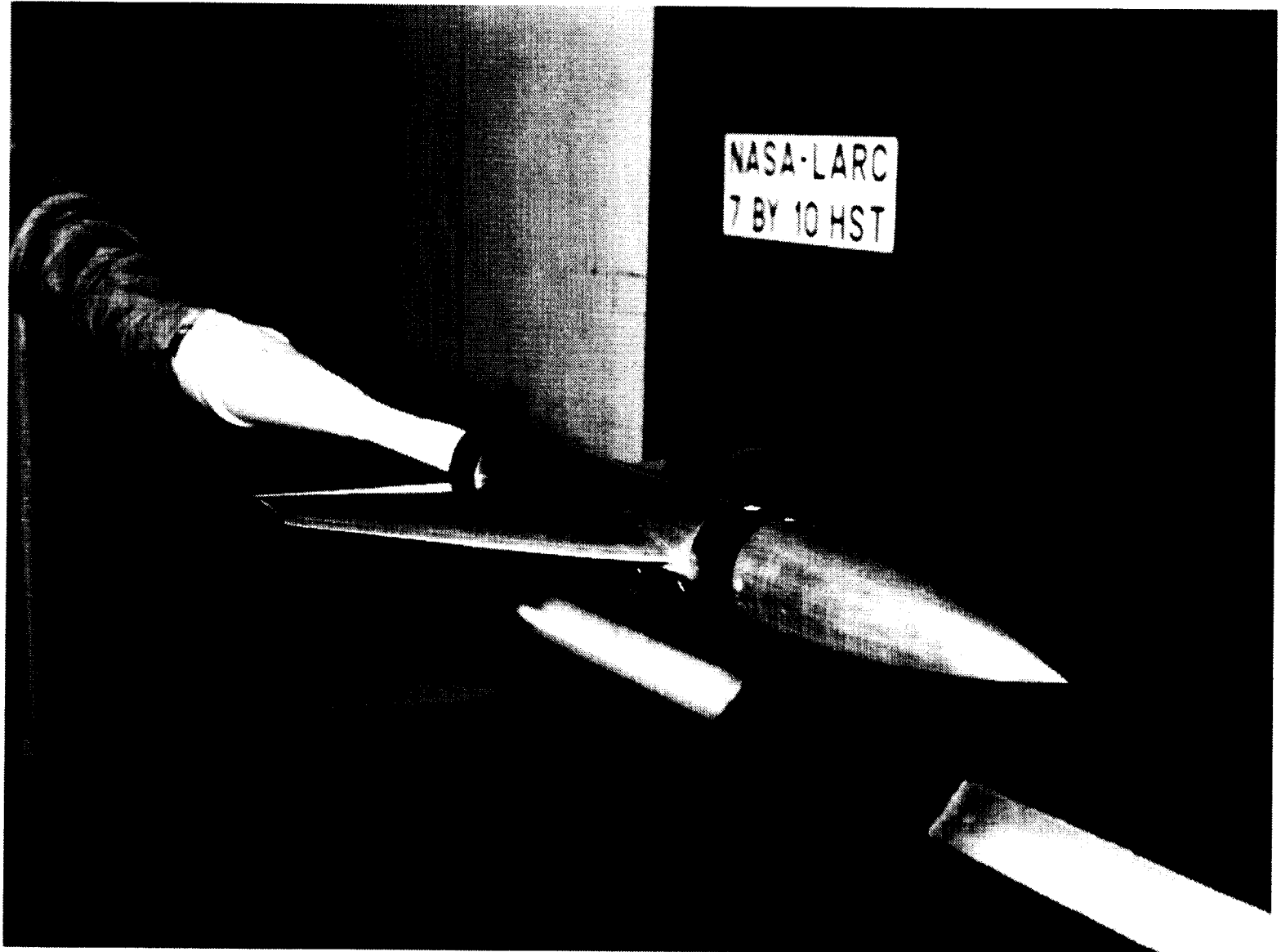
L-90-10324

(a) Baseline.

Figure 2. Model in tunnel.
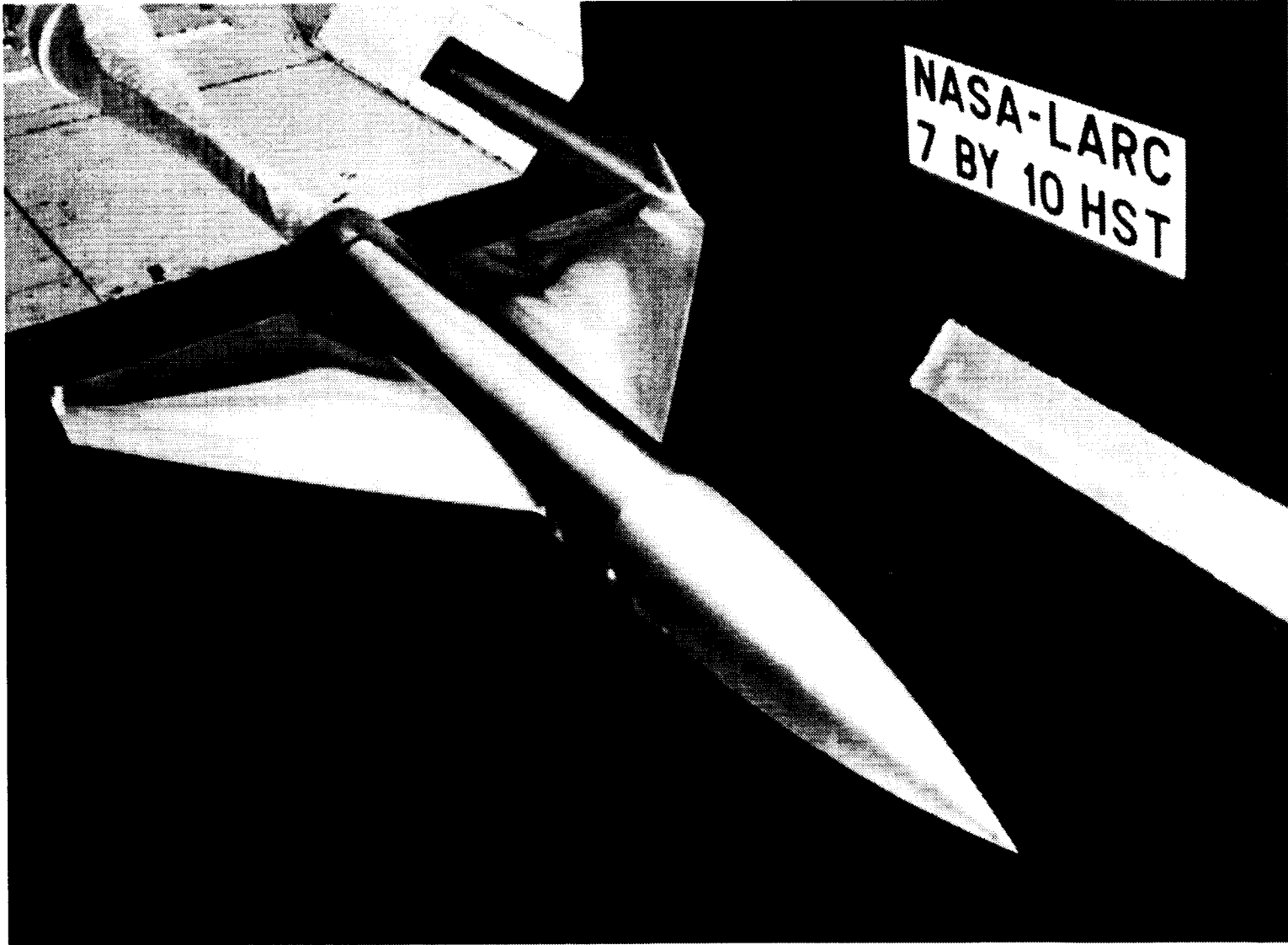
L-90-10670

(b) Winglet.

Figure 2. Concluded.

25
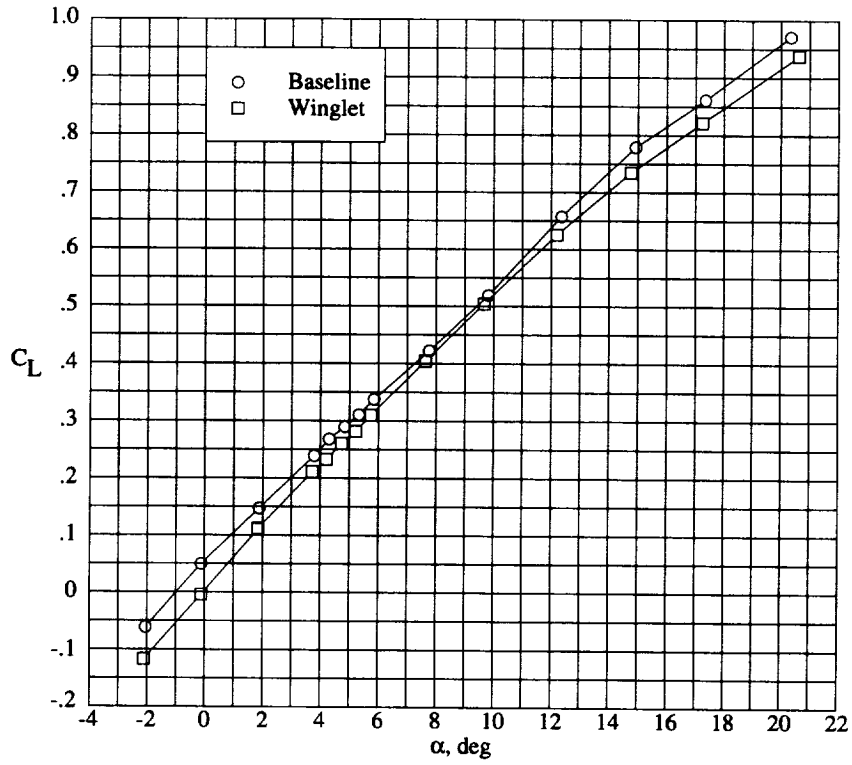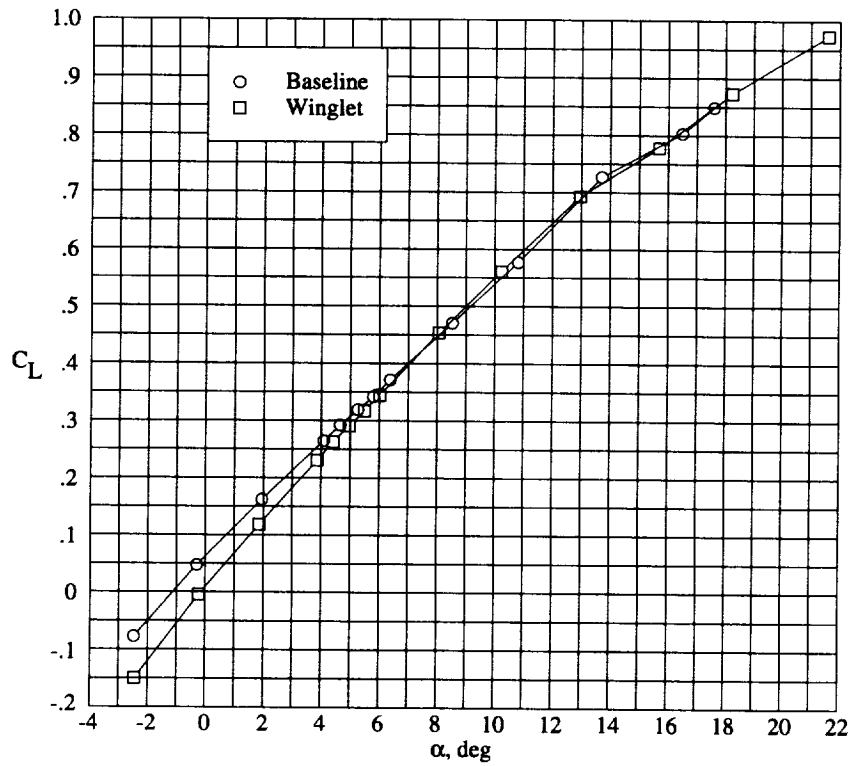
(a) $M = 0.30$.

(b) $M = 0.60$.

Figure 3. Experimental performance data—lift curve.
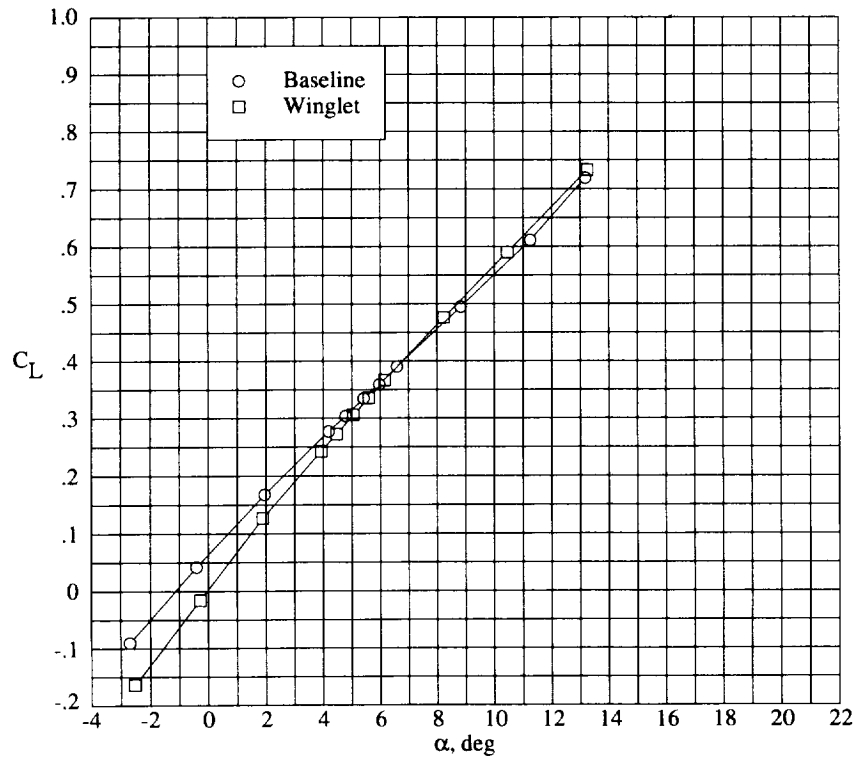
(c) $M = 0.70$.
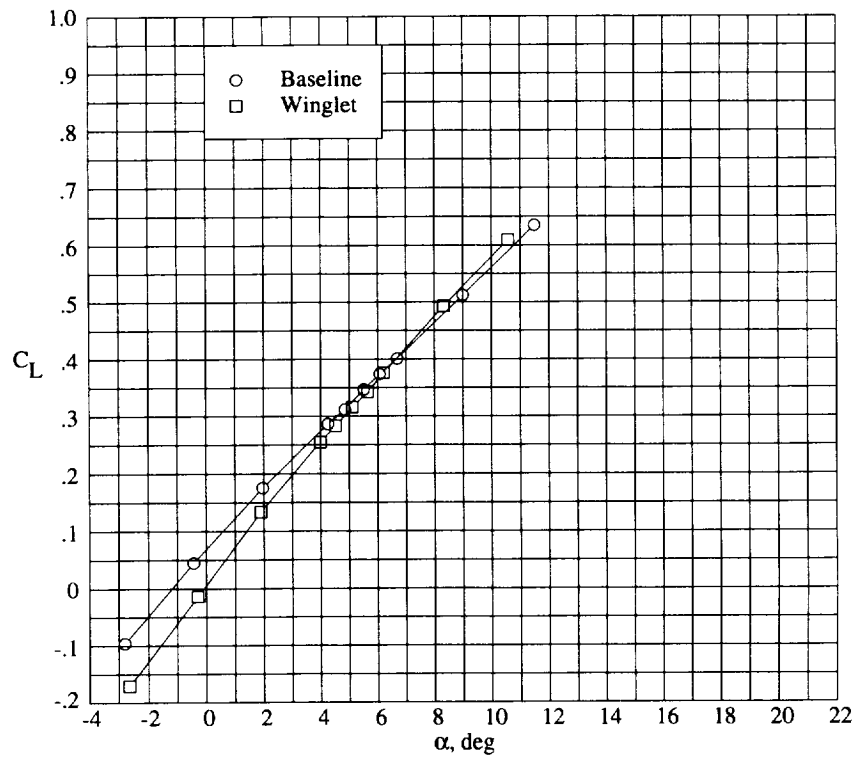
(d) $M = 0.75$.

Figure 3. Continued.
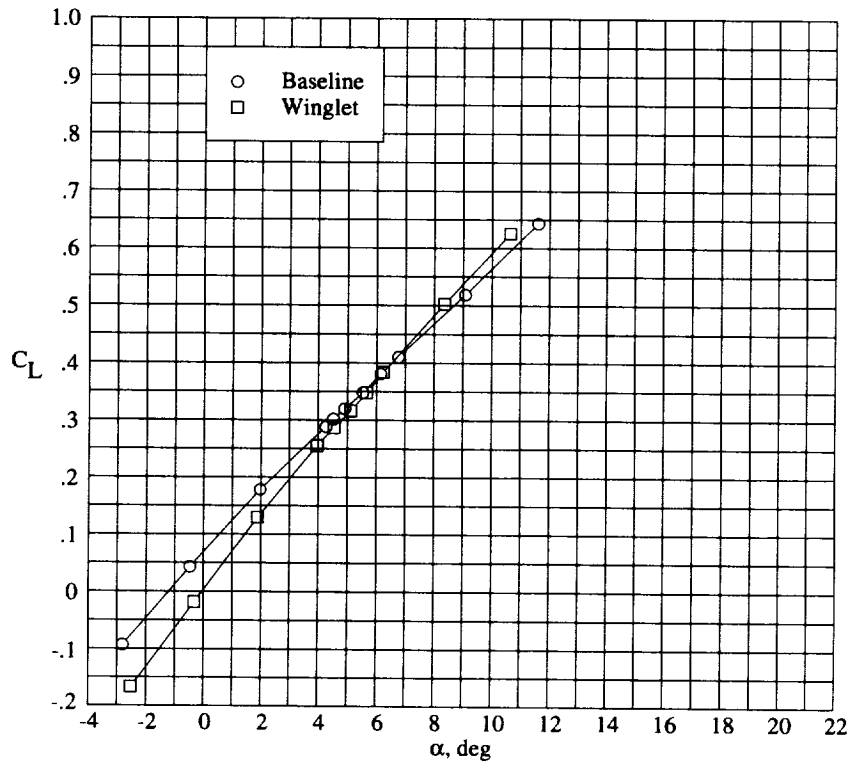
(e) $M = 0.775$.
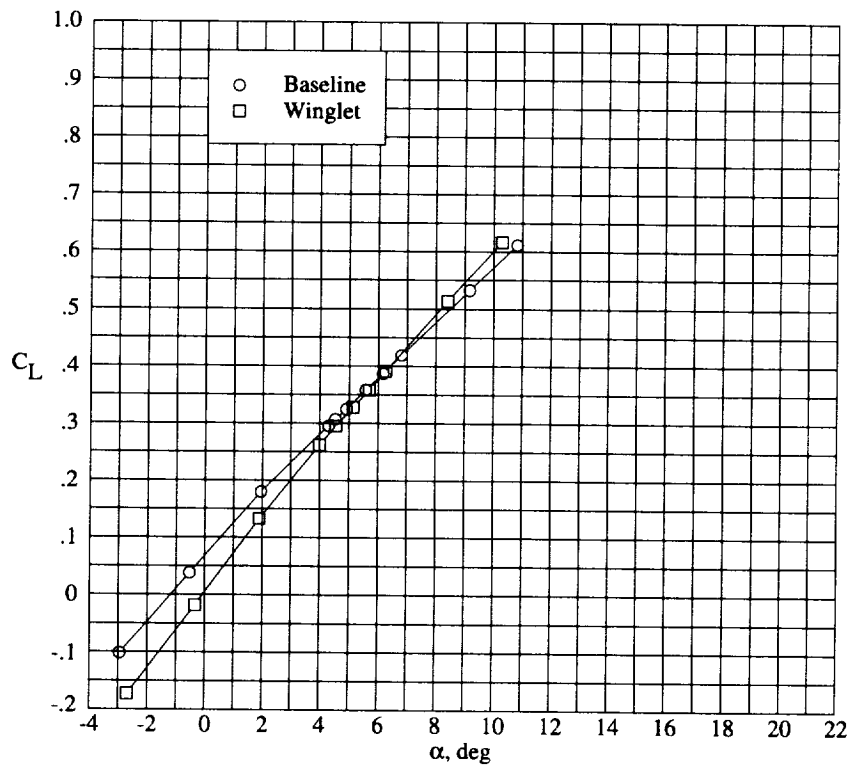
(f) $M = 0.80$.

Figure 3. Continued.

28
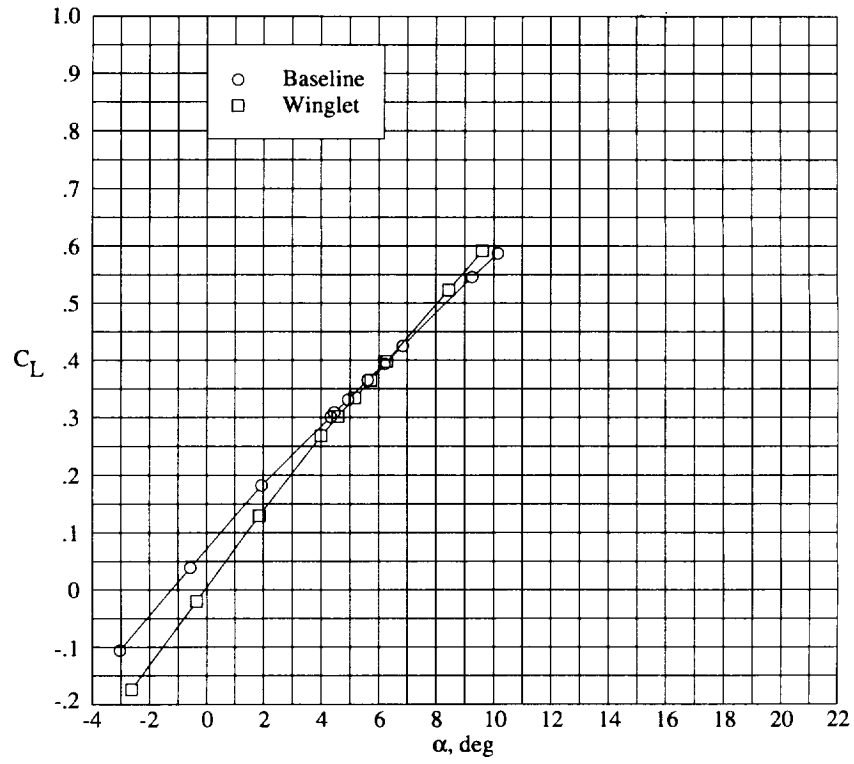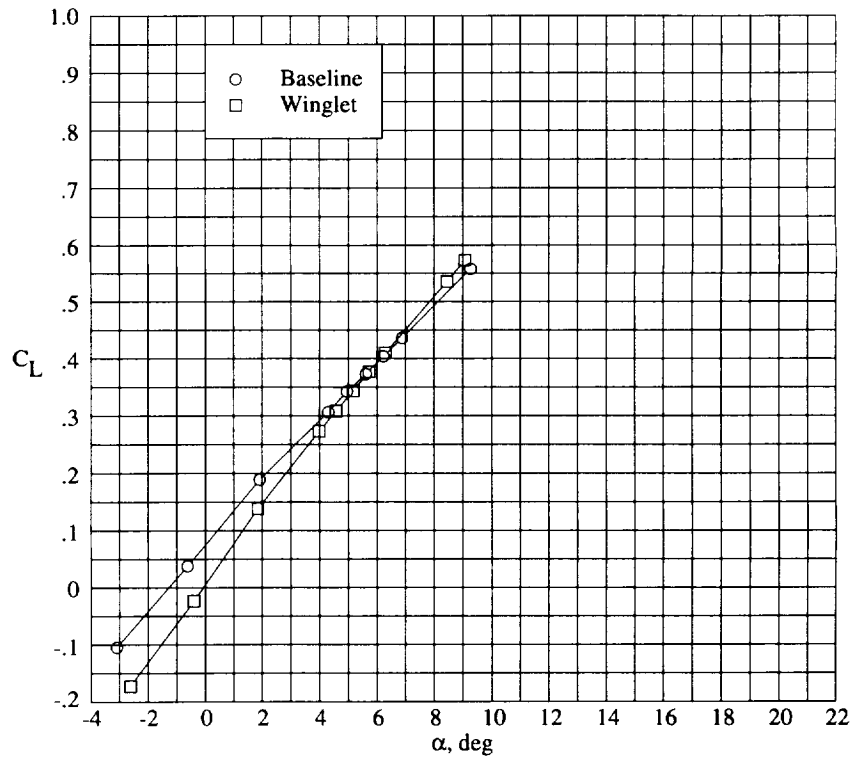
(g) $M = 0.825$.

(h) $M = 0.85$.

Figure 3. Concluded.
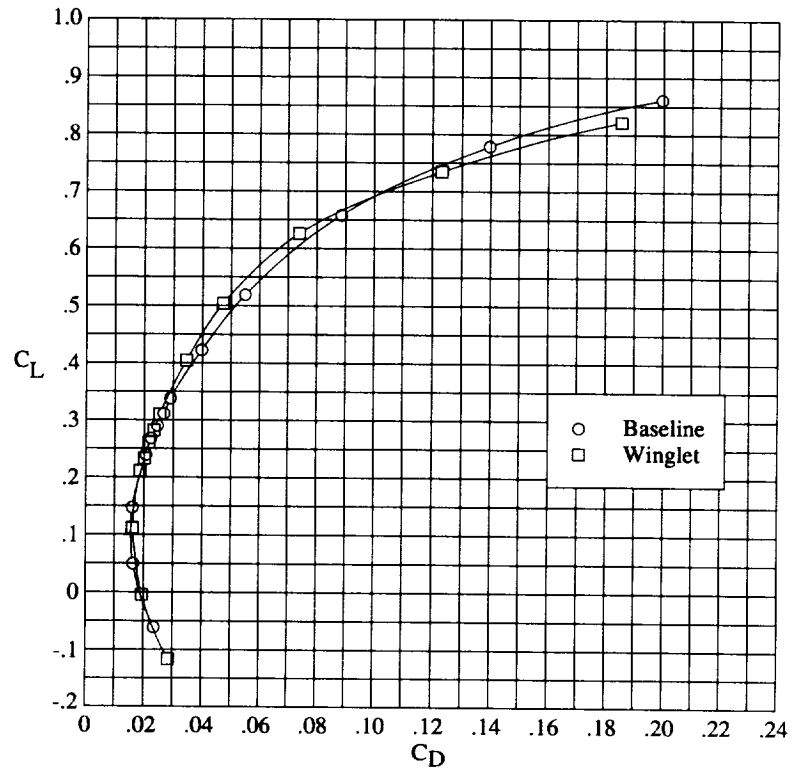
(a) $M = 0.30$.
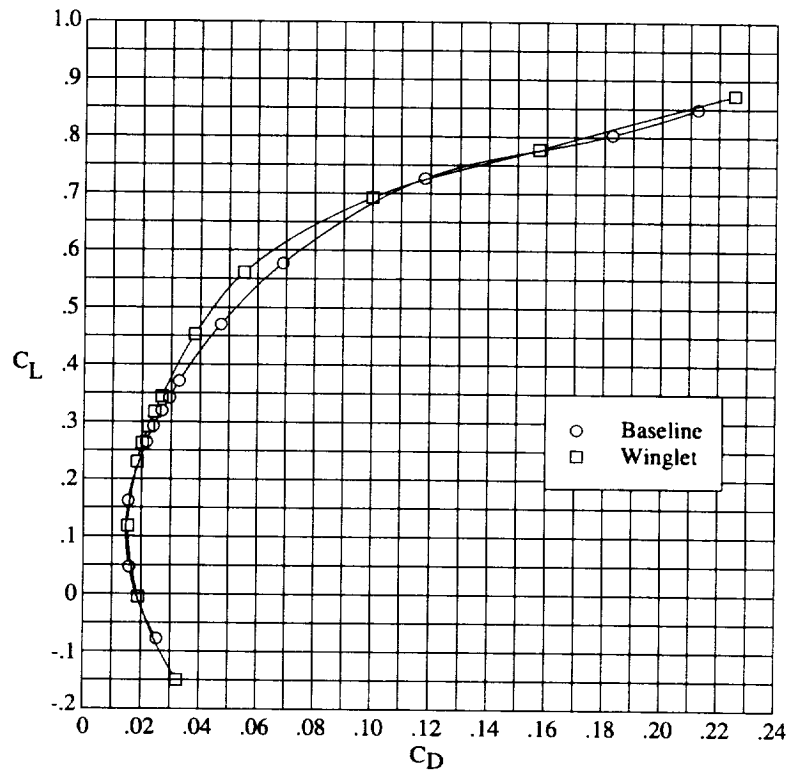
(b) $M = 0.60$.

Figure 4. Experimental performance data—drag polar.
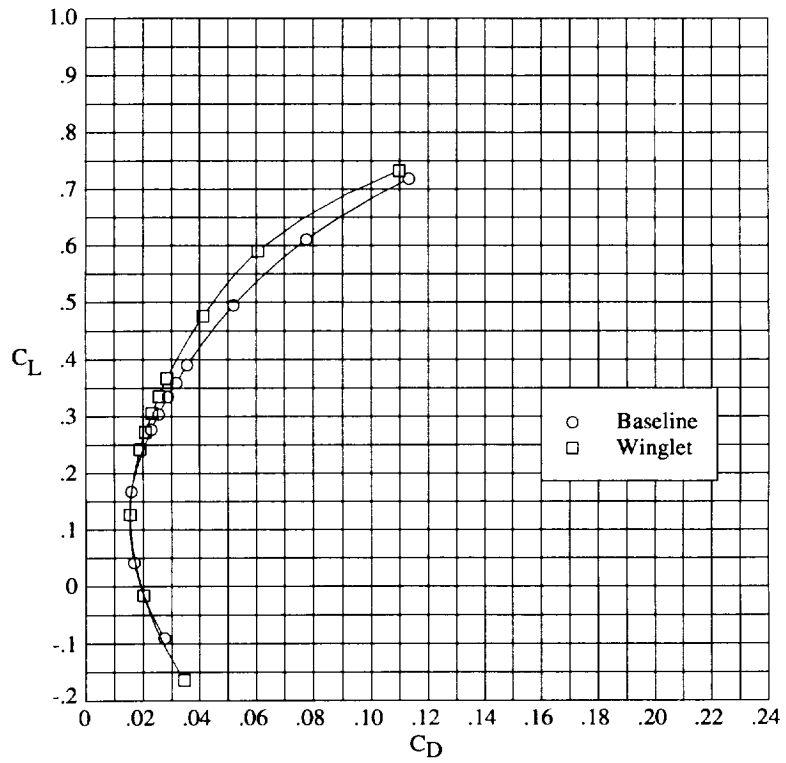
(c) $M = 0.70$.
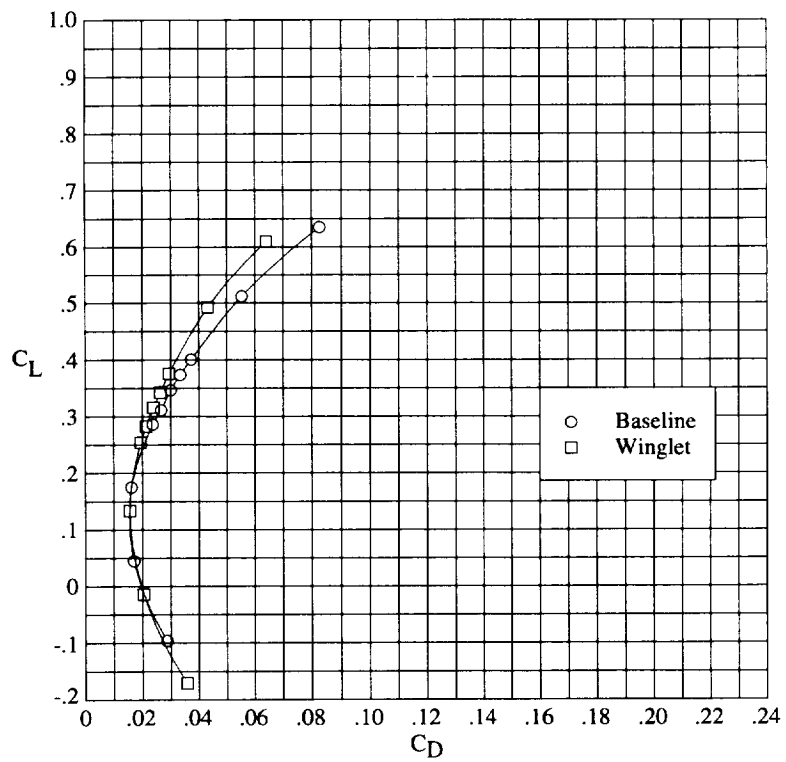
(d) $M = 0.75$.

Figure 4. Continued.
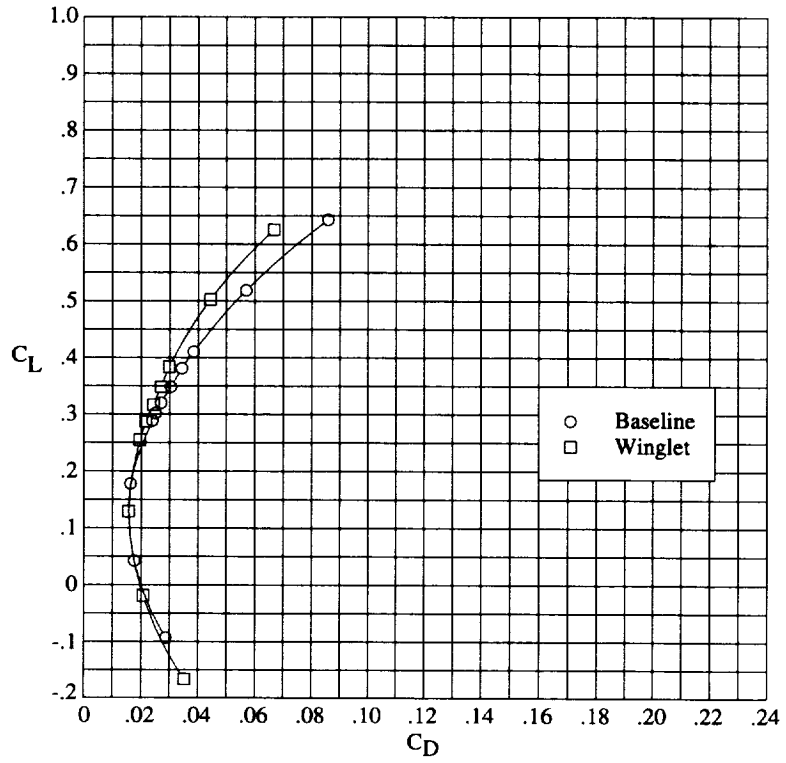
(e) $M = 0.775$.
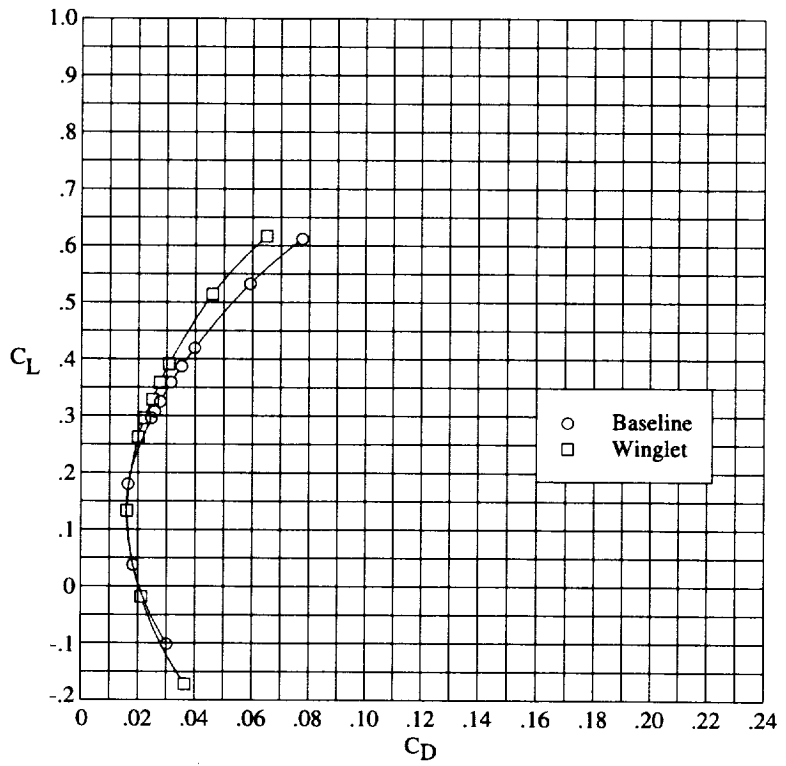
(f) $M = 0.80$.

Figure 4. Continued.

32
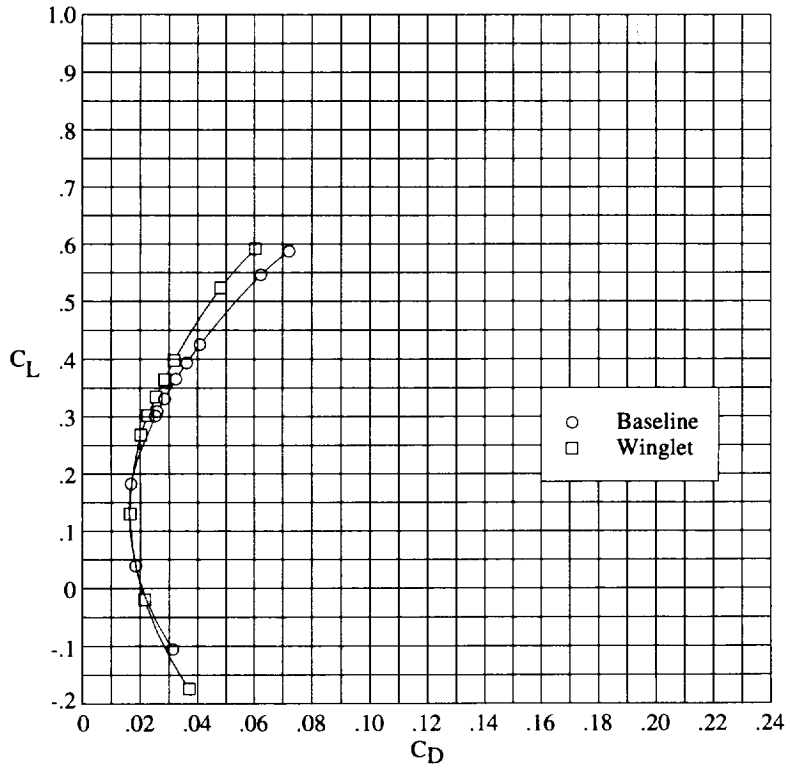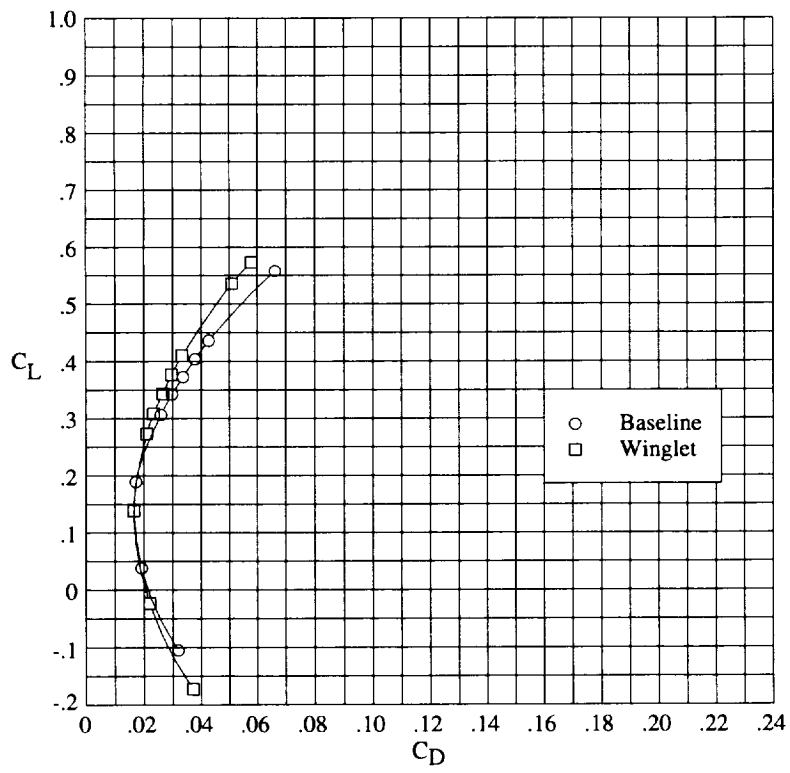
(g) $M = 0.825$.

(h) $M = 0.85$.

Figure 4. Concluded.
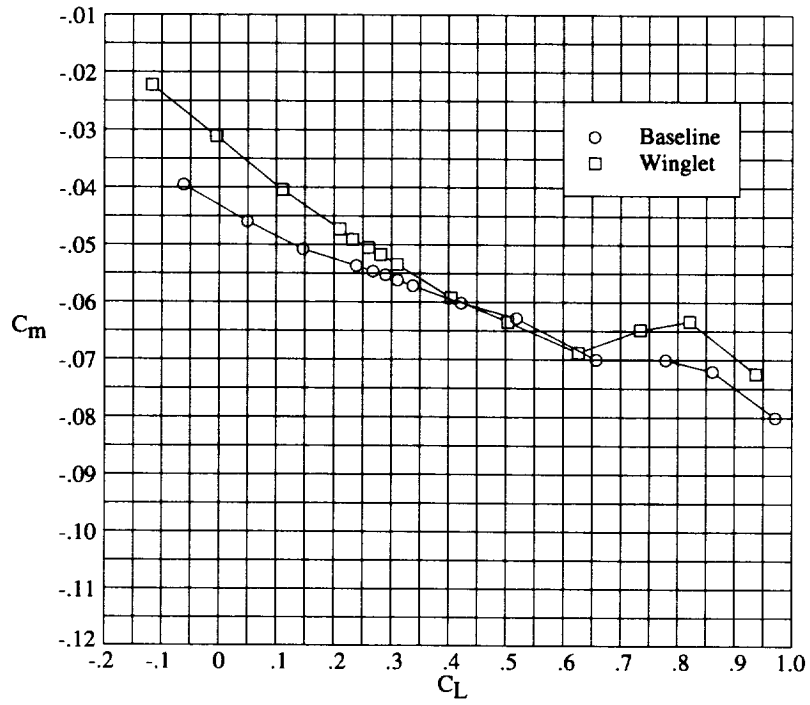
(a) $M = 0.30$.
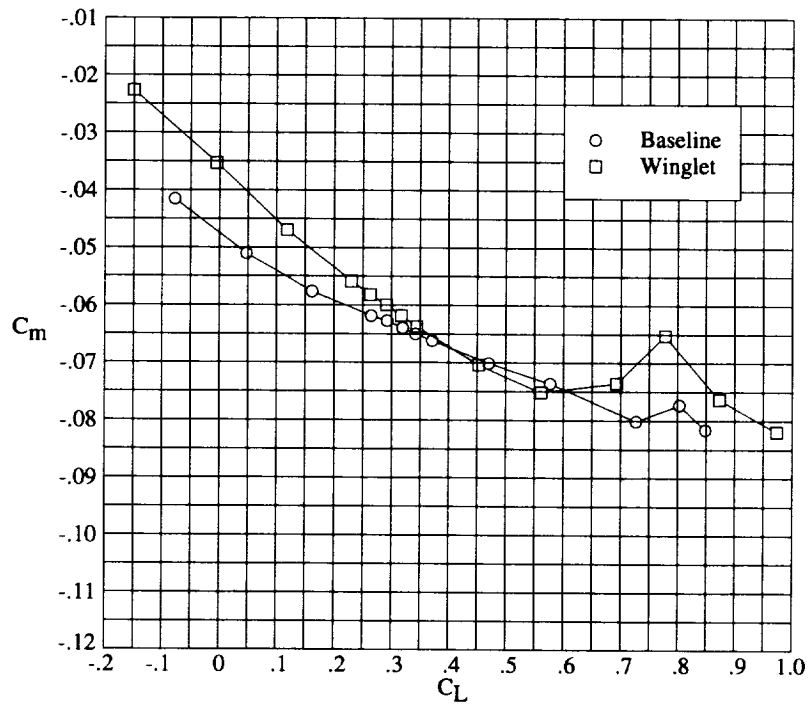
(b) $M = 0.60$.

Figure 5. Experimental performance data—pitching moment.
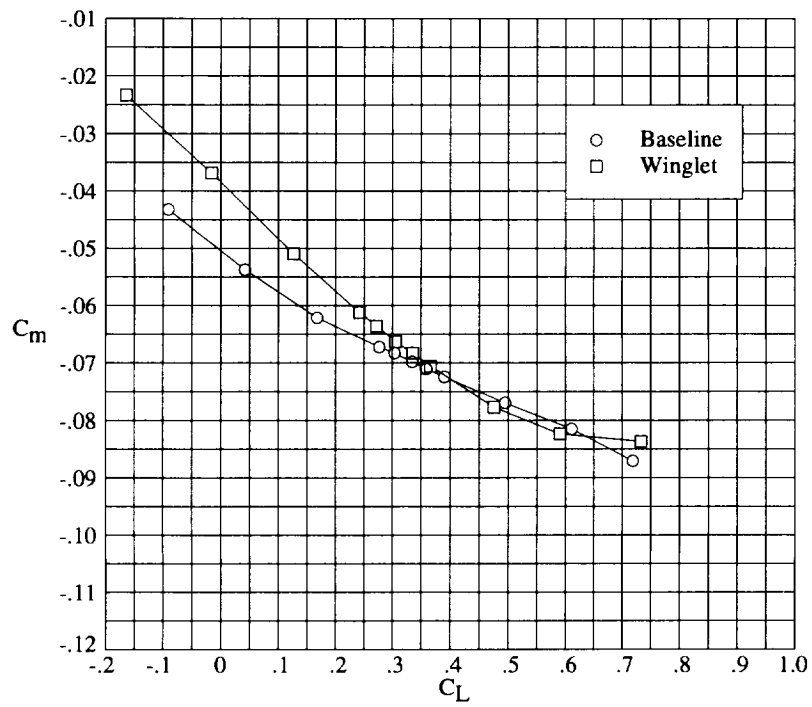
(c) $M = 0.70$.
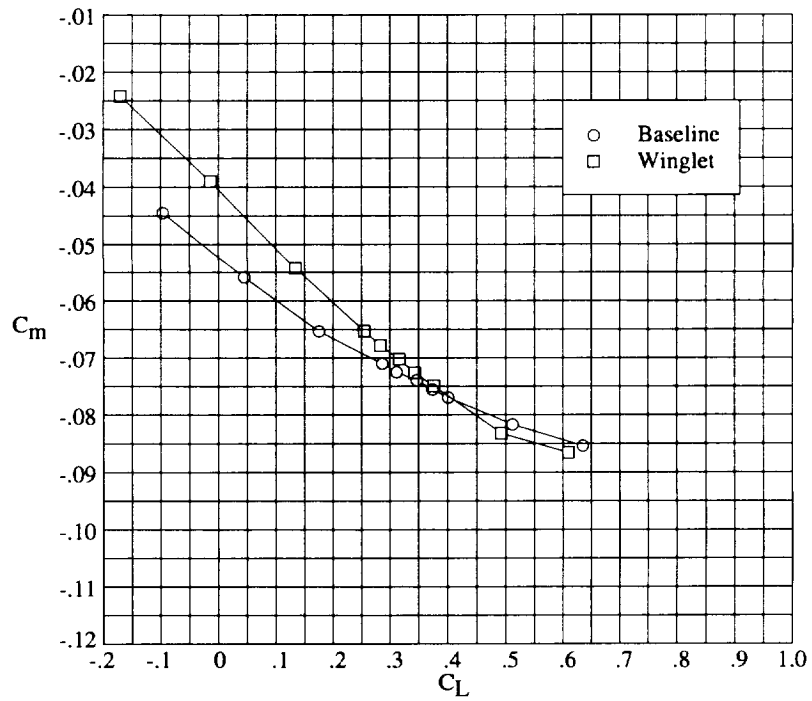
(d) $M = 0.75$.

Figure 5. Continued.
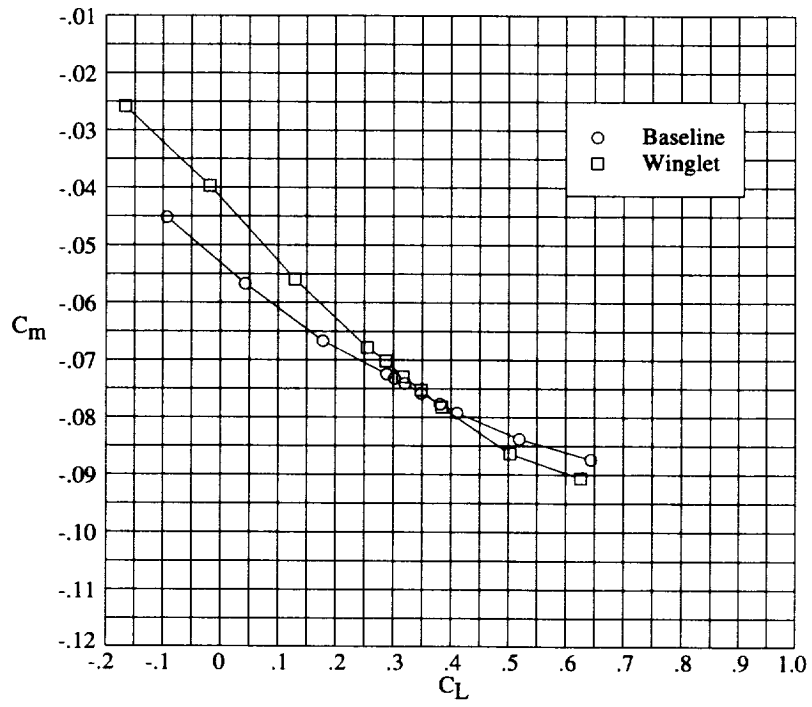
(e) $M = 0.775$.
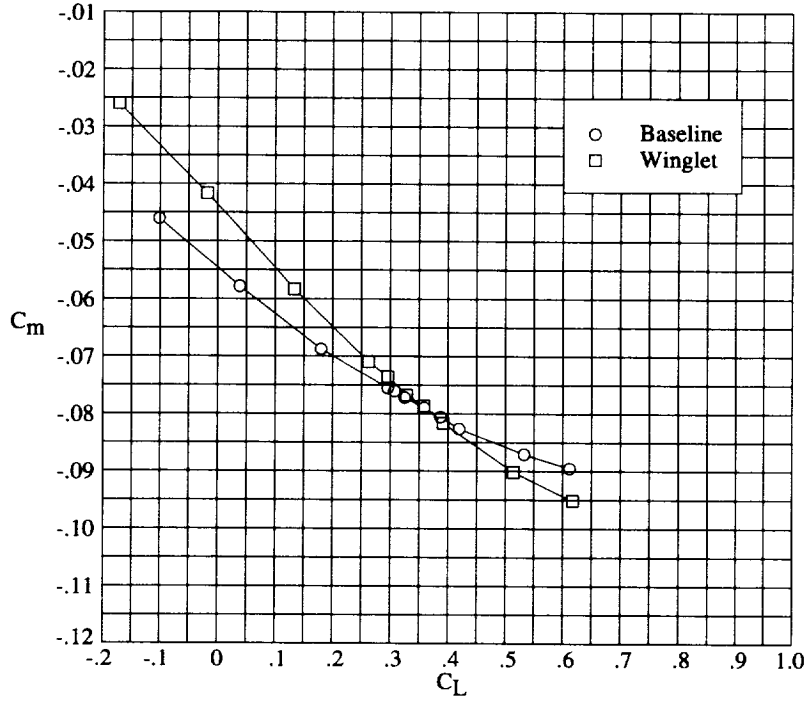
(f) $M = 0.80$.

Figure 5. Continued.
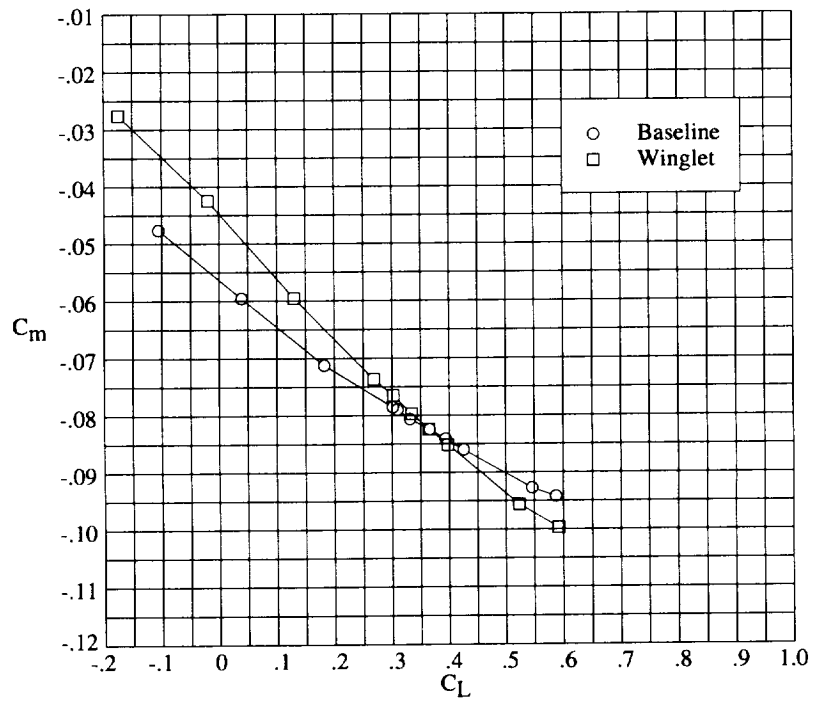
(g) $M = 0.825$.
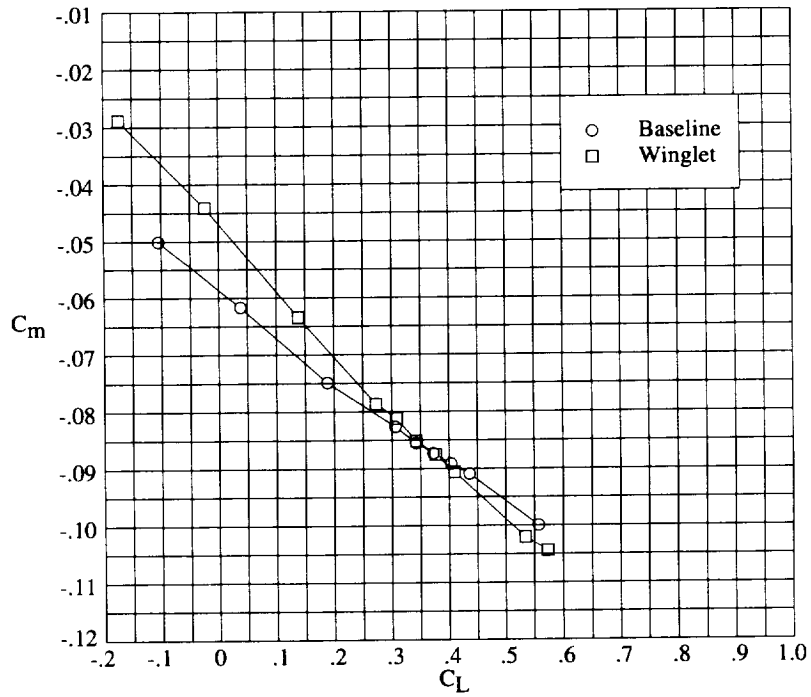
(h) $M = 0.85$.

Figure 5. Concluded.
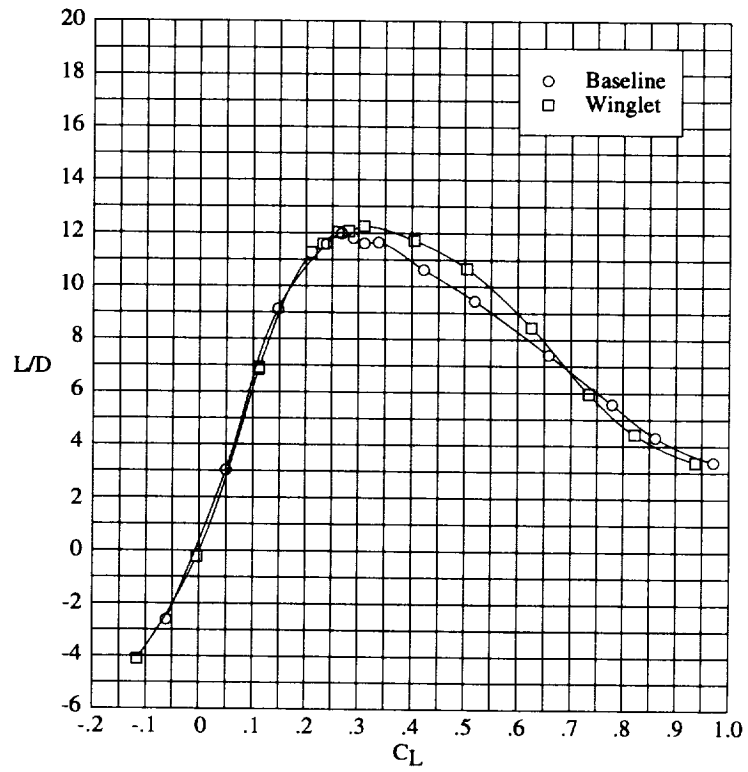
(a) $M = 0.30$.
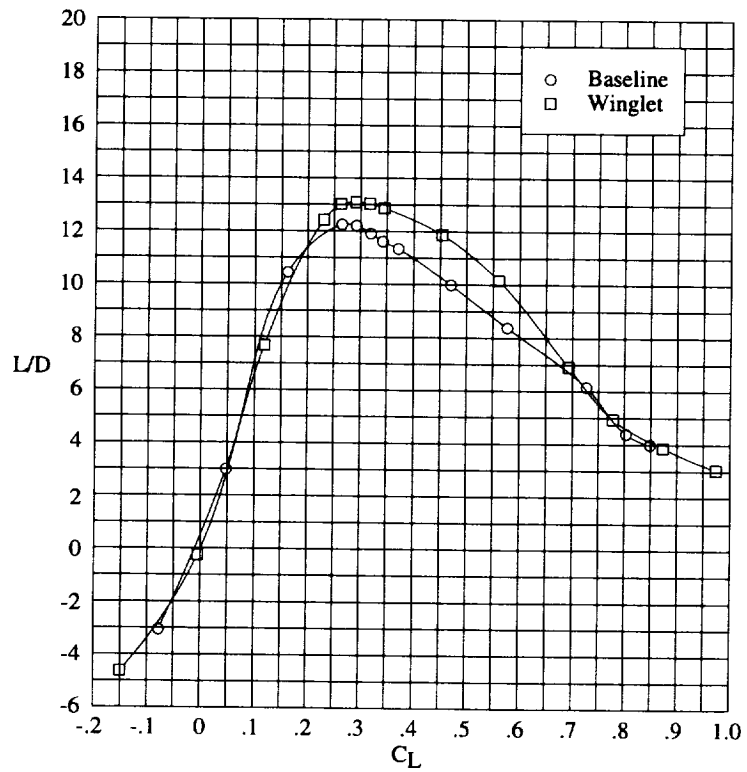
(b) $M = 0.60$.

Figure 6. Experimental performance data—lift-drag ratio.
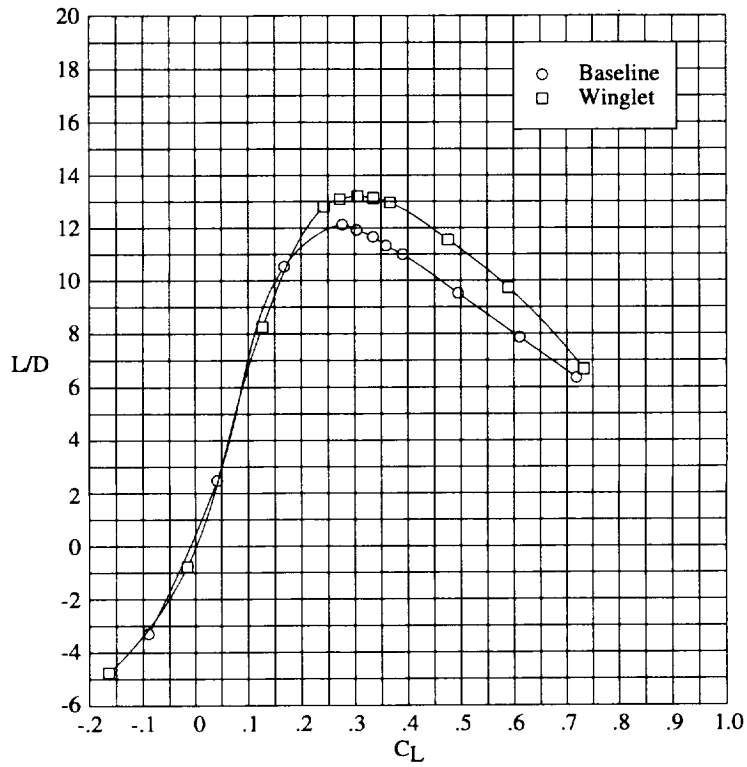
(c) $M = 0.70$.
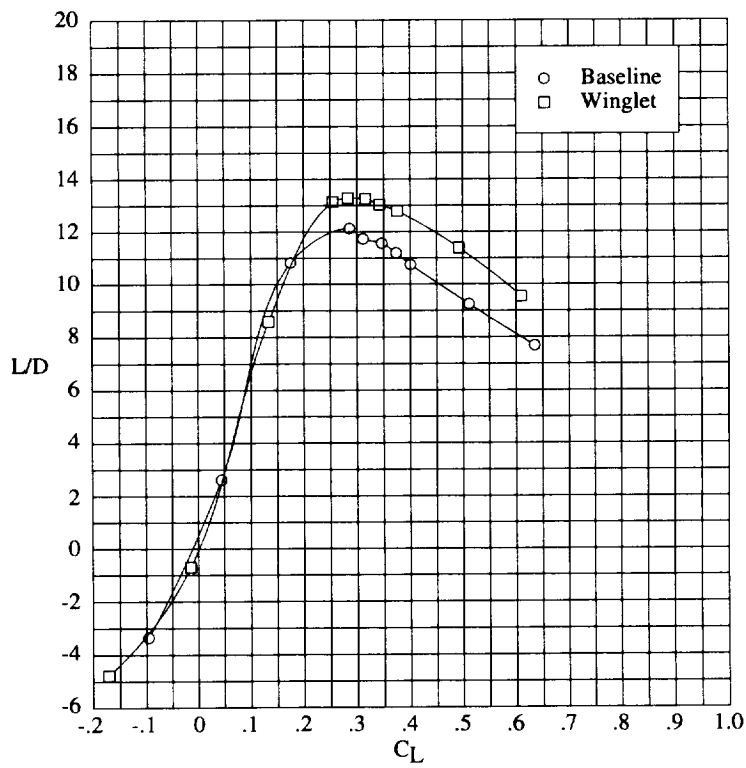
(d) $M = 0.75$.

Figure 6. Continued.
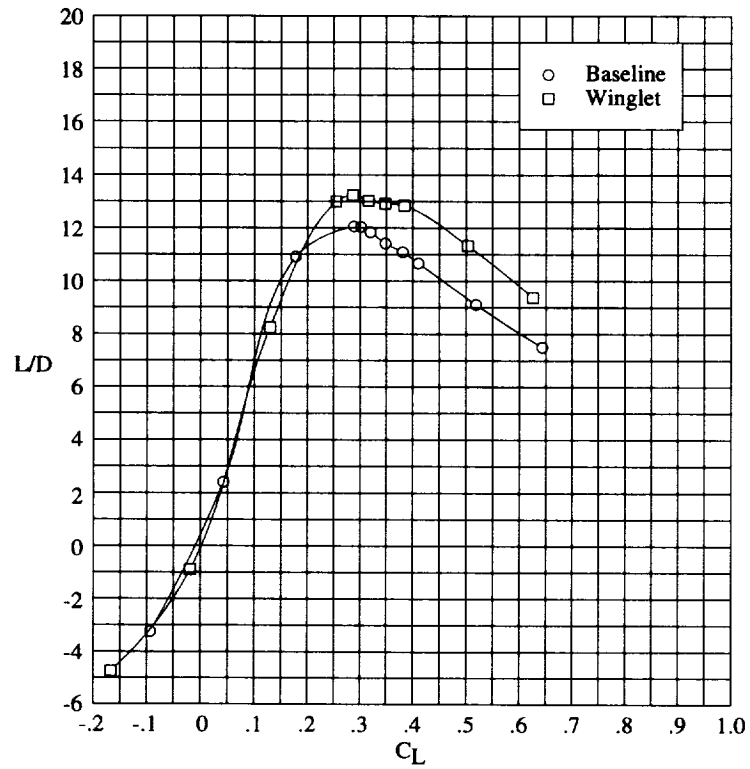
(e) $M = 0.775$.
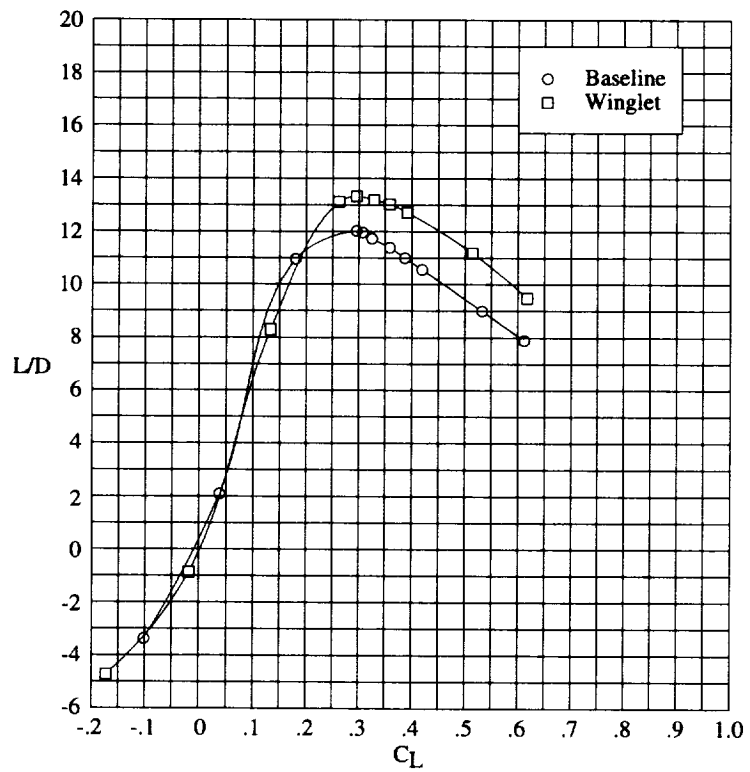
(f) $M = 0.80$.

Figure 6. Continued.
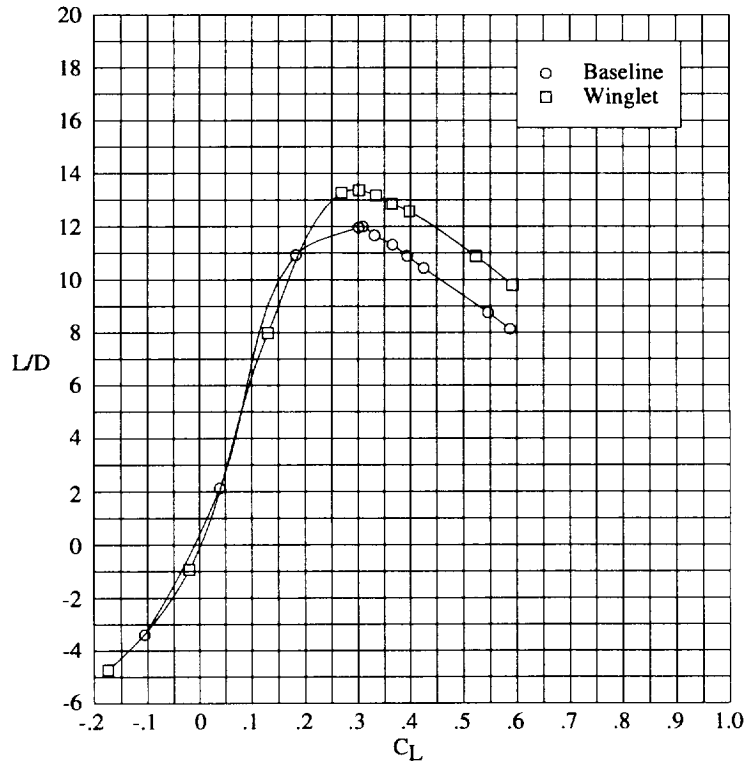
(g) $M = 0.825$.
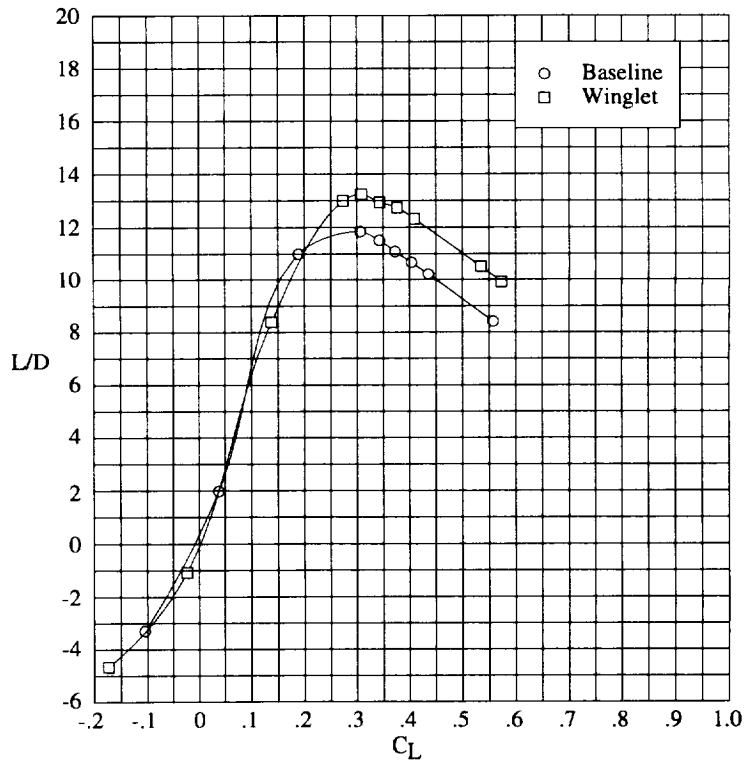
(h) $M = 0.85$.

Figure 6. Concluded.
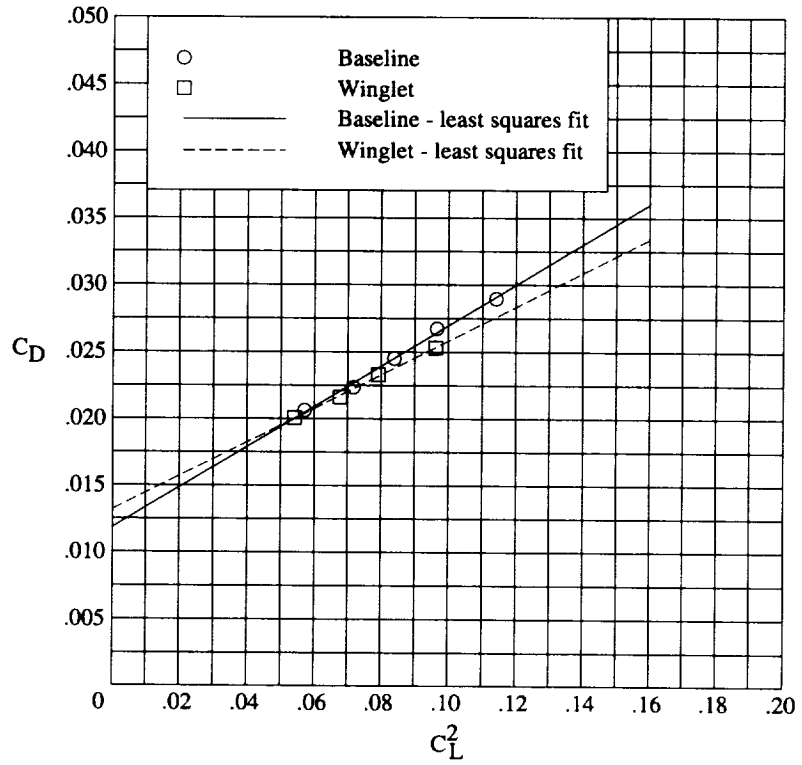
(a) $M = 0.30$.
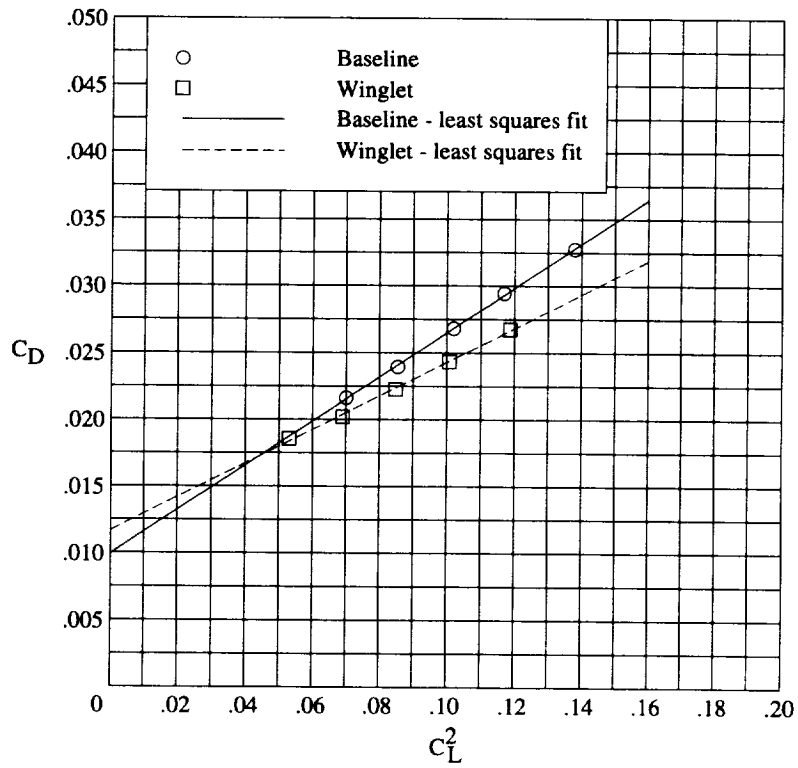
(b) $M = 0.60$.

Figure 7. Experimental performance data—minimum drag projection.
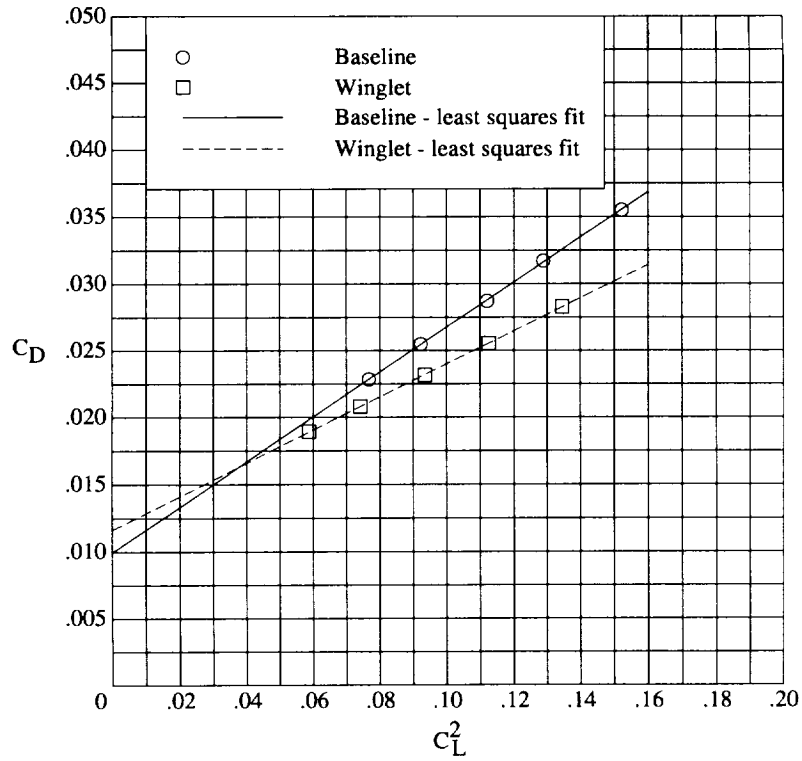
(c) $M = 0.70$.
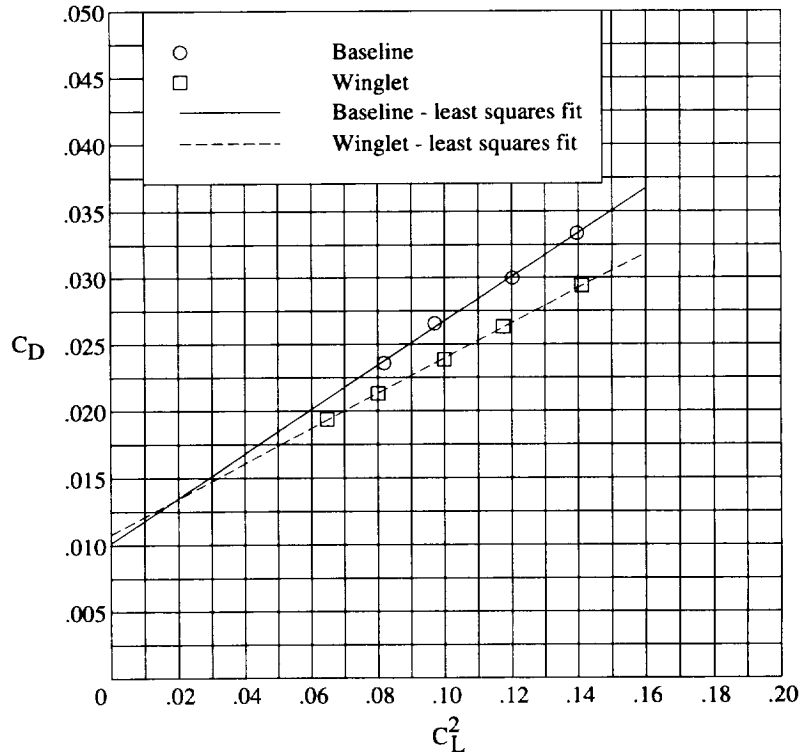
(d) $M = 0.75$.

Figure 7. Continued.
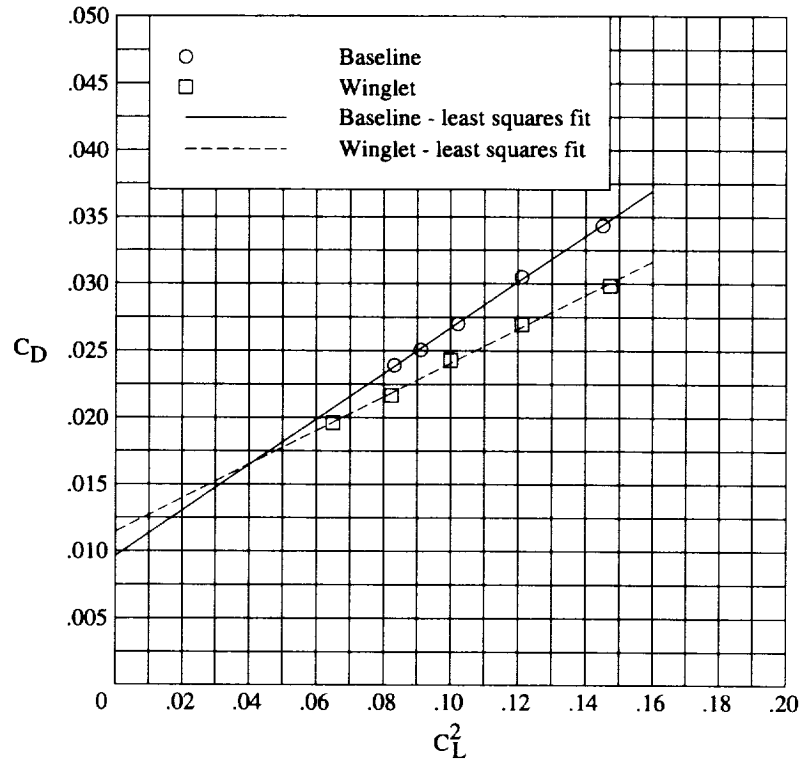
(e) $M = 0.775.$
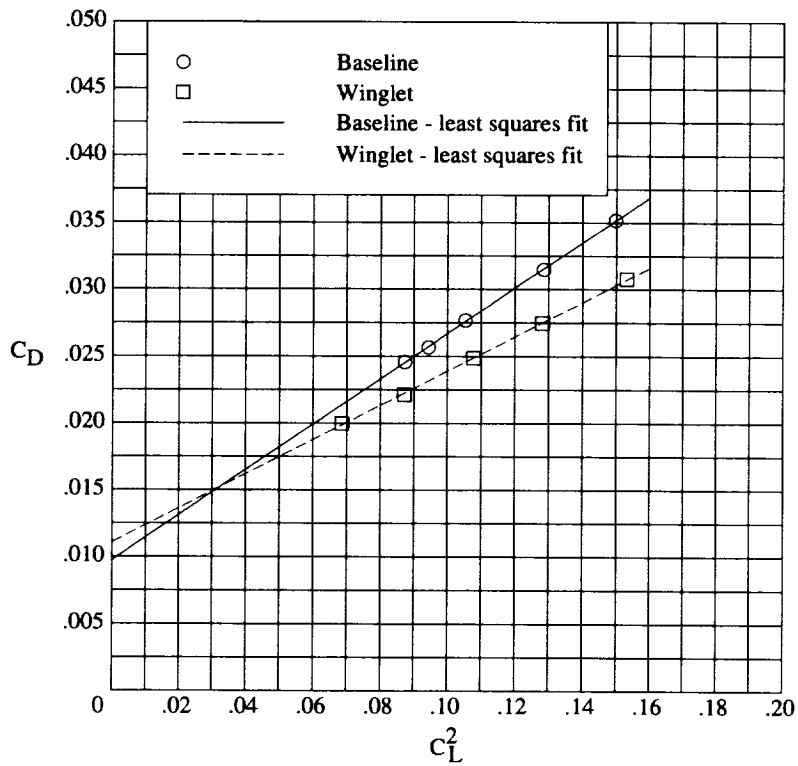
(f) $M = 0.80.$

Figure 7. Continued.
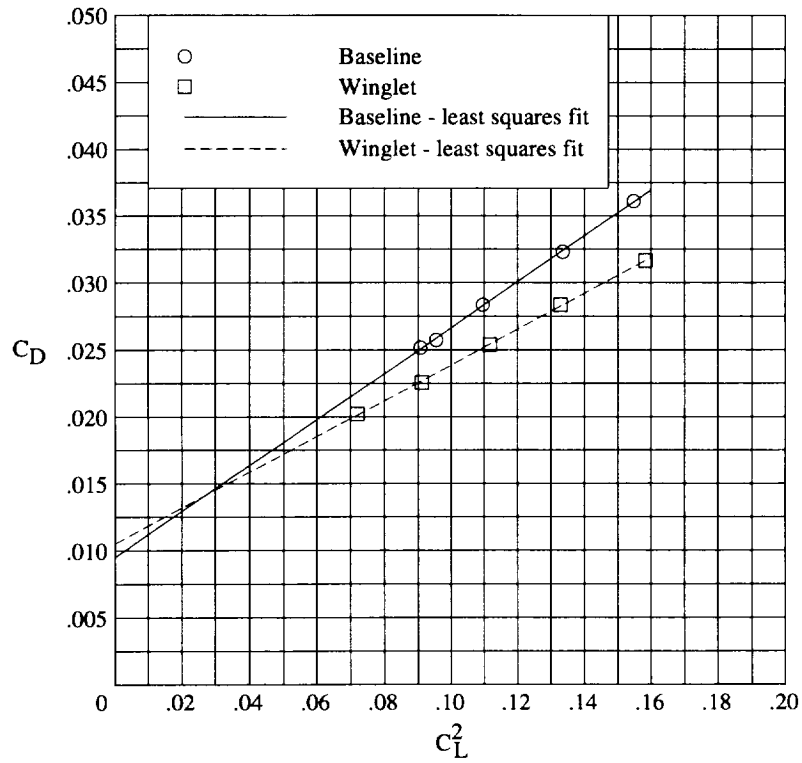
(g) $M = 0.825$.
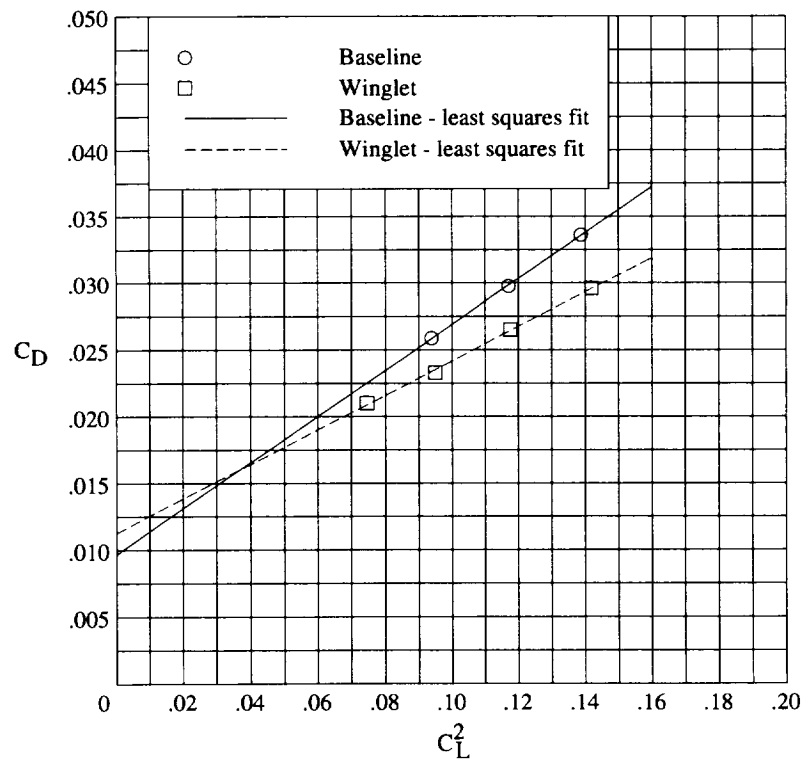
(h) $M = 0.85$.

Figure 7. Concluded.
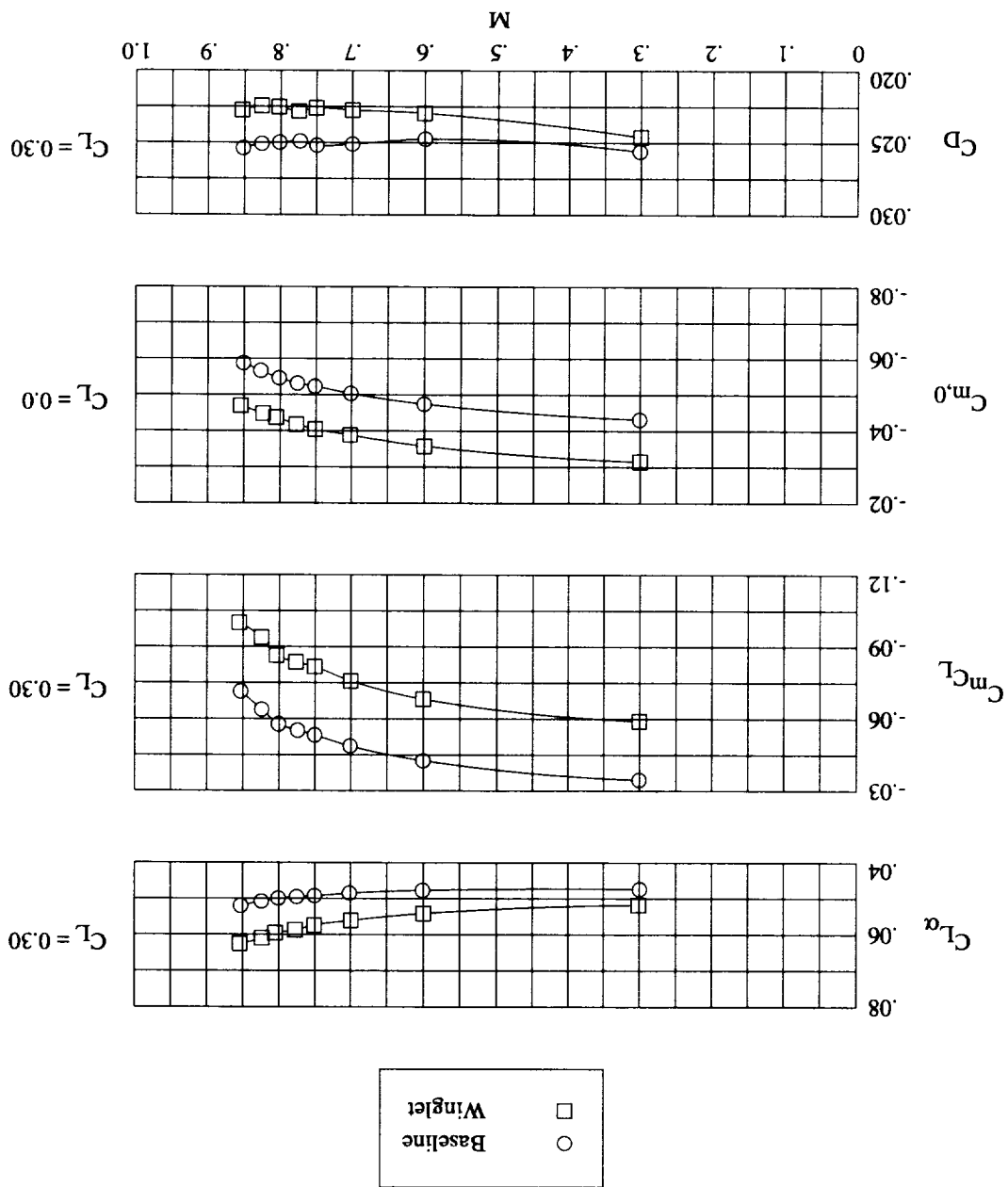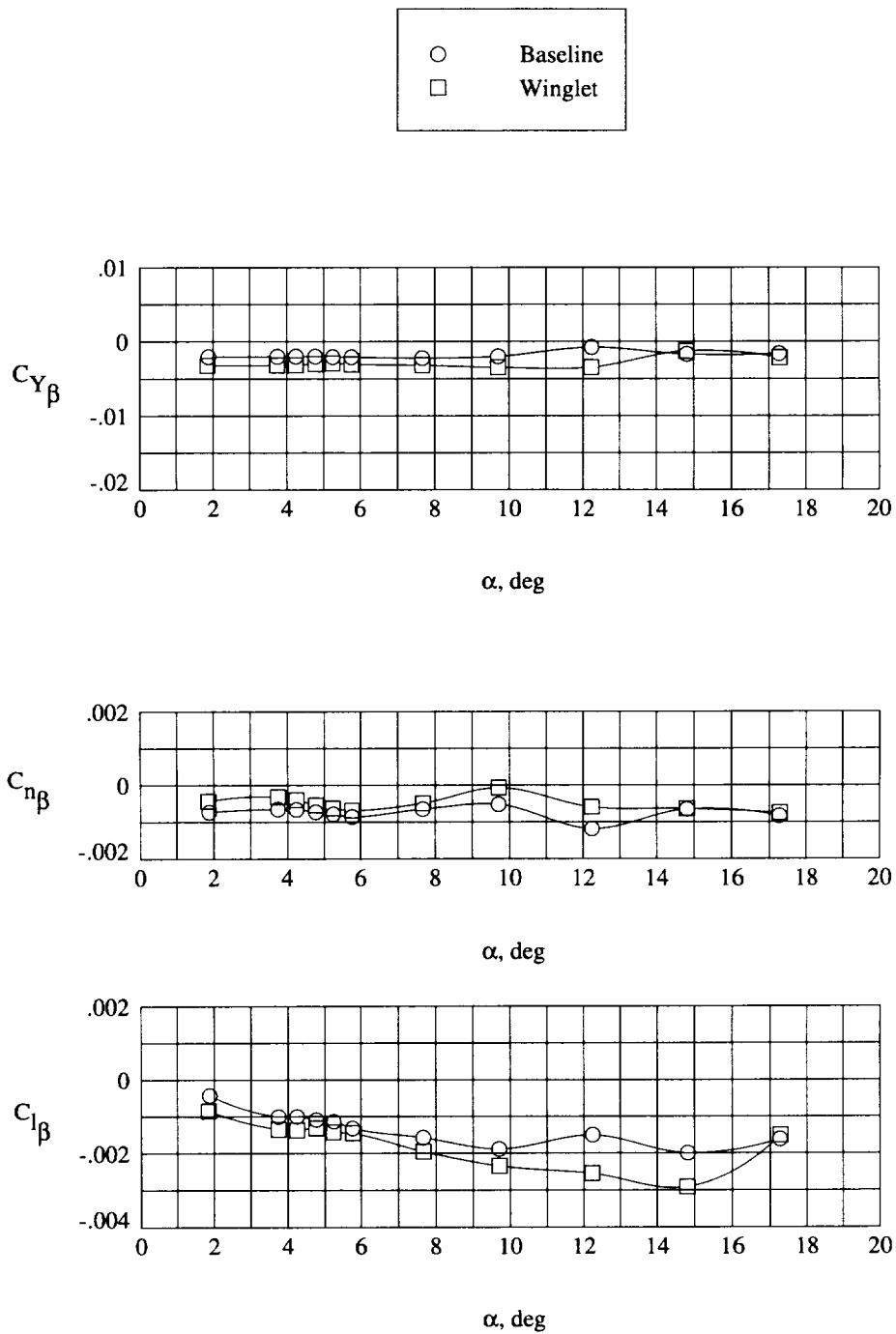
(a) $M = 0.30$.

Figure 9. Experimental lateral-directional stability data.
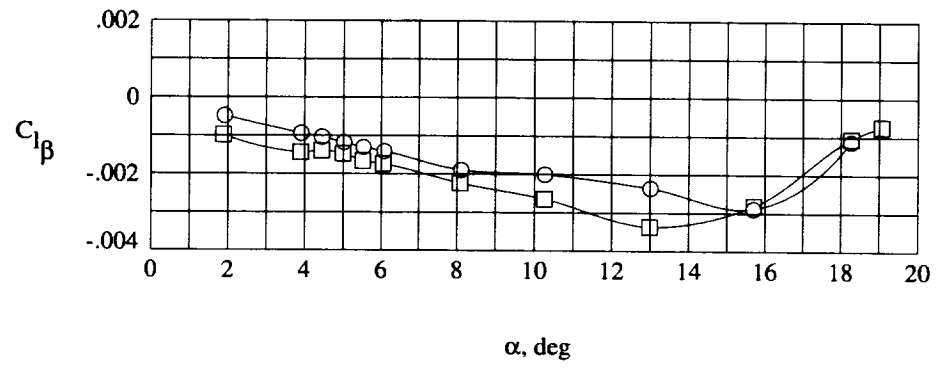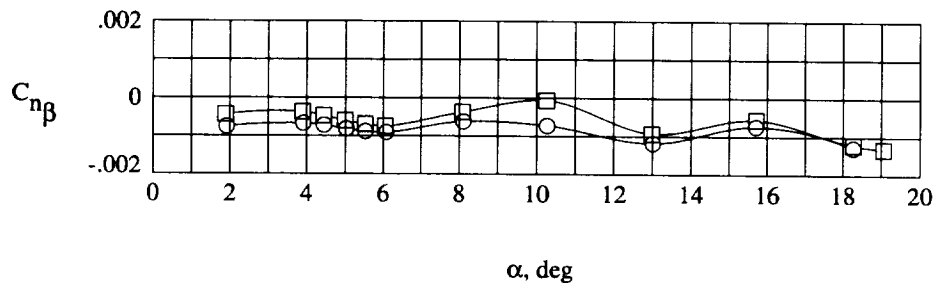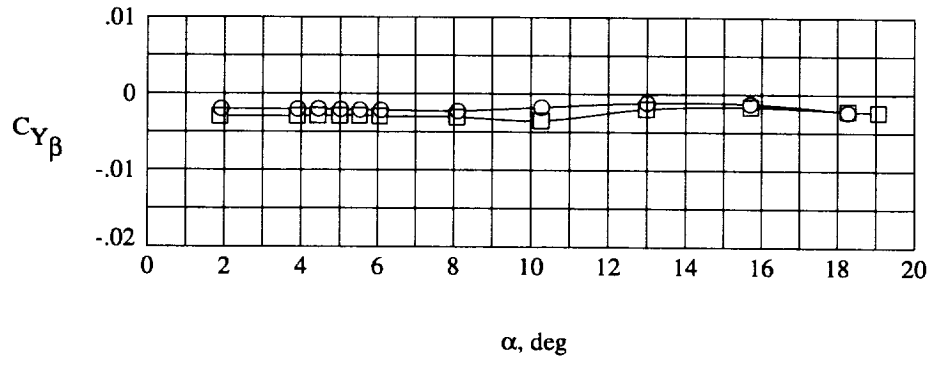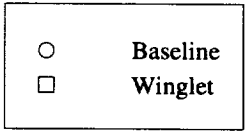
(b) $M = 0.60$.

Figure 9. Continued.
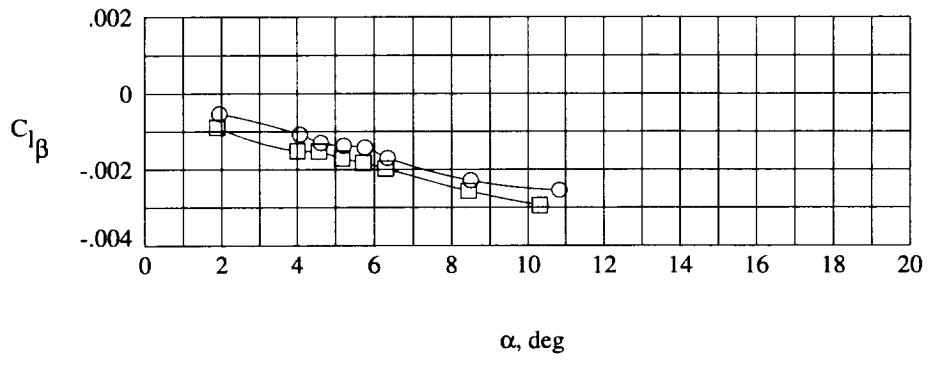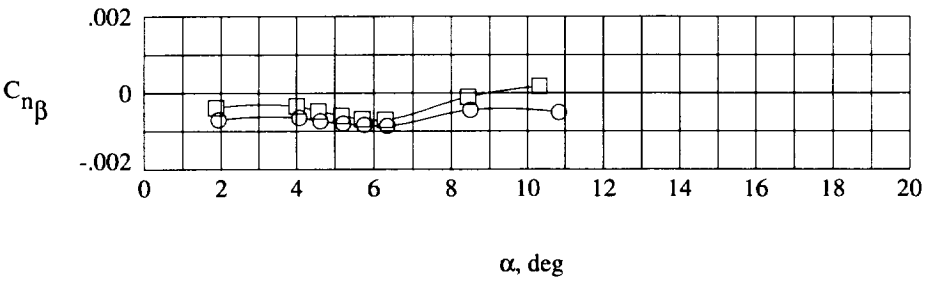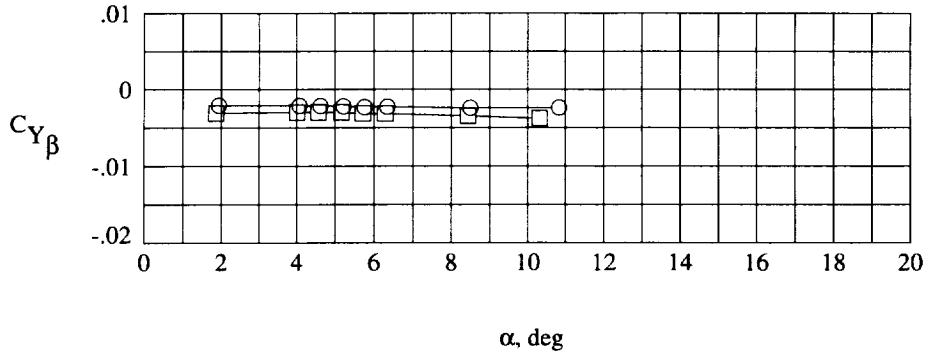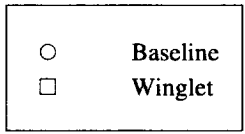
(c) $M = 0.80$.

Figure 9. Concluded.
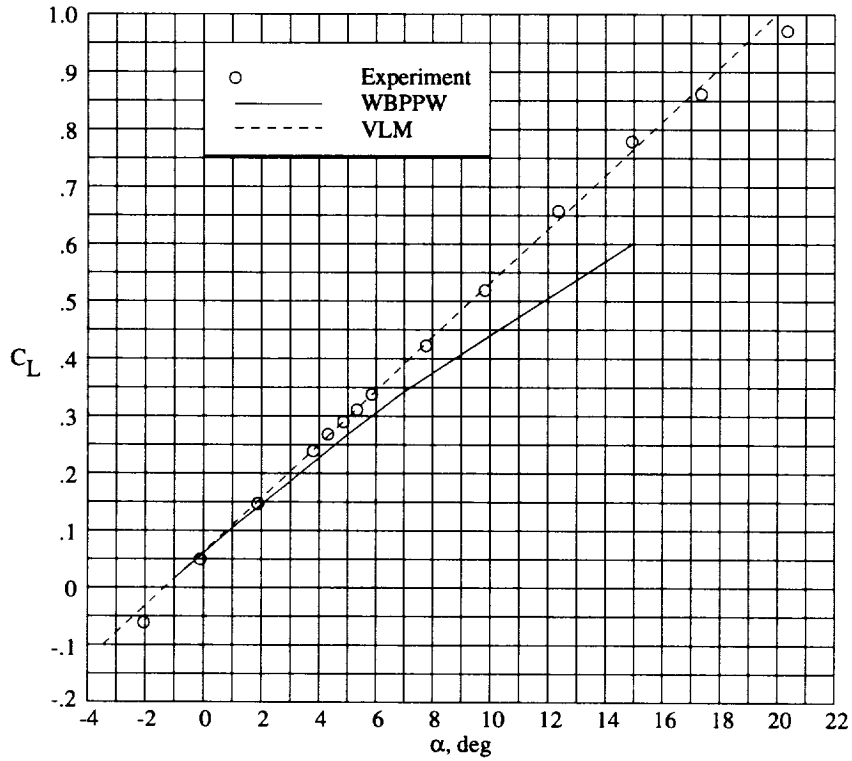
(a) Baseline; $M = 0.30$.
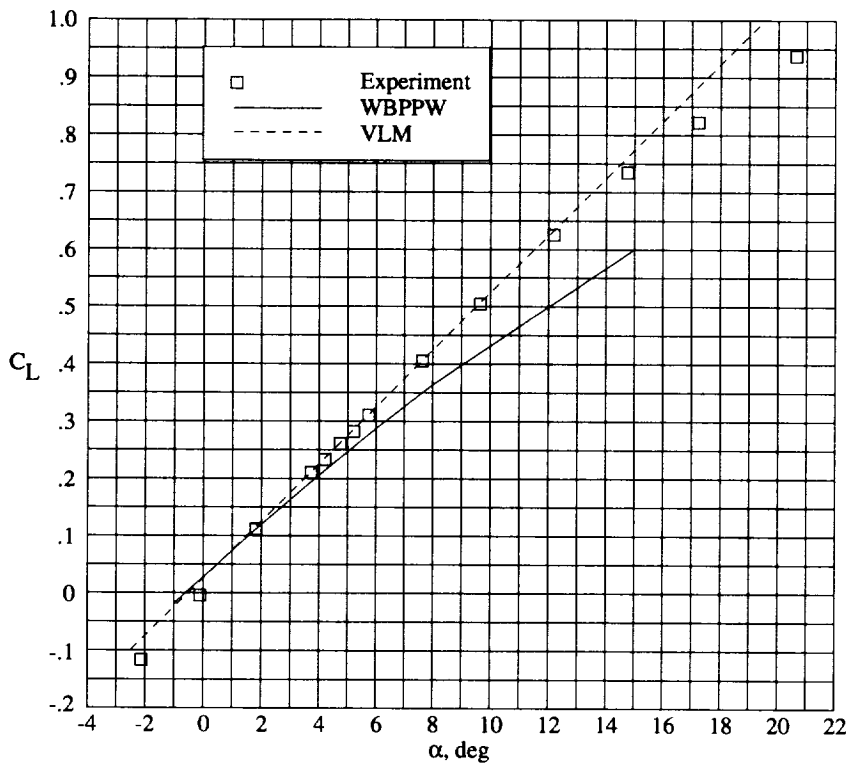
(b) Winglet; $M = 0.30$.

Figure 10. Comparison of computed lift with experiment.
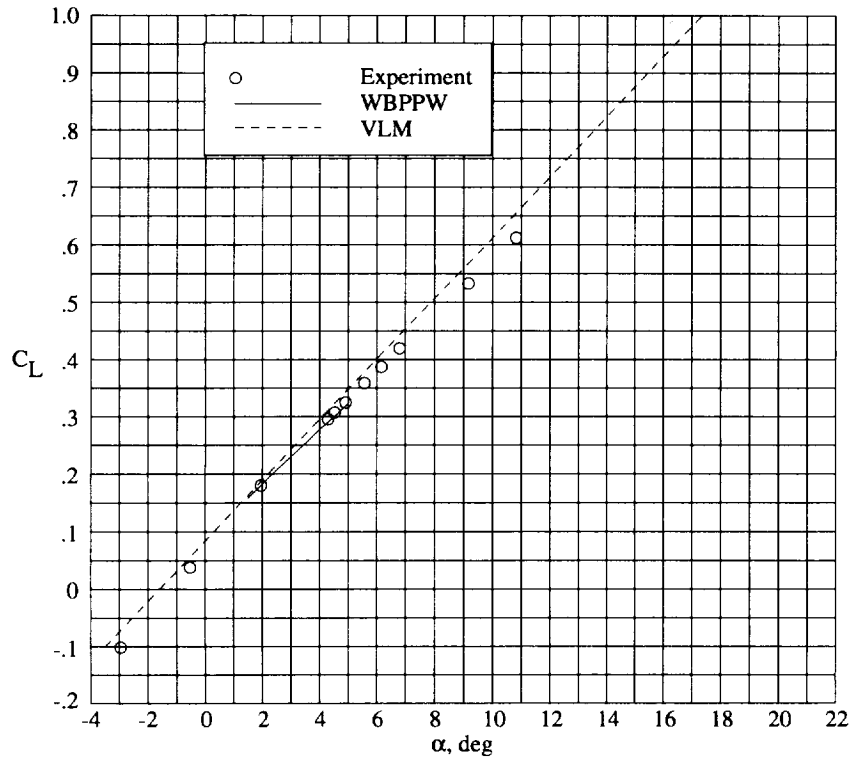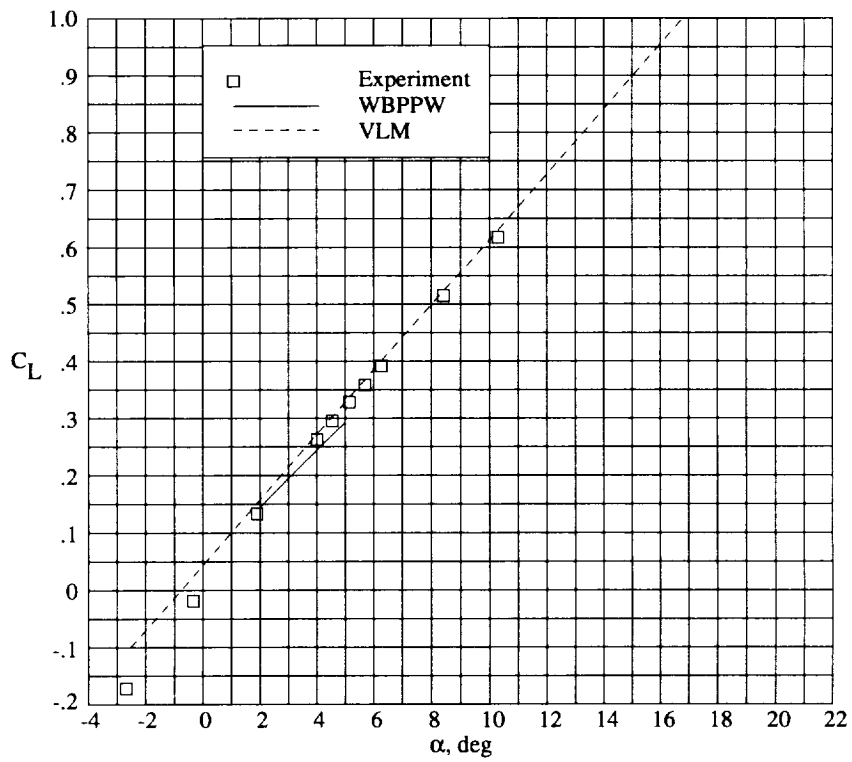
(c) Baseline; $M = 0.80$.

(d) Winglet; $M = 0.80$.

Figure 10. Concluded.
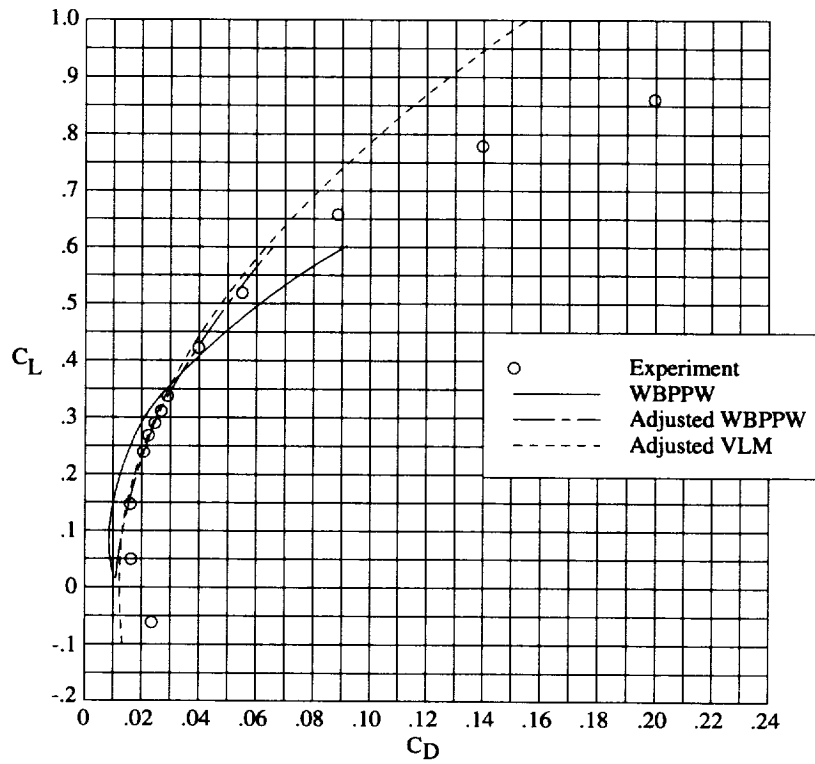
(a) Baseline; $M = 0.30$.
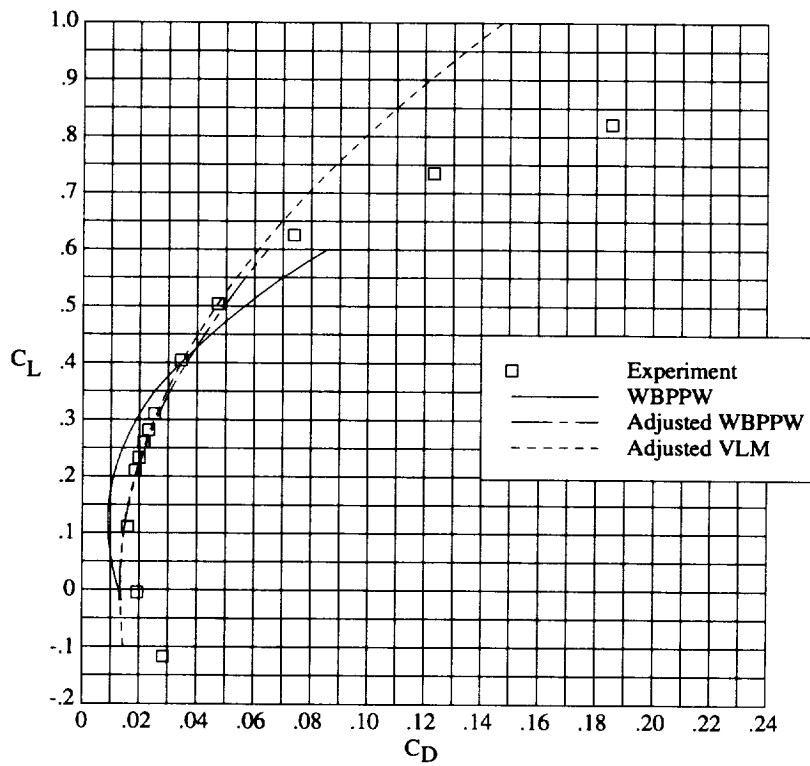
(b) Winglet; $M = 0.30$.

Figure 11. Comparison of computed drag with experiment.
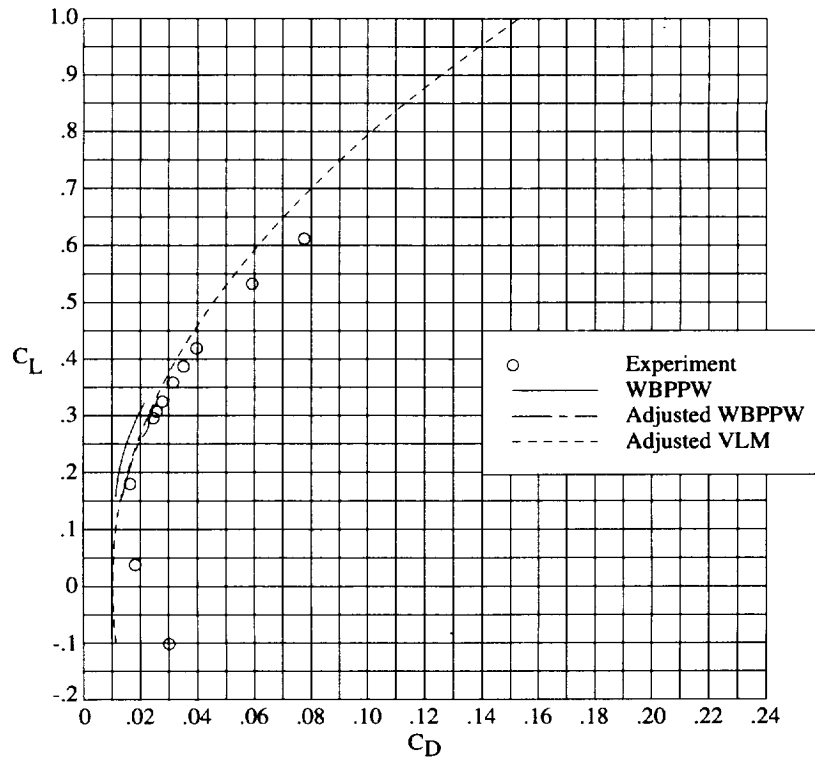
(c) Baseline; $M = 0.80$.
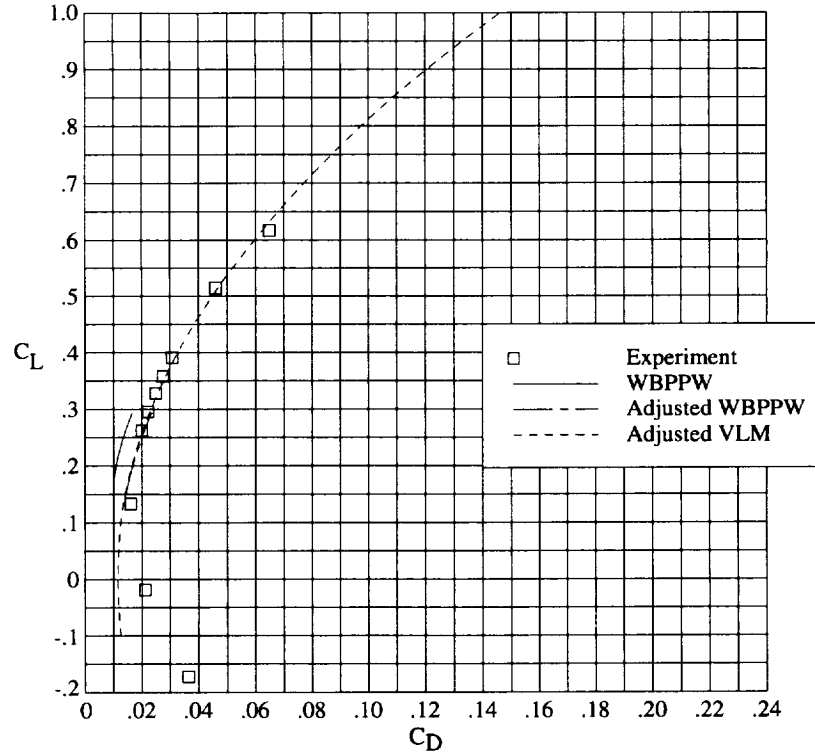
(d) Winglet; $M = 0.80$.

Figure 11. Concluded.
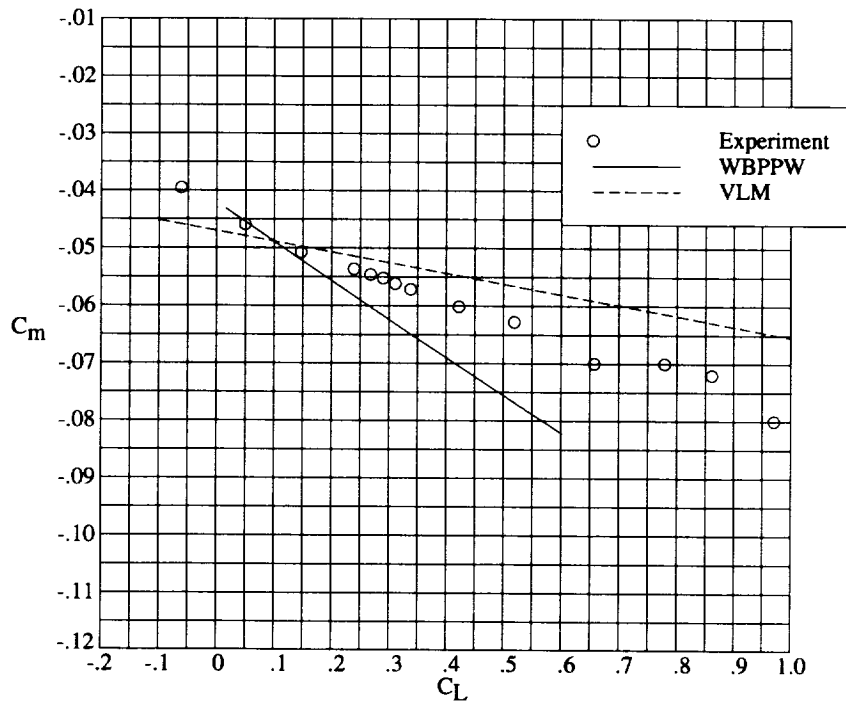
(a) Baseline; $M = 0.30$.
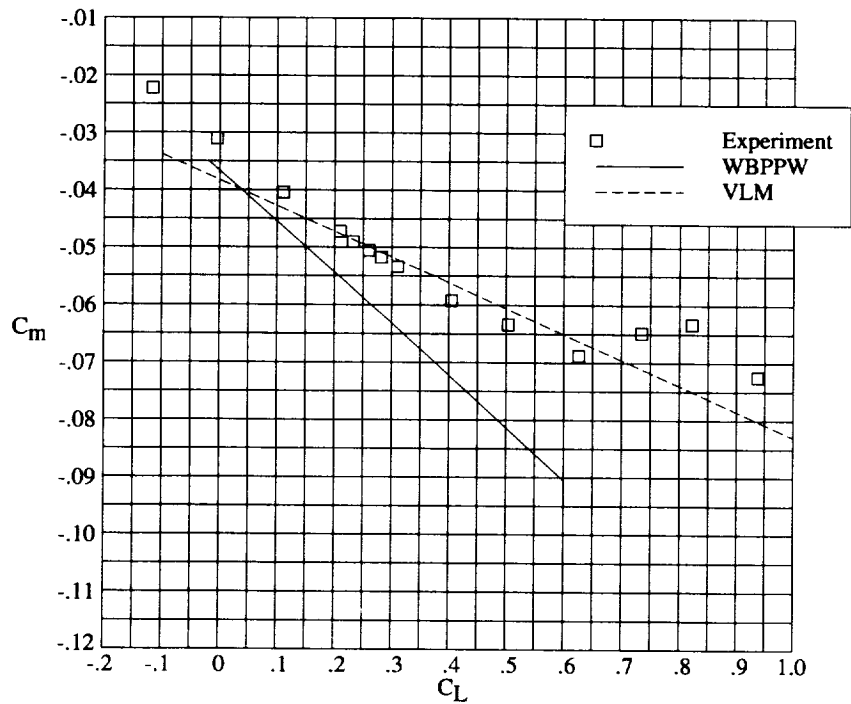
(b) Winglet; $M = 0.30$.

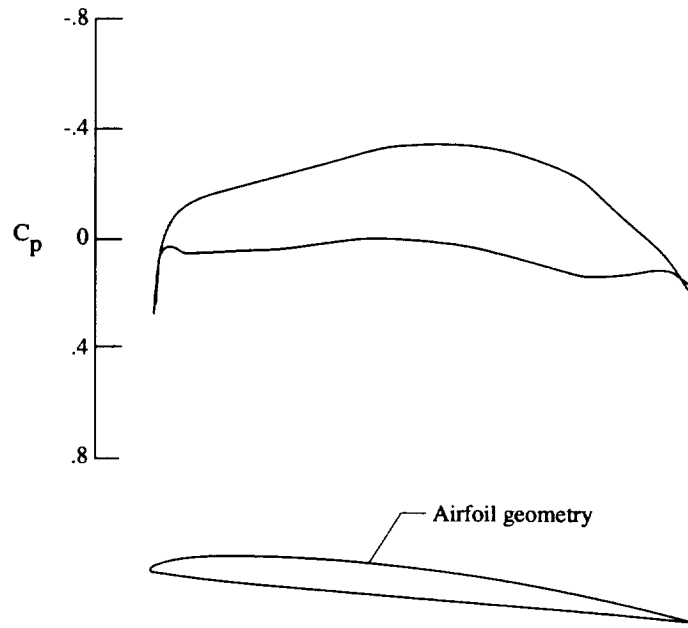Figure 12. Comparison of computed pitching moment with experiment.
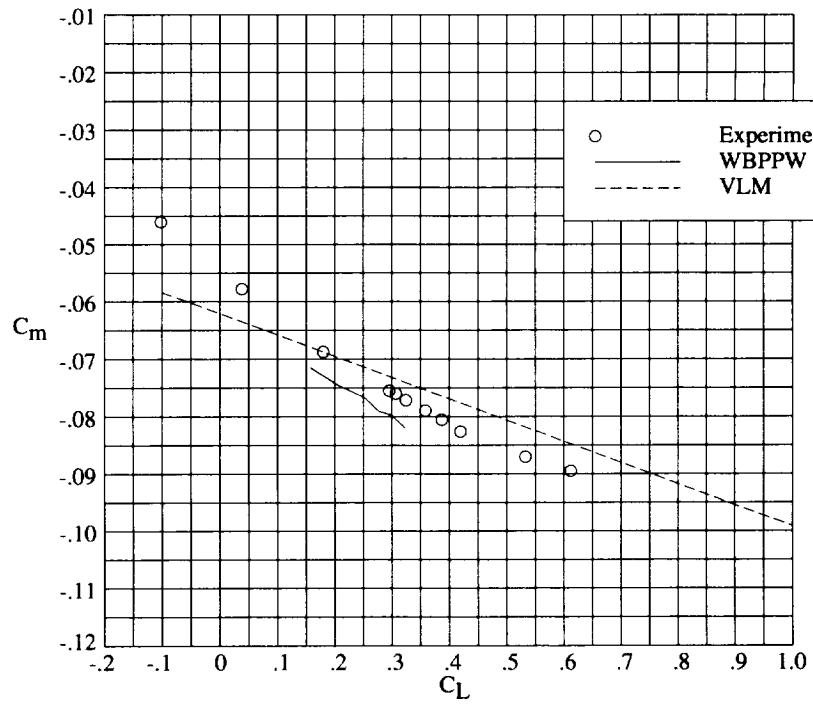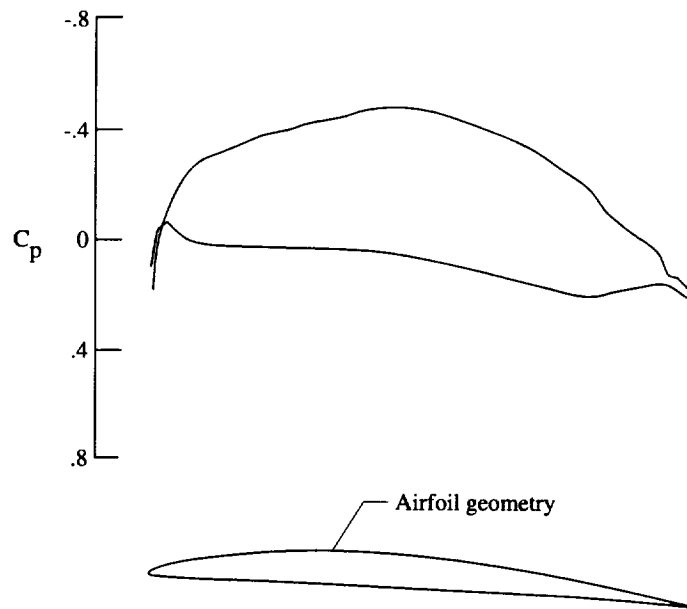
(c) Baseline; $M = 0.80$.
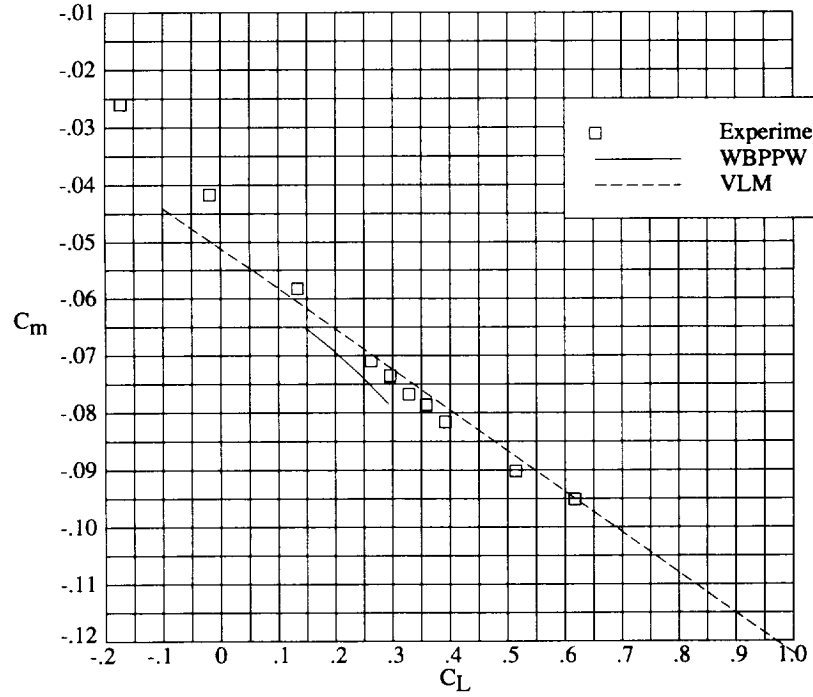
(d) Winglet; $M = 0.80$.

Figure 12. Concluded.

(a) $\eta = 0.186$.

(b) $\eta = 0.603$.

Figure 13. Typical pressure distribution. $M = 0.80$; $\alpha = 4.2°$.

REPORT DOCUMENTATION PAGE

Public reporting burden for this collection of information is estimated to average 1 hour per response, including the time for reviewing instructions, searching existing data sources, gathering and maintaining the data needed, and completing and reviewing the collection of information. Send comments regarding this burden estimate or any other aspect of this collection of information, including suggestions for reducing this burden, to Washington Headquarters Services, Directorate for Information Operations and Reports, 1215 Jefferson Davis Highway, Suite 1204, Arlington, VA 22202-4302, and to the Office of Management and Budget, Paperwork Reduction Project (0704-0188), Washington, DC 20503.

1. AGENCY USE ONLY (Leave blank)	2. REPORT DATE February 1996	3. REPORT TYPE AND DATES COVERED Technical Paper

4. TITLE AND SUBTITLE
Effects of Winglets on the Drag of a Low-Aspect-Ratio Configuration

5. FUNDING NUMBERS
WU 505-59-10-30

6. AUTHOR(S)
Leigh Ann Smith and Richard L. Campbell

7. PERFORMING ORGANIZATION NAME(S) AND ADDRESS(ES)

NASA Langley Research Center
Hampton, VA 23681-0001

8. PERFORMING ORGANIZATION REPORT NUMBER
L-17456

9. SPONSORING/MONITORING AGENCY NAME(S) AND ADDRESS(ES)

National Aeronautics and Space Administration
Washington, DC 20546-0001

10. SPONSORING/MONITORING AGENCY REPORT NUMBER
NASA TP-3563

11. SUPPLEMENTARY NOTES

12a. DISTRIBUTION/AVAILABILITY STATEMENT

Unclassified–Unlimited
Subject Category 02
Availability: NASA CASI (301) 621-0390

12b. DISTRIBUTION CODE

13. ABSTRACT (Maximum 200 words)
A wind-tunnel investigation has been performed to determine the effect of winglets on the induced drag of a low-aspect-ratio wing configuration at Mach numbers between 0.30 and 0.85 and a nominal angle-of-attack range from $-2°$ to $20°$. Results of the tests at the cruise lift coefficient showed significant increases in lift-drag ratio for the winglet configuration relative to a wing-alone configuration designed for the same lift coefficient and Mach number. Further, even larger increases in lift-drag ratio were observed at lift coefficients above the design value at all Mach numbers tested. The addition of these winglets had a negligible effect on the static lateral-directional stability characteristics of the configuration. No tests were made to determine the effect of these winglets at supersonic Mach numbers, where increases in drag caused by winglets might be more significant. Computational analyses were also performed for the two configurations studied. Linear and small-disturbance formulations were used. The codes were found to give reasonable performance estimates sufficient for predicting changes of this magnitude.

14. SUBJECT TERMS
Aircraft design; Drag reduction; Fighter aircraft; Winglets

15. NUMBER OF PAGES
60

16. PRICE CODE
A04

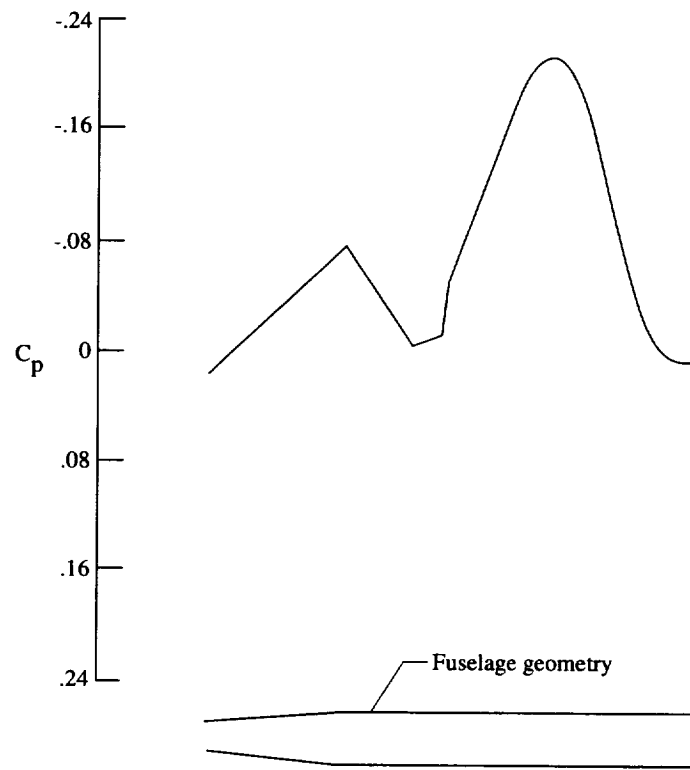| 17. SECURITY CLASSIFICATION OF REPORT Unclassified	18. SECURITY CLASSIFICATION OF THIS PAGE Unclassified	19. SECURITY CLASSIFICATION OF ABSTRACT Unclassified	20. LIMITATION OF ABSTRACT

Figure 14. Typical body pressure distribution. $M = 0.80$; $\alpha = 4.2°$.